Chapter 2
Active RC Filters Using Opamps

In this chapter, we consider the design aspects of active resistor–capacitor (RC) filters using operational amplifiers (opamps). This topic has been covered extensively in the past three decades in several classic textbooks [2.1, 2.2, 2.3, 2.4, 2.5, 2.6, 2.7, 2.8, 2.9, 2.10, 2.11, 2.12, 2.13]. There are numerous second-order filters structures available in the literature using one, two, three, or four opamps [2.14]. The choice of a particular structure is dependent on (a) the number of opamps used, (b) power consumption, (c) orthogonal control of pole-frequency, pole-Q, gain and transmission zeroes, (d) component spread, and (e) sensitivity to passive and active components. The designer shall also consider the dynamic range available through noise and distortion analysis. We illustrate the concepts through some examples chosen among several well-known structures. This enables readers to derive for themselves the results for other circuits of interest.

2.1 Amplifiers Using Opamps

In this section we consider finite gain inverting and noninverting amplifiers. The opamp frequency-dependent gain $A(s)$ is modeled by a single-pole model given by

$$A(s) = -\frac{B}{s + \omega_a} \tag{2.1}$$

where B is the gain bandwidth product denoted as $A_o\omega_a$, A_o is the dc gain, and ω_a is the open-loop cutoff frequency. Usually ω_a is very small, for example, the popular bipolar opamp μA741, say $2\pi \times 10$ rad/s and $A_o = 100{,}000$ for a typical bipolar opamp, so that $B = 2\pi \times 10^6$ rad/s. Taking into account the finite bandwidth of the opamp, the gain of the inverting amplifier of Fig. 2.1a can be derived as

P.V.A. Mohan, *VLSI Analog Filters: Active RC, OTA-C, and SC*,
Modeling and Simulation in Science, Engineering and Technology,
DOI 10.1007/978-0-8176-8358-0_2,

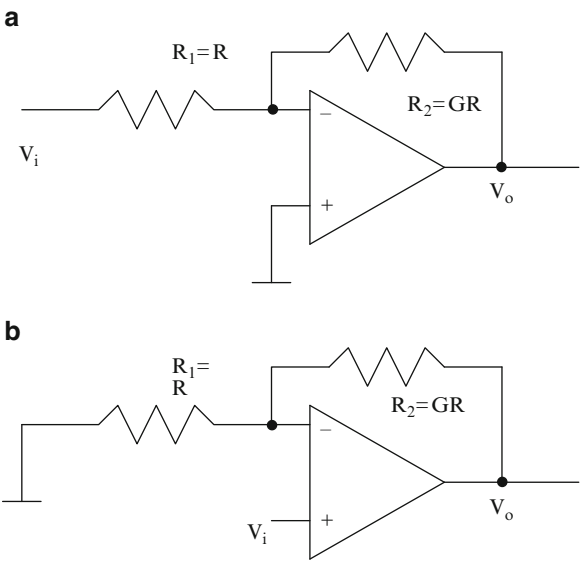

Fig. 2.1 (**a**) An inverting amplifier, and (**b**) a noninverting amplifier

$$\frac{V_o}{V_i} = -\frac{G}{1+\frac{(G+1)s}{B}} \tag{2.2}$$

where $G = R_2/R_1$. Thus, effectively, the cutoff frequency or bandwidth of the inverting amplifier is $B/(G + 1)$. In a similar manner, the gain of the noninverting amplifier of Fig. 2.1b can be derived as

$$\frac{V_o}{V_i} = \frac{(G+1)}{1+\frac{(G+1)s}{B}} \tag{2.3}$$

where $G = R_2/R_1$. Note that the cutoff frequency of a unity gain buffer (noninverting amplifier), that is, $G = 0$, is B whereas for an inverting amplifier of gain unity, the bandwidth is $B/2$ [2.15].

Considering the frequency response of the form (ignoring the frequency-independent gain factor),

$$A(s) = \frac{V_o}{V_i} = \frac{1}{1+as} \tag{2.4a}$$

where $a = 1/B$ and B is the unity gain bandwidth of the opamp, the gain and phase are given approximately for frequencies far smaller than the bandwidth B of the opamp as

$$A = \sqrt{(A(j\omega))^2} \cong 1 - \frac{a^2\ \omega^2}{2} \tag{2.4b}$$

$$\varphi \cong -a\,\omega \tag{2.4c}$$

The use of finite gain amplifiers in filters will lead to certain undesirable problems due to the introduced phase shift, which is considered in a later section.

To extend the frequency response (increase the bandwidth) of the amplifier, it is necessary to use passive or active compensation techniques [2.16]–[2.21]. In these, we effectively realize a transfer function of the form

$$A(s) = \frac{V_o}{V_i} = -\frac{K(1+as)}{1+as+b\,s^2} \tag{2.5}$$

where $a = \alpha/B$ and $b = \beta/B^2$. As a result, the gain and phase become

$$A = \sqrt{(A(j\omega))^2} \cong 1 + b\,\omega^2 \tag{2.6a}$$

$$\varphi \cong -ab\,\omega^3 \tag{2.6b}$$

Thus the phase response will have a third-order dependence on (ω/B) against first-order dependence for an uncompensated opamp given by (2.4c).

One method of *passive compensation* [2.16] is shown in Fig. 2.2a, wherein a capacitor C_c across the input resistor is used. The transfer function of this circuit can be obtained as

$$\frac{V_o}{V_i} = -\frac{R_2}{R_1}\,\frac{(1+s\,C_c\,R_1)}{1+\frac{s}{B}\left(1+\frac{R_2}{R_1}\right)+s^2\left(\frac{C_c\,R_2}{B}\right)} \tag{2.7}$$

Thus, under the condition $C_c\,R_1 = \frac{1}{B}\left(1+\frac{R_2}{R_1}\right)$, the first-order terms dependent on B will become equal, thus reducing the effect of finite bandwidth of the opamp on the amplifier frequency response.

Another technique, known as *active compensation*, uses another OA to compensate the effect of finite bandwidth of the opamp [2.18] and is shown in Fig. 2.2b. The pair of OAs together as shown within dotted lines is denoted as "composite OA." The transfer function of this circuit is given by

$$\frac{V_o}{V_i} = -\frac{R_2}{R_1}\,\frac{\left(1+\frac{s}{B_2}\right)}{1+\frac{s}{B_2}+\frac{s^2}{B_1\,B_2}\left(1+\frac{R_2}{R_1}\right)} \tag{2.8}$$

Thus, without needing any matching of bandwidths of the opamps, the circuit realizes active compensation. In the case of a unity gain buffer [2.17], the circuit of Fig. 2.2c has the gain given by

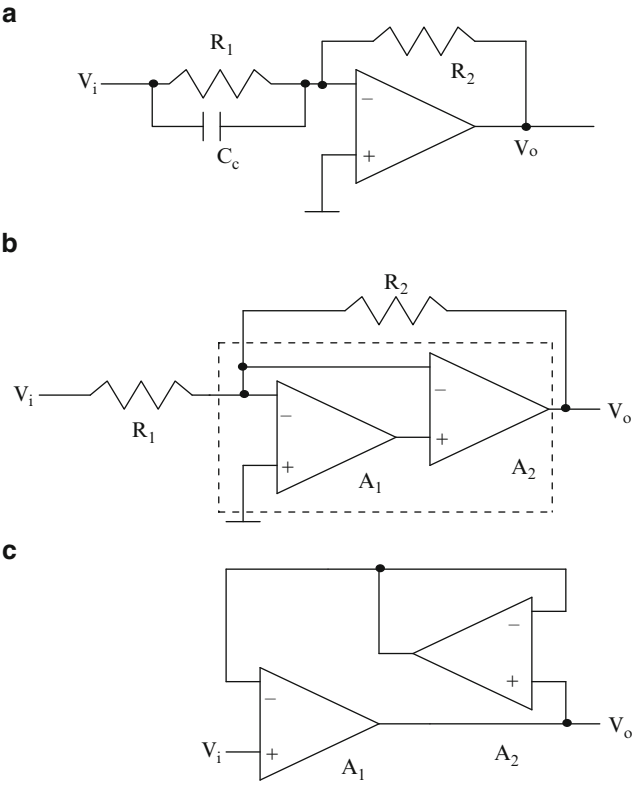

Fig. 2.2 Improved inverting amplifiers (**a**) using passive compensation, (**b**) using active compensation, and (**c**) improved buffer ((c) Adapted from [2.17] ©IEEE 1979)

$$\frac{V_o}{V_i} = \frac{\left(1 + \frac{s}{B_2}\right)}{1 + \frac{s}{B_1} + \frac{s^2}{B_1 B_2}} \tag{2.9}$$

Note that matching of OA bandwidths is needed to achieve exact compensation.

Example 2.1 Using WINSPICE, evaluate the frequency response of the actively compensated inverting amplifier for gain 10 of Fig. E.2.1. Use the opamp macromodel with opamp finite dc gain 100,000 and bandwidth 1 MHz. Compare the results with the uncompensated amplifier of Fig. 2.1a.

The SPICE code is listed below. Note that the opamp is modeled as a controlled voltage source with gain 100,000 using dependent voltage source E1 and the finite bandwidth is modeled by a first-order RC network (using R7, C2) with a pole-frequency of 1 MHz. The bandwidth expansion can be observed. Note that peaking can occur in the resultant composite amplifier frequency response.

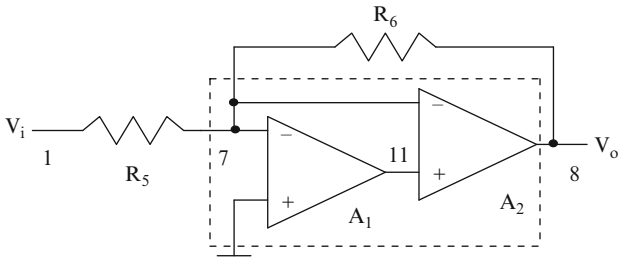

Fig. E.2.1

```
*Nonideal composite inverting amplifier
Vin1 1 0 ac 1 v
R5 1 7 1 k
R6 7 8 10 k
E1 0 9 7 0 100,000
R7 9 10 1 k
C2 10 0 15.9 uf
E2 11 0 10 0 1
E3 0 12 7 11 100,000
R8 12 13 1 k
C3 13 0 15.9 uf
E4 8 0 13 0 1
*Nonideal Inverting amplifier
R1 1 2 1 K
R2 2 6 10 k
E5 0 4 2 0 100,000
R3 4 5 1 k
C1 5 0 15.9 uf
E6 6 0 5 0 1
.ac dec 10 1 100,000 K
```

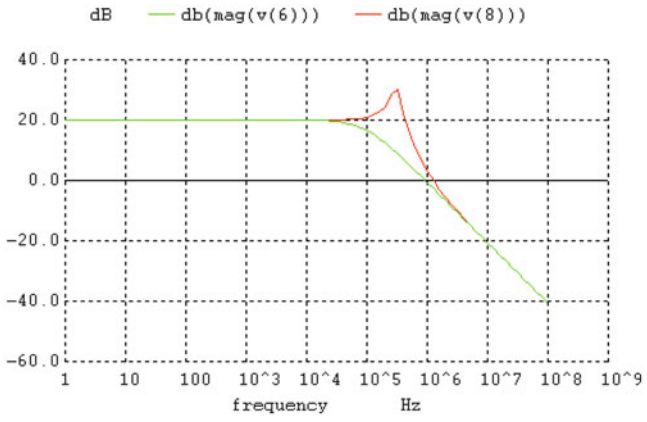

Fig. E.2.2

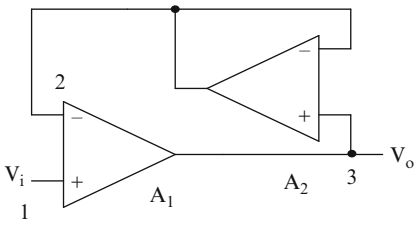

Example 2.2 Using WINSPICE, evaluate the frequency response of the actively compensated buffer amplifier of Fig. E.2.2. Use the opamp macro model with opamp finite dc gain 100,000 and bandwidth 1 MHz.

The SPICE listing is given below. The bandwidth enhancement can be seen clearly.

```
*Nonideal composite noninverting buffer amplifier
Vin1 1 0 ac 1 v
E1 4 0 1 2 100,000
R1 4 5 1 k
C1 5 0 15.9 uf
E2 3 0 5 0 1
E3 6 0 3 2 100,000
R3 6 7 1 k
C2 7 0 15.9 uf
E4 2 0 7 0 1
E5 9 0 1 8 100,000
R4 9 10 1 K
C3 10 0 15.9uF
E6 8 0 10 0 1
.ac dec 10 1 100,000 K
```

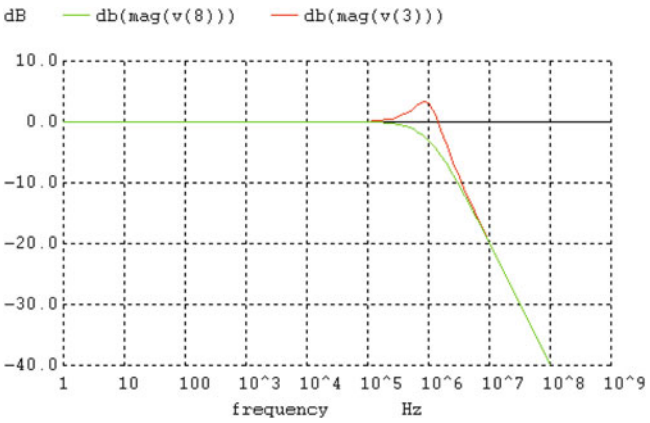

Another interesting active compensation scheme was suggested by Boutin [2.19], which uses a negative impedance converter (NIC). This circuit, presented in Fig. 2.3a, has the transfer function given by

$$\frac{V_o}{V_i} = -\frac{R_2}{R_1}\left(\frac{1}{1+\frac{s}{B}\left(1+\frac{R_2}{R_1}-\frac{R_2}{R_N}\right)}\right) \tag{2.10}$$

Evidently, under the condition $\frac{1}{R_1}+\frac{1}{R_2}=\frac{1}{R_N}$, the gain will be frequency independent. Note, however, that we need an ideal negative resistance, which is not possible in practice.

Two circuits for obtaining negative resistance are presented in Fig. 2.3b, c. Note that in both these circuits, a resistance R is placed between V_i and $2V_i$, thus effectively making a current $(V_i - 2V_i)/R = -V_i/R = V_i/(-R)$ to flow simulating a negative resistance. Since the opamp is nonideal, these two circuits realize a nonideal negative resistance.

The use of the negative resistance [2.20] of Fig. 2.3b in the circuit of Fig. 2.3a in place of $-R_N$ yields the circuit of Fig. 2.3d, whose transfer function is given by

$$\frac{V_o}{V_i} = -\frac{R_2}{R_1}\left(\frac{1+\frac{2s}{B_2}}{1+s\left(\frac{2}{B_2}-\frac{1}{B_1}\left(\frac{R_2}{R_1}+1-\frac{R_2}{R_3}\right)\right)+\frac{2s^2}{B_1 B_2}\left(\frac{R_2}{R_1}+1-\frac{R_2}{R_3}\right)}\right) \tag{2.11}$$

Under the condition $\frac{1}{R_1}+\frac{1}{R_2}=\frac{1}{R_3}$, the first-order terms become equal, thus achieving compensation.

Example 2.3 Analyze using SPICE the compensated amplifier using NIC shown in Fig. E.2.3.

Note that $R_3 = -R_1R_2/(R_1 + R_2)$ is chosen for exact compensation. The uncompensated amplifier response is also presented to illustrate the bandwidth enhancement.

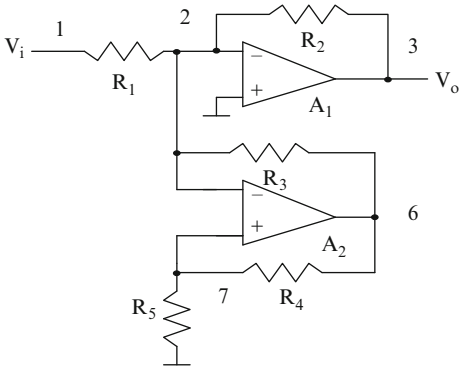

Fig. E.2.3

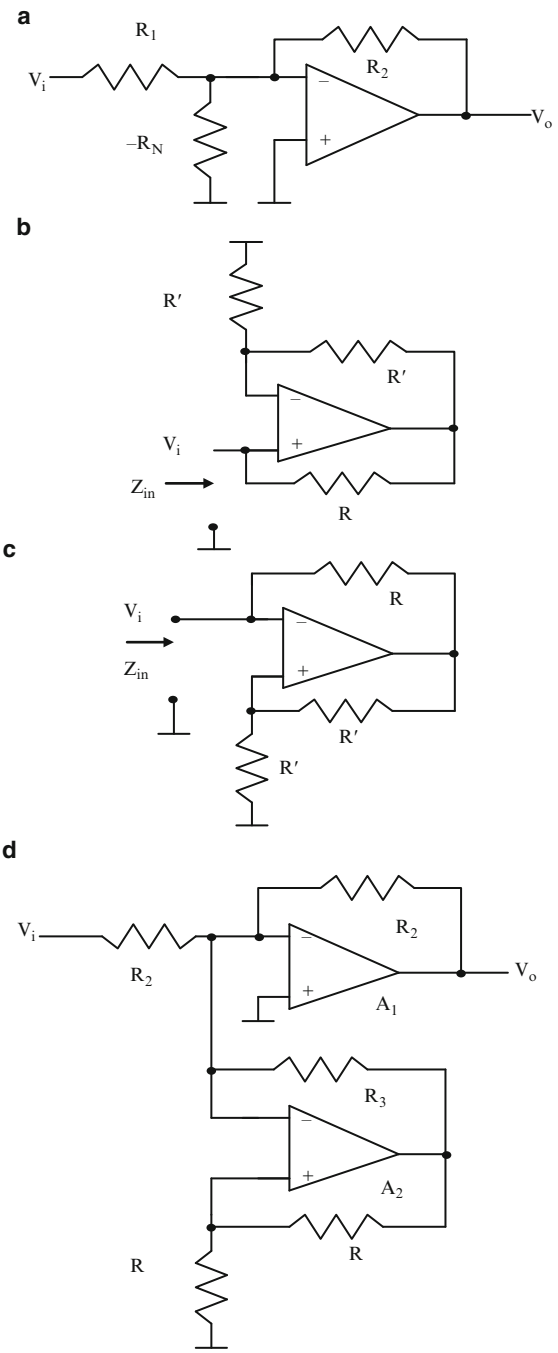

Fig. 2.3 (**a**) Boutin's active compensation scheme of amplifier using NIC, (**b**) and (**c**) circuits for NIC realization, and (**d**) complete circuit following (a) and (b) ((a) Adapted from [2.19] ©IEE 1981, (d) Adapted from [2.20] ©AEU 1988)

```
*Amplifier using NIC compensation
R1 1 2 1 K
R2 2 3 1 K
R3 2 6 500
R4 6 7 1 k
R5 7 0 1 K
E1 0 4 2 0 100,000
R6 4 5 1 k
C1 5 0 15.9 uf
E2 3 0 5 0 1
E3 8 0 2 7 100,000
R7 8 9 1 K
C2 9 0 15.9 uf
E4 6 0 9 0 1
*Normal amplifier
R8 1 10 1 K
R9 10 11 1 K
E5 0 12 10 0 100,000
R10 12 13 1 k
C3 13 0 15.9 uf
E6 11 0 13 0 1
vin 1 0 ac 1 V
.ac dec 10 1 100,00 K
```

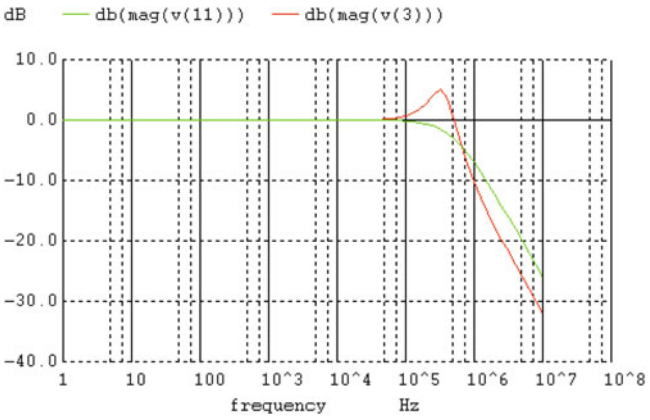

2.2 Integrators Using Opamps

An inverting integrator using an opamp is shown in Fig. 2.4a. In the case of an opamp with infinite bandwidth, the transfer function realized is

$$\frac{V_o}{V_i} = -\frac{1}{sCR} \tag{2.12a}$$

The transfer function of the integrator taking into account the model of (2.1) is given by

$$\frac{V_o}{V_i} = -\frac{1}{sCR\left(1+\frac{1}{BCR}+\frac{s}{B}\right)} \tag{2.12b}$$

Thus, a real pole is created because of the finite bandwidth of the OA. Expressing the integrator transfer function as

$$\frac{V_o}{V_i} = -\frac{1}{R(j\omega)+jX(j\omega)} \tag{2.13a}$$

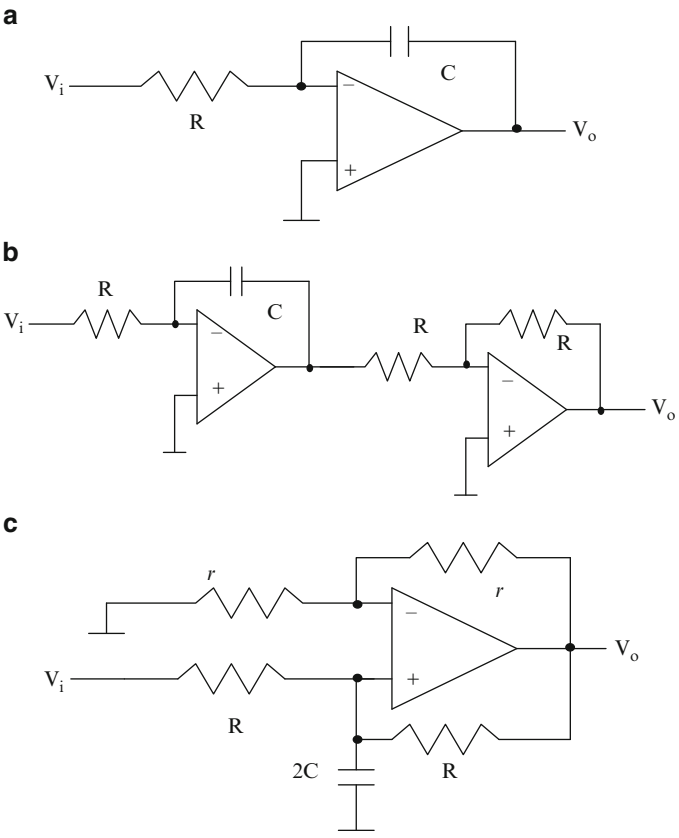

Fig. 2.4 (**a**) An inverting integrator (**b**) a non-inverting integrator and (**c**) Deboo's non-inverting integrator, Actively compensated integrators: (**d**) Akerberg–Mossberg scheme [2.24], (**e–g**) Brackett and Sedra schemes [2.21] and (**h**) Ravichandran and Rao [2.18] (**b–d**),(**f**),(**g**) Adapted from [2.21] ©IEEE 1976)

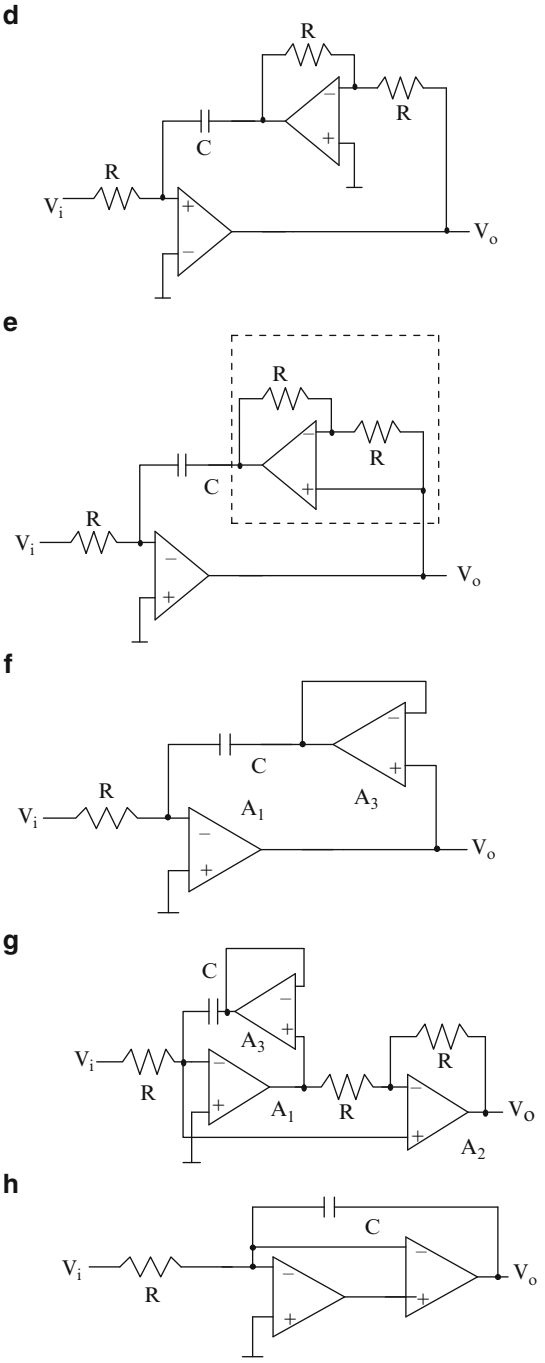

Fig. 2.4 (continued)

its Q-factor [2.21] can be defined as

$$Q_{integ} = \frac{X(j\omega)}{R(j\omega)} \tag{2.13b}$$

Thus, for the integrator of Fig. 2.4a, using (2.12b) and (2.13b) we obtain the Q-factor as

$$Q_{integ} = -\left(\frac{B}{\omega} + \frac{1}{\omega CR}\right) \tag{2.14}$$

A noninverting integrator can be obtained by cascading an inverting integrator with a unity gain inverting amplifier [2.21] as shown in Fig. 2.4b. The transfer function of this integrator, taking into account the nonideal opamp, is given by

$$\frac{V_o}{V_i} = \frac{1}{\left(sCR + \frac{s}{B} + \frac{s^2 CR}{B}\right)\left(1 + \frac{2s}{B}\right)} \tag{2.15a}$$

The Q-factor for this integrator can be obtained using (2.13b) as

$$Q_{integ} = -\left(\frac{BCR + 1 - \frac{2\omega^2 CR}{B}}{3\omega CR + \frac{2\omega}{B}}\right) \cong -\frac{B}{3\omega} \tag{2.15b}$$

Evidently, the Q-factor is lower than that of the inverting integrator given by (2.14).

Since the noninverting integrator of Fig. 2.4b needs two opamps, a single amplifier-based integrator has been suggested by Deboo [2.22] (shown in Fig. 2.4c). The transfer function of this integrator is given by

$$\frac{V_o}{V_i} = \frac{1}{sCR + \frac{2s}{B} + \frac{2s^2 CR}{B}} \tag{2.16a}$$

The resulting Q-factor can be derived as

$$Q_{integ} = -\left(\frac{BCR + 2}{2\omega CR}\right) \cong -\frac{B}{2\omega} \tag{2.16b}$$

Note that the Deboo integrator uses a negative resistance formed by resistors R', r, and r and opamp A_1 (see Fig. 2.3b). Its Q-factor is less than that of the inverting integrator but more than the two-amplifier based noninverting integrator of Fig. 2.4b.

The Q-factor of the noninverting integrator can be made equal to that of the inverting integrator by using an ingenious integrator described by Akerberg and

Mossberg [2.24] and shown in Fig. 2.4d. The transfer function of this integrator can be derived as

$$\frac{V_o}{V_i} = \frac{\left(1+\frac{2s}{B}\right)}{\frac{2s^3CR}{B^2} + s^2\left(\frac{2}{B^2}+\frac{CR}{B}\right) + s\left(\frac{1}{B}+CR\right)} \tag{2.17a}$$

The resulting Q-factor is given as

$$Q_{integ} = -\left(\frac{\frac{B}{\omega}+\frac{1}{\omega CR}+\frac{4\omega}{CRB^2}}{1-\frac{4\omega^2}{B^2}}\right) \cong \frac{B}{\omega} \tag{2.17b}$$

Another actively compensated integrator [2.21] is shown in Fig. 2.4e, which realizes the same transfer function as that of Fig. 2.4d. Note that the block within dotted lines has a gain $\frac{1}{1+\frac{2s}{B_2}}$ and the opamp A_1 is an inverting amplifier, whereas in the circuit of Fig. 2.4d, the opamp A_1 is a noninverting amplifier and A_2 and resistor R realize a gain $\frac{-1}{1+\frac{2s}{B_2}}$. Thus, the circuit is the same except for the sign of the integrator transfer function.

Active compensation also can be achieved using a buffer amplifier [2.21] as shown in Fig. 2.4f. The transfer function of this circuit can be derived as

$$\frac{V_o}{V_i} = \frac{-\left(1+\frac{s}{B_3}\right)}{sCR\left(1+\frac{1}{CRB_1}+\frac{s}{B_1}\left(1+\frac{1}{CRB_3}\right)+\frac{s^2}{B_1B_3}\right)} \tag{2.18}$$

A noninverting integrator can be obtained with the same integrator Q-factor by augmenting the compensated inverting integrator of Fig. 2.4f using an additional opamp and two resistors, as shown in Fig. 2.4g. The transfer function of this circuit [2.21] is given as

$$\frac{V_o}{V_i} = \frac{\left(1+\frac{s}{B_3}\right)}{sCR\left(1+\frac{1}{CRB_1}+\frac{s}{B_1}\left(1+\frac{1}{CRB_3}\right)+\frac{s^2}{B_1B_3}\right)} \frac{\left(1+\frac{2s}{B_1}\right)}{\left(1+\frac{2s}{B_2}\right)} \tag{2.19}$$

It can be seen that when $B_1 = B_2$, the second fraction will become unity, thus realizing the same transfer function as an inverting integrator except for the sign.

We next consider another actively compensated integrator [2.18] shown in Fig. 2.4h that does not need any additional passive components. The transfer function of this integrator can be derived as

$$\frac{V_o}{V_i} = \frac{-\left(1+\frac{s}{B_2}\right)}{\frac{s^3CR}{B_1B_2}+\frac{s^2}{B_1B_2}(1+B_1CR)+sCR} \tag{2.20a}$$

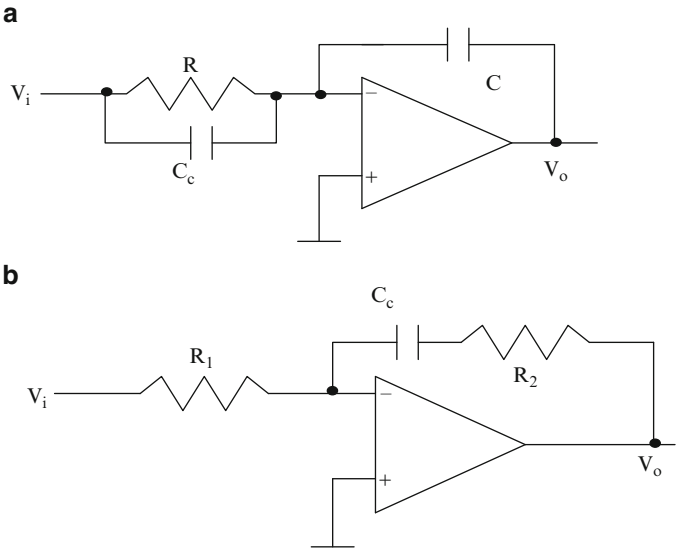

Fig. 2.5 (**a**, **b**) Passive compensation of inverting integrators

The resulting Q-factor (assuming $B_1 = B_2 = B$) is given as

$$Q_{integ} = -\left(\frac{B^3 + \frac{\omega^2}{CR}}{\omega^3 + \frac{B\omega}{CR}}\right) = -\left(\frac{\frac{B^3}{\omega^3} + \frac{\omega_o}{\omega}}{1 + \frac{B\omega_o}{\omega^2}}\right) \tag{2.20b}$$

For $\omega_o = 1/CR = \omega$,

$$Q_{integ} = -\left(\frac{\frac{B^3}{\omega^3} + 1}{1 + \frac{B}{\omega}}\right) \cong -\frac{B^2}{\omega^2} \tag{2.20c}$$

which is much larger than B/ω of an uncompensated integrator.

An integrator can be compensated by adding a small capacitance C_c across the input feeding resistance R [2.23] as shown in Fig. 2.5a. The transfer function of this circuit can be obtained as

$$\frac{V_o}{V_i} = \frac{-(1 + s\,C_c R)}{sCR\left(1 + \frac{s}{B}\left(1 + \frac{C_c}{C}\right) + \frac{1}{BCR}\right)} \tag{2.21a}$$

Evidently, under the condition

$$C_c = \frac{C}{BCR - 1} \cong \frac{1}{BR} \tag{2.21b}$$

compensation is achieved.

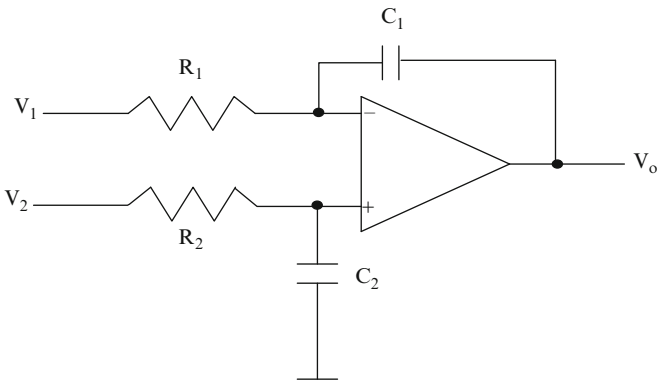

Fig. 2.6 A differential integrator

In another technique [2.25] shown in Fig. 2.5b, an integrator has been shown to be compensated using an additional series resistance with the integrating capacitor. In this technique, the transfer function can be obtained as

$$\frac{V_o}{V_i} = -\frac{1}{sCR_1}\left(\frac{(1+sCR_2)}{1+\frac{1}{BCR_1}+\frac{s}{B}\left(1+\frac{R_2}{R_1}\right)}\right) \tag{2.22}$$

It can be seen that under the condition $BCR_2 = \left(1+\frac{R_2}{R_1}\right)$, the s-terms in the numerator and denominator are equal thus achieving first-order cancellation of the effect of the finite bandwidth on the amplifier.

A differential integrator is shown in Fig. 2.6 whose transfer function considering an ideal opamp is given by

$$V_o = \frac{-V_1\,(1+s\,C_2\,R_2)+V_2\,(1+s\,C_1\,R_1)}{s\,C_1\,R_1\,(1+s\,C_2\,R_2)} \tag{2.23}$$

Thus, a differential integrator is obtained when $C_1R_1 = C_2R_2$, that is, the two time constants shall match.

2.3 First-Order Filters Using Opamps

2.3.1 Low-Pass Filters

A first-order low-pass filter can be obtained by damping the integrator capacitor in the integrators described earlier as shown in Fig. 2.7a. The transfer function of this circuit is given by

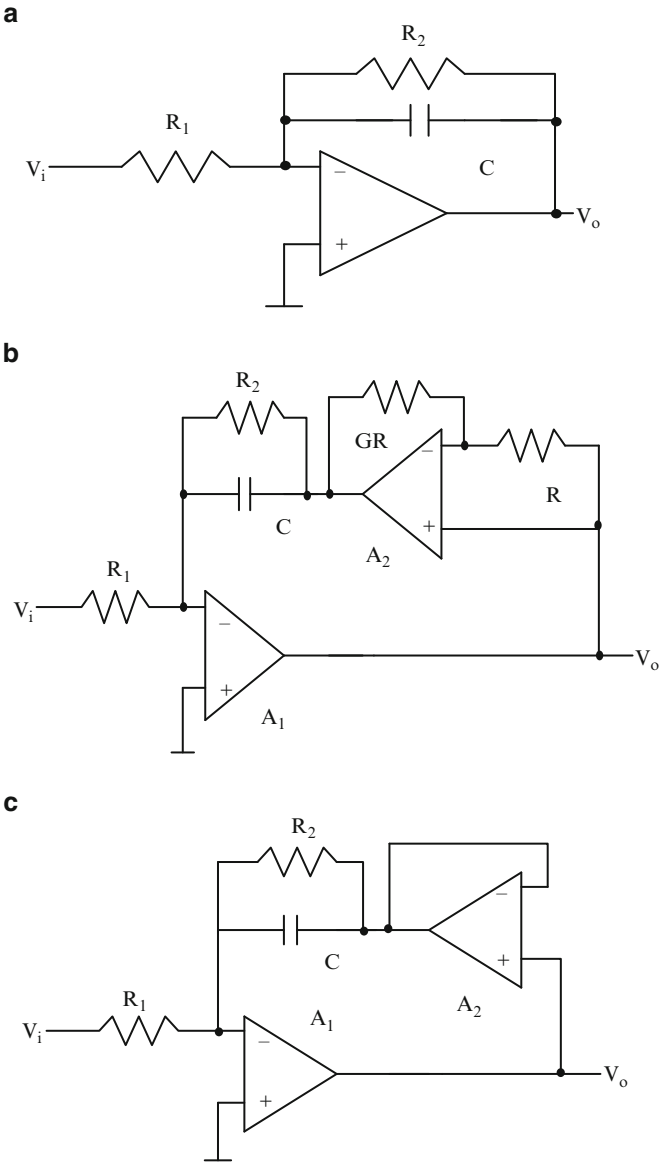

Fig. 2.7 (**a**) A first-order low-pass filter, (**b**) and (**c**) actively compensated first-order low-pass filters

$$\frac{V_o}{V_i} = -\frac{R_2}{R_1}\left(\frac{1}{1 + s\left(C R_2 + \frac{1}{B}\left(1 + \frac{R_2}{R_1}\right)\right) + s^2\left(\frac{C R_2}{B}\right)}\right) \tag{2.24}$$

showing that two real poles exist. The circuit can be compensated using another OA with two resistors as shown in Fig. 2.7b. The resulting transfer function can be shown to be

$$\frac{V_o}{V_i} = -G\left(\frac{1 + \frac{(G+1)s}{B_2}}{1 + s\left(C R_2 + \frac{G+1}{B_1}\right) + s^2\left(\frac{(G+1)^2}{B_1 B_2} + \frac{C R_2}{B_1}\right) + \frac{s^3 C R_2 (G+1)}{B_1 B_2}}\right) \tag{2.25}$$

where $G = R_2/R_1$. Note that the first-order term $s(G + 1)/B$ in the numerator and denominator (assuming $B_1 = B_2 = B$) will compensate the lossy integrator.

An alternative compensated lossy integrator is shown in Fig. 2.7c whose transfer function is given by

$$\frac{V_o}{V_i} = -G\left(\frac{1 + \frac{s}{B_2}}{1 + s\left(C R_2 + \frac{G+1}{B_1}\right) + s^2\left(\frac{(G+1)}{B_1 B_2} + \frac{C R_2}{B_1}\right) + \frac{s^3 C R_2}{B_1 B_2}}\right) \tag{2.26}$$

2.3.2 *First-Order All-Pass Filters*

We next consider the realization of first-order all-pass filters [2.26] which is possible using the two circuits of Fig. 2.8a, b. The transfer functions of these circuits are, respectively, as follows.

$$\frac{V_o}{V_i} = \frac{(1 - sCR)}{(1 + sCR)\left(1 + \frac{2s}{B}\right)} \tag{2.27a}$$

and

$$\frac{V_o}{V_i} = -\frac{(1 - sCR)}{(1 + sCR)\left(1 + \frac{2s}{B}\right)} \tag{2.27b}$$

2.4 Sallen–Key Active RC Low-Pass Filter

Consider the Sallen–Key active RC filter [2.27] of Fig. 2.9a. We use this as a vehicle to explain the design concepts. Consider that the opamp has finite gain A. Then, the following equations can be easily written at the nodes 1, 2, and 3,

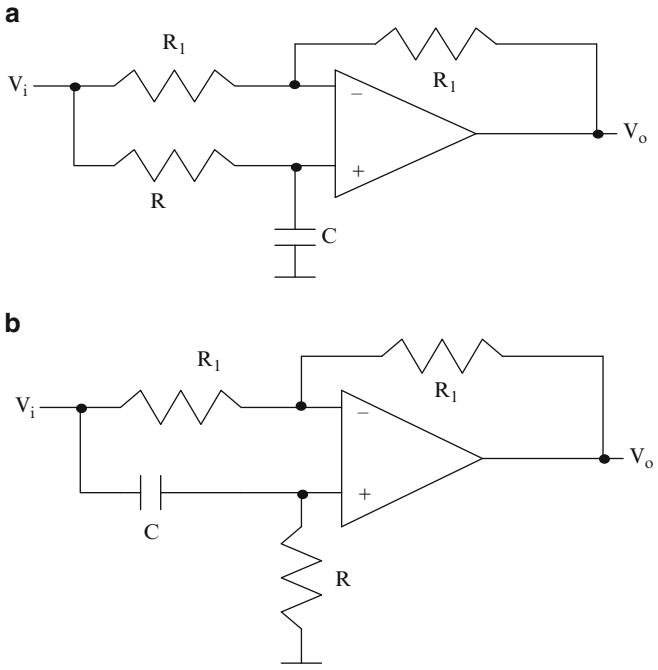

Fig. 2.8 (**a**, **b**) First-order all-pass filters using one opamp

$$\frac{V_i - V_1}{R_1} + \frac{V_2 - V_1}{R_2} + (V_0 - V_1)sC_1 = 0 \tag{2.28a}$$

$$\frac{V_1 - V_2}{R_2} = V_2\, s\, C_2 \tag{2.28b}$$

$$\left(V_2 - \frac{V_0}{K}\right)A = V_0 \tag{2.28c}$$

where A is the gain of the opamp. Solving these equations, we obtain the transfer function of the filter as

$$\frac{V_o}{V_i} = \frac{K}{s^2 C_1 C_2 R_1 R_2 \left(1+\frac{K}{A}\right) + s\left((C_1 R_1 + C_2 (R_1 + R_2))\left(1+\frac{K}{A}\right) - K C_1 R_1\right) + \left(1+\frac{K}{A}\right)} \tag{2.29a}$$

Note that in the case where we consider an ideal opamp (i.e., $A = \infty$), the transfer function of (2.29a) is simplified as

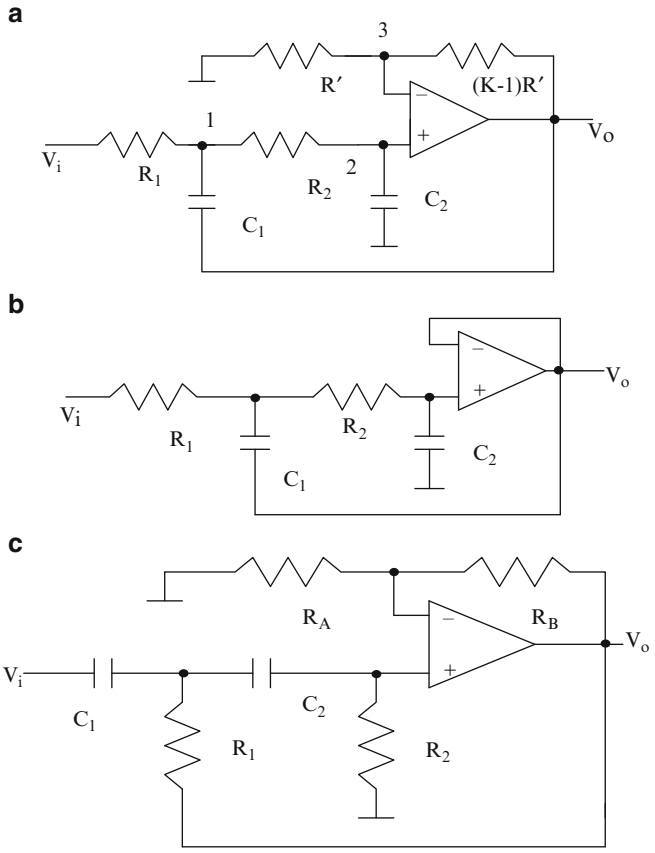

Fig. 2.9 (**a**) Sallen–Key active RC low-pass filter using amplifier gain K, (**b**) with $K = 1$ using a buffer, and (**c**) Sallen–Key high-pass filter using a noninverting amplifier of gain K

$$\frac{V_o}{V_i} = \frac{K}{s^2\ C_1\ C_2\ R_1\ R_2 + s(C_1\ R_1 + C_2\ (R_1 + R_2) - K\ C_1\ R_1) + 1} \tag{2.29b}$$

The next step is to match the transfer function with the desired second-order low-pass transfer function. Since the s-term and s^2 term in the numerator are zero, the transfer function is a low-pass type. The denominator of the transfer function can be compared with the standard second-order denominator

$$D(s) = s^2 + s\left(\frac{\omega_o}{Q_p}\right) + {\omega_p}^2 \tag{2.30a}$$

to obtain the pole-frequency and pole-Q as follows.

$$\omega_p = \frac{1}{\sqrt{C_1\ C_2\ R_1\ R_2}} \tag{2.30b}$$

and

$$Q_p = \frac{\sqrt{C_1\ C_2\ R_1\ R_2}}{(C_1\ R_1 + C_2\,(R_1 + R_2) - K\,C_1\ R_1)} \tag{2.30c}$$

There are many component choices possible. However, two popular choices are (a) using equal resistors ($R_1 = R_2 = R$) and equal capacitors ($C_1 = C_2 = C$) and $K > 1$; (b) $K = 1$ (see Fig. 2.9b) using unequal resistors and capacitors.

In choice (a), the expressions for pole-frequency and pole-Q simplify as

$$\omega_p = \frac{1}{RC} \text{ and } Q_p = \frac{1}{3 - K} \tag{2.31}$$

For choice (b), the corresponding expression for pole-frequency is given by (2.30b) and the expression for pole-Q is

$$Q_p = \sqrt{\frac{C_1}{C_2}}\frac{\sqrt{R_1\ R_2}}{(R_1 + R_2)} \tag{2.32a}$$

It can be seen from (2.32a) that the spread in capacitor values can be minimized when $R_1 = R_2$:

$$\frac{C_1}{C_2} = 4\,Q_p^2 \tag{2.32b}$$

which can be quite large for large Q_p values.

It is thus easily possible to design the circuit for a given pole-frequency and pole-Q Q_p. Note that the dc gain in both cases can be obtained by substituting $s = j\omega = 0$ in (2.29b). There is no degree of freedom to control the dc (low-frequency) gain. On the other hand, in choice (a), the pole-Q is independently controlled by K. The property of independent control of pole-frequency, pole-Q, and gain is known as *orthogonal tunability*.

2.4.1 *Effect of Finite Gain of the Opamp*

Next, let us consider the effect of opamp finite dc gain. Evidently, by matching denominator coefficients of the denominator of (2.29a) with (2.30a), the pole-frequency is seen to be independent of the finite gain of the opamp. However, the pole-Q is dependent on A as follows.

$$Q_p = \frac{\left(1+\frac{K}{A}\right)\sqrt{C_1\ R_1\ C_2\ R_2}}{\left((C_1\ R_1 + C_2\ (R_1+R_2)\right)\left(1+\frac{K}{A}\right) - K\,C_1\ R_1)} \tag{2.33}$$

Evidently, for large gain of the opamp, the sensitivity to A becomes zero as A tends to the limit ∞.

2.4.2 *Effect of Finite Bandwidth of the Opamp*

On the other hand, let us investigate the effect of finite bandwidth of the opamp. For this purpose, we need to employ the single-pole model of the opamp. Note that the opamp is usually designed to be a three-pole system [2.28] and has a dominant pole which is at very low frequencies, and has second and third poles at very large frequencies. The dominant pole is intentionally created by connecting a compensation capacitor inside the opamp circuitry by the opamp designer. Such an approach ensures stability of the opamp when 100% negative feedback is used, for example, when the opamp is connected as a buffer.

From (2.29a), using the model of (2.1), we obtain the denominator of the transfer function as a third-degree expression:

$$D(s) = \left(s^3\ \frac{C_1\ C_2\ R_1\ R_2\,K}{B} + s^2\left(C_1\ C_2\ R_1\ R_2 + \frac{K}{B}\left(C_1\ R_1 + C_2\ (R_1+R_2)\right)\right)\right.$$
$$\left. + s\left(C_1\ R_1 + C_2\ (R_1+R_2) - K\,C_1\ R_1 + \frac{K}{B}\right) + 1\right) \tag{2.34}$$

Evidently, a parasitic real pole is created and the original (ideal) pole-frequency and pole-Q would have changed. It is therefore necessary to find out the deviation in pole-frequency and pole-Q of the active filter due to the opamp finite bandwidth. The cubic equation can be solved to find the roots and from that information, the real pole, pole-frequency, and pole-Q corresponding to the complex pole pair can be estimated. However, most often, designers need to have a quick assessment of the expected deviations.

For this purpose, an approximation suggested by Akerberg and Mossberg [2.24] can be used. In this, the s^3 term is written as $-s{\omega_p}^2$ so that the third-order system becomes a second-order system. From this, the modified pole-frequency and pole-Q can be found following the conventional definitions. Note, however, that this is true for high pole-Qs. For low pole-Qs, one can find them by exactly solving the cubic equation. Using the Akerberg–Mossberg approximation, we have from (2.34), the approximated denominator of the transfer function as

$$\begin{aligned} \mathrm{D}'(\mathrm{s}) = s^2 \left(C_1\ C_2\ R_1\ R_2 + \frac{K}{B}(C_1\ R_1 + C_2\ (R_1 + R_2)) \right) \\ + s\,(C_1\ R_1 + C_2\,(R_1 + R_2) - K\,C_1\ R_1) + 1 \end{aligned} \tag{2.35}$$

Thus, the shifted pole-frequency $\hat{\omega}_p$ and shifted pole-Q $\hat{Q}_p$ can be seen by identifying (2.35) with

$$s^2 \left(\frac{1}{\hat{\omega}_p^2} \right) + s \left(\frac{1}{\hat{\omega}_p\, \hat{Q}_p} \right) + 1$$

as

$$\frac{\omega_p^2}{\hat{\omega}_p^2} = 1 + \frac{K}{B}(C_1\ R_1 + C_2\,(R_1 + R_2))\,\omega_p^2 \tag{2.36}$$

and

$$\frac{1}{\hat{\omega}_p\ \hat{Q}_p} = \frac{1}{\omega_p\ Q_p} \tag{2.37}$$

Evidently, from (2.36), we can observe that the pole-frequency $\hat{\omega}_p$ decreases due to opamp finite bandwidth and we note also from (2.37) that the pole-Q $\hat{Q}_p$ increases by a similar amount. As an illustration for case (b), $K = 1$, we have

$$\frac{\omega_p^2}{\hat{\omega}_p^2} = 1 + \left(2\,Q_p + \frac{1}{Q_p} \right) \frac{\omega_p}{B} \tag{2.38a}$$

and for case (a), $K \neq 1$,

$$\frac{\omega_p^2}{\hat{\omega}_p^2} = 1 + 3 \left(3 - \frac{1}{Q_p} \right) \frac{\omega_p}{B} \tag{2.38b}$$

Note that several solutions have been suggested to get rid of the problem of opamp finite bandwidth by (a) *predistortion*, (b) *passive compensation* of opamp, and (c) *active compensation* of opamp. However, these need either extra passive or active components or the performance of the compensated filters varies with power supply voltage and temperature. The predistortion technique is based on (2.38a) and considers the design of the circuit with lower pole-Q and higher pole-frequency than desired.

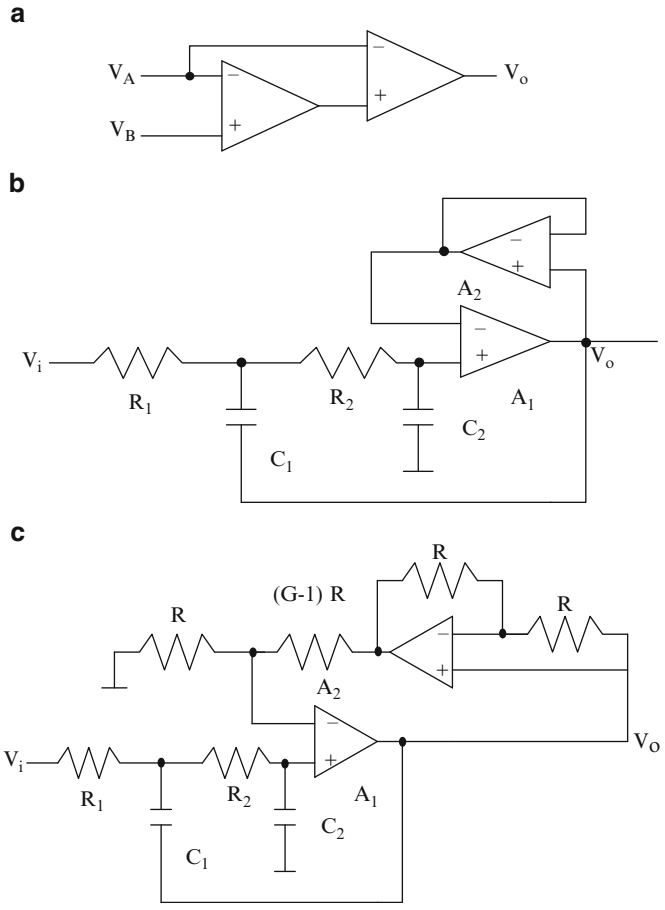

Fig. 2.10 (**a**) A composite opamp, (**b**) Sallen–Key filter with $K = 1$ using composite opamp-based buffer, and (**c**) Sallen–Key filter using composite opamp for $K \neq 1$

2.4.3 Active Compensation of Sallen–Key Filter with K = 1

The Sallen–Key filter using the composite opamp of Fig. 2.10a to realize a unity gain buffer is shown in Fig. 2.10b. The transfer function of the buffer stage using composite opamps is given by (2.9). The denominator of the transfer function of the actively compensated Sallen–Key filter of Fig. 2.10b is given by

$$D(s) = s^4\left(\frac{C_1\,C_2\,R_1\,R_2}{B^2}\right) + s^3\left(\frac{C_1\,C_2\,R_1\,R_2}{B} + \frac{C_1\,R_1 + C_2\,R_1 + C_2\,R_2}{B^2}\right)$$
$$+ s^2\left(\frac{1}{B^2} + \frac{C_2\,R_1 + C_2\,R_2}{B} + C_1\,C_2\,R_1\,R_2\right) + s\left(\frac{1}{B} + C_2\,R_1 + C_2\,R_2) + 1\right) \tag{2.39}$$

Using Akerberg–Mossberg approximation, it can be shown that the modified pole-frequency is given as

$$\frac{\omega_p^2}{\widehat{\omega}_p^2} = 1 + \frac{\omega_p}{Q_p B} \tag{2.40}$$

which may be compared with (2.38a) to note the significant improvement.

A noninverting amplifier needed in the Sallen–Key filter can also be actively compensated using the circuit shown in Fig. 2.10c within dotted lines which needs an additional OA and two resistors. The transfer function of this block is

$$H(s) = \frac{G\left(1 + \frac{sG}{B_2}\right)}{1 + \frac{Gs}{B_1} + \frac{G^2 s^2}{B_1 B_2}} \tag{2.41}$$

Under the matching condition $B_1 = B_2$, this composite amplifier also realizes a third-order dependence of phase but much larger than that of a buffer due to the G^3 term. The reader is urged to study the effect of using this compensated Sallen–Key filter.

2.4.4 Sensitivity Analysis

The active and passive components used in filters typically have large tolerances due to manufacturing processes. The effect of these variations on the pole-frequency and pole-Q from the nominal design values of the filters needs to be analyzed. This can be carried out through sensitivity analysis. The sensitivity of a filter parameter such as transfer function magnitude H to a component x_i is defined as

$$S_{x_i}^H = \frac{\partial H}{\partial x_i} \cdot \frac{x_i}{H} = \frac{\partial H}{H} \Big/ \frac{\partial x_i}{x_i} = \frac{\%\ change\ in\ H}{\%\ change\ in\ x_i} \tag{2.42}$$

In other words, we would like to know the percentage change in H for a given change of 1% in component value. Generally, the sensitivity should be small and closer to unity. Note that the sensitivity can be positive or negative, meaning that H may increase due to the 1% increase in component value or may decrease.

The computation of sensitivity can be easily done by noting some tricks. As an illustration, consider the following expression for pole-frequency of a typical active RC filter,

$$\omega_o = \frac{1}{\sqrt{R_1\ R_2\ C_1\ C_2}} \tag{2.43}$$

The following can be easily written,

$$S_{R_1}^{\omega_o} = S_{R_2}^{\omega_o} = S_{C_1}^{\omega_o} = S_{C_2}^{\omega_o} = -\frac{1}{2}$$

In other words, if the term under consideration is in the denominator, the sensitivity will have negative sign and the "exponent" of that variable in the expression is the sensitivity.

Some general formulae are presented next. The sensitivity of a fraction (p/q) to any component can be shown to be

$$S_x^{p/q} = S_x^p - S_x^q \tag{2.44}$$

As an illustration, consider the sensitivity evaluation of Q_p given by (2.30c) to the various components:

$$Q_p = \frac{\sqrt{C_1\ C_2\ R_1\ R_2}}{(C_1\ R_1 + C_2\,(R_1 + R_2) - K\,C_1\ R_1)} = \frac{N}{D} \tag{2.45}$$

We have

$$\begin{aligned} S_{C_1}^{Q_p} &= S_{C_1}^N - S_{C_1}^D = \frac{1}{2} - \frac{C_1\ R_1 - K\,C_1\ R_1}{C_1\ R_1 + C_2\,(R_1 + R_2) - K\,C_1\ R_1} \\ &= \frac{1}{2} - \frac{C_1\ R_1\,(1-K)\,Q_p}{\sqrt{C_1\ R_1\ C_2\ R_2}} \end{aligned} \tag{2.46a}$$

The expressions for other sensitivities can be very similarly written as follows.

$$S_{R_1}^{Q_p} = S_{R_1}^N - S_{R_1}^D = \frac{1}{2} - \frac{Q_p\,(C_1\ R_1 + C_2\ R_1 - K\,C_1\ R_1)}{\sqrt{C_1\ R_1\ C_2\ R_2}} \tag{2.46b}$$

$$S_{R_2}^{Q_p} = S_{R_2}^N - S_{R_2}^D = \frac{1}{2} - \frac{C_2\ R_2\ Q_p}{\sqrt{C_1\ R_1\ C_2\ R_2}} \tag{2.46c}$$

$$S_{C_2}^{Q_p} = S_{C_2}^N - S_{C_2}^D = \frac{1}{2} - \frac{C_2\,(R_1 + R_2)\,Q_p}{\sqrt{C_1\ R_1\ C_2\ R_2}} \tag{2.46d}$$

$$S_K^{Q_p} = S_K^N - S_K^D = \frac{K\,C_1\ R_1\ Q_p}{\sqrt{C_1\ R_1\ C_2\ R_2}} \tag{2.46e}$$

It is very important to remember that sensitivity formulae should be written for the original equation with all component values distinctly present. As an illustration for the choice $K = 1, R_1 = R_2$ the sensitivities are as follows.

$$S_{C_1}^{Q_p} = -S_{C_2}^{Q_p} = \frac{1}{2}, S_{R_1}^{Q_p} = S_{R_2}^{Q_p} = 0$$

For the case $K \neq 1$, we have the following.

$$S_{C_1}^{Q_p} = 2\,Q_p - \frac{1}{2}, S_{R_1}^{Q_p} = \frac{3\,Q_p}{2} - 1, S_{R_2}^{Q_p} = \frac{1}{2} - Q_p, S_{C_2}^{Q_p} = \frac{1}{2} - 2\,Q_p, S_K^{Q_p} = 3\,Q_p - 1$$

It will be useful to substitute the parameter under consideration in the sensitivity expression to get a meaningful insight to the magnitude of the sensitivity. For example, in (2.46) above, the value of Q_p has been substituted to obtain the various sensitivities in terms of Q_p. At this stage, the assumptions made in design such as $R_1 = R_2$, and so on can be made. The reader is referred to Appendix A for information on the evaluation of the overall variation in the magnitude of the transfer function.

In the earlier section, we considered a single-amplifier low-pass filter. A high-pass filter can be easily obtained by replacing resistors with capacitors and capacitors with resistances. This leads to a transformation known as low-pass to high-pass transformation denoted as an $s \rightarrow 1/s$ transformation. A high-pass filter thus obtained is shown in Fig. 2.9c.

Example 2.4 Analyze using SPICE, the Sallen–Key filter using (a) an ideal unity gain amplifier, (b) using a μA 741 operational amplifier, and (c) an actively compensated unity gain amplifier. We use the model of the μA741 opamp. The ideal pole-frequency and pole-Q are 159.09 KHz and 5, respectively.

The SPICE listing and frequency responses for the three cases are presented below. The actual 741 model is defined as a subcircuit Xopamp. This is available from manufacturers at their websites. It can be seen that a nonideal opamp results in a decrease in pole-frequency and increase in pole-Q. On the other hand, the use of an actively compensated opamp results in a pole-frequency closer to the ideal value and Q enhancement is still present.

```
*Uncompensated Sallen–Key filter using opamp macromodel (infinite bandwidth)
Vin 1 0 1v ac
R3 1 6 1 K
R4 6 7 1 K
C3 6 8 10 nF
C4 7 0 .10 nF
E1 8 0 7 0 1
*Uncompensated Sallen–Key filter using Actual 741 model.
R1 1 2 1 K
```

```
R2 2 3 1 K
C1 2 4 10 nF
C2 3 0 .10 nF
xopamp1 3 4 vpos vneg 4 xyz
v1 vpos 0 dc 12
v2 0 vneg dc 12
*Actively Compensated Sallen–Key filter
R5 1 9 1 K
R6 9 10 1 K
C5 9 11 10 nF
C6 10 0 .10 nF
Xopamp2 10 12 vpos vneg 11 xyz
Xopamp3 11 12 vpos vneg 12 xyz
.ac lin 100 10 600 K
.subckt xyz 1 2 3 4 5
c1 11 12 8.661E-12
c2 6 7 30.00E-12
dc 5 53 dx
de 54 5 dx
dlp 90 91 dx
dln 92 90 dx
dp 4 3 dx
egnd 99 0 poly(2) (3.0) (4.0) 0 .5 .5
fb 7 99 poly(5) vb vc ve vlp vln 0 10.61E6–10E6 10E6 +10E6 –10E6
ga 6 0 11 12 188.5E-6
gcm 0 6 10 99 5.961E-9
iee 10 4 dc 15.16E-6
hlim 90 0 vlim 1 K
q1 11 2 13 qx
q2 12 1 14 qx
r2 6 9 100.0E3
rc1 3 11 5.305E3
rc2 3 12 5.305E3
re1 13 10 1.836E3
re2 14 10 1.836E3
ree 10 99 13.19E6
r01 8 5 50
ro2 7 99 100
rp 3 4 18.16E3
vb 9 0 dc 0
vc 3 53 dc 1
ve 54 4 dc 1
vlim 7 8 dc 0
vlp 91 0 dc 40
vln 0 92 dc 40
```

.model dx D(Is = 800.0E–18 Rs = 1)
.model qx NPN(Is = 800E–18 Bf = 93.75)
.ends

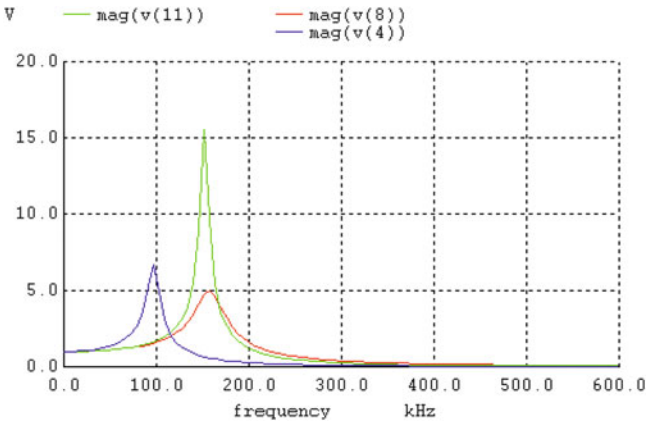

The SPICE simulation of the second-order Sallen–Key low-pass filter using a unity gain amplifier is presented next. The CMOS opamp Schematic [2.103] is shown in Fig. E.2.4. The program listing also gives an ideal Sallen–Key filter for comparison. The filter is designed for a pole-frequency of 795.45 KHz and pole-Q of 2.5.

*Sallen–Key ideal opamp
R3 1 6 100 K
R4 6 7 100 K
C3 6 8 10 pF
C4 7 0 0.4 pF
E1 8 0 7 0 1

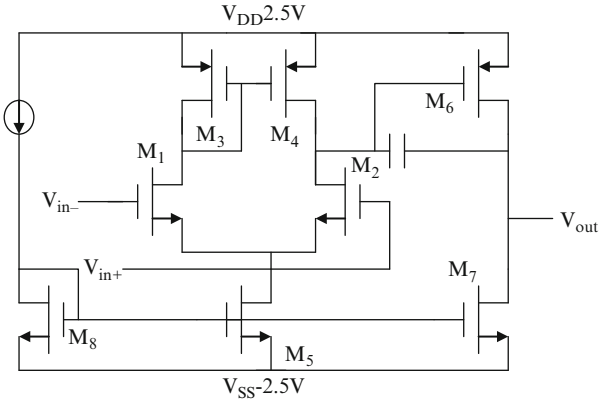

Fig. E.2.4 SPICE code of opamps (Adapted from [2.103]©OUP 2002)

```
*Sallen–Key filter using CMOS opamp
Vin 1 0 0.1v ac
R5 1 9 100 K
R6 9 10 100 K
C5 9 11 10 pF
C6 10 0 0.4 pf
Xopamp1 10 11 11 vpos vneg OPAMP
.ac lin 100 10 2000 K
v1 vpos 0 dc 2.5
v2 0 vneg dc 2.5
.SUBCKT OPAMP 1 2 6 8 9
M1 4 2 3 3 NMOS1 W = 3U L = 1U AD = 18P AS = 18P PD = 18U PS = 18U
M2 5 1 3 3 NMOS1 W = 3U L = 1U AD = 18P AS = 18P PD = 18U PS = 18U
M3 4 4 8 8 PMOS1 W = 15U L = 1U AD = 90P AS = 90P PD = 42U PS = 42U
M4 5 4 8 8 PMOS1 W = 15U L = 1U AD = 90P AS = 90P PD = 42U PS = 42U
M5 3 7 9 9 NMOS1 W = 4.5U L = 1U AD = 27P AS = 27P PD = 21U PS = 21U
M6 6 5 8 8 PMOS1 W = 94U L = 1U AD = 564P AS = 564P PD = 200U PS =
    200U
M7 6 7 9 9 NMOS1 W = 14U L = 1U AD = 84P AS = 84P PD = 40U PS = 40U
M8 7 7 9 9 NMOS1 W = 4.5U L = 1U AD = 27P AS = 27P PD = 21U PS = 21U
CC 5 6 3.0P
.MODEL NMOS1 NMOS VTO = 0.70 KP = 110U GAMMA = 0.4 LAMBDA =
    0.04 PHI = 0.7 MJ = 0.5 MJSW = 0.38 CGBO = 700P CGSO = 220P CGDO =
    220P CJ = 770U CJSW = 380P LD = 0.016U TOX = 14N
.MODEL PMOS1 PMOS VTO = -0.70 KP = 50U GAMMA = 0.57 LAMBDA =
    0.05 PHI = 0.8 MJ = 0.5 MJSW = 0.35 CGBO = 700P CGSO = 220P CGDO =
    220P CJ = 560U CJSW = 350P LD = 0.014U TOX = 14N
IBIAS 8 7 30U
.ENDS
.END
```

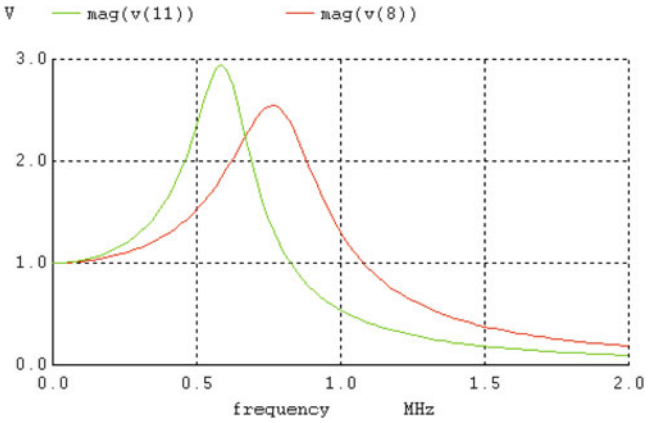

2.5 Second-Order Filters Based on Multiple Feedback

2.5.1 *Friend's Biquad*

There are other second-order filters using a single opamp known as *single-amplifier biquads* (SAB) that can realize many transfer functions based on the choice of component values. One such popular biquad is known as *Friend's biquad* [2.29]. This is shown in Fig. 2.11a and is also known as a *multiple feedback* filter since it uses both negative and positive feedback. This circuit, however, cannot realize a low-pass and all-pass transfer function for which alternative circuits shown in Figs. 2.12 and 2.13 can be used. We first denote

$$V_x = \alpha V_i + \beta V_o \tag{2.47}$$

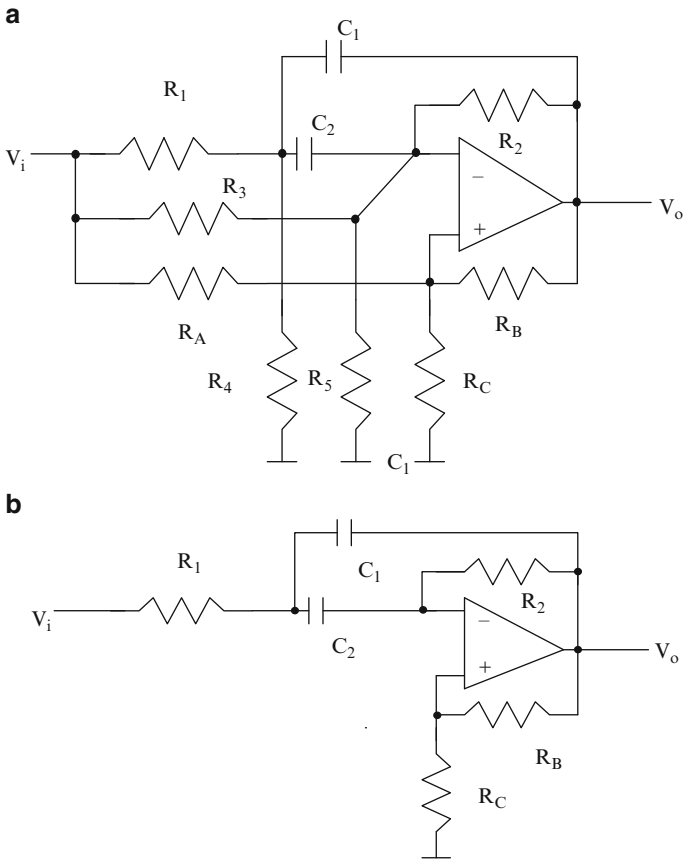

Fig. 2.11 (**a**) Friend's biquad, and (**b**) Deliyannis band-pass filter (Adapted from [2.29] ©IEEE 1975)

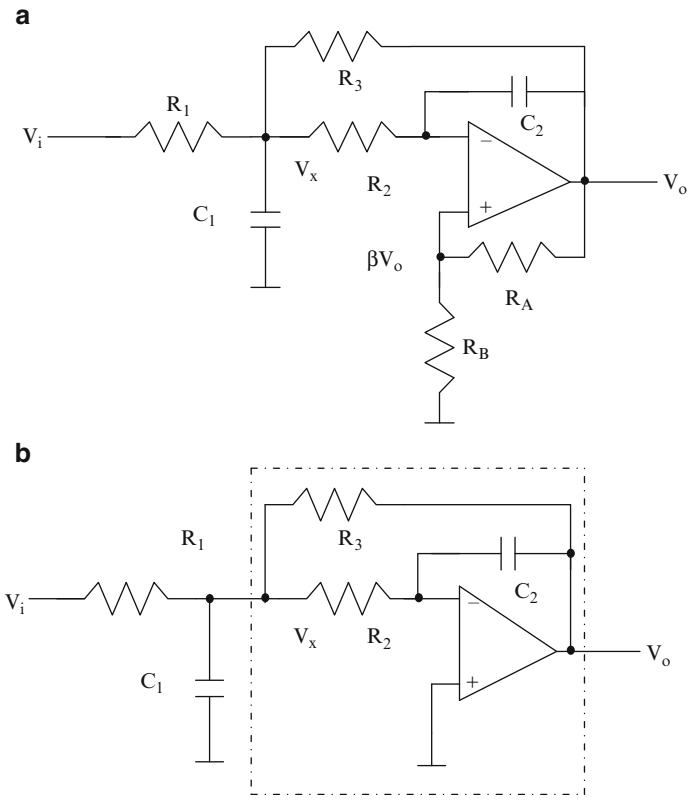

Fig. 2.12 (**a**) Multiple feedback- type second-order active RC low-pass filter with positive feedback, and (**b**) with no positive feedback (Adapted from [2.29] ©IEEE 1975)

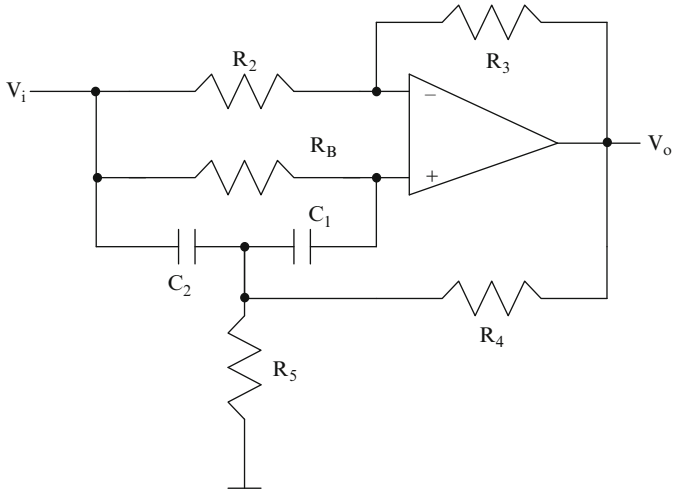

Fig. 2.13 Steffen's all-pass-type single-amplifier biquad (Adapted from [2.29] ©IEEE1975)

where

$$\alpha = \frac{R_C\ R_B}{R_A\ R_B + R_B\ R_C + R_A\ R_C} \tag{2.48}$$

and

$$\beta = \frac{R_C\ R_A}{R_A\ R_B + R_B\ R_C + R_A\ R_C} \tag{2.49}$$

The transfer function of the circuit of Fig. 2.11a can be derived as

$$\frac{V_o}{V_i} = -\frac{s^2\,\alpha C_2\ C_1 + s\left(\alpha C_2\left(\frac{1}{R_1}+\frac{1}{R_4}\right) - \frac{C_2}{R_1} - (C_1+C_2)\left(\frac{\alpha}{R_2}+\frac{\alpha}{R_5}-\frac{1-\alpha}{R_3}\right) + \left(\frac{1}{R_1}+\frac{1}{R_4}\right)\left(\frac{\alpha}{R_2}+\frac{\alpha-1}{R_5}+\frac{\alpha}{R_5}\right)\right)}{s^2\ C_2\ C_1\,(1-\beta) + s\left((C_1+C_2)\left(\frac{1-\beta}{R_2}-\frac{\beta}{R_3}-\frac{\beta}{R_5}\right) - \frac{\beta C_2}{R_1} - \frac{\beta C_2}{R_4}\right) + \left(\frac{1}{R_1}+\frac{1}{R_4}\right)\left(\frac{1-\beta}{R_2}-\frac{\beta}{R_3}-\frac{\beta}{R_5}\right)} \tag{2.50}$$

Note that the several degrees of freedom available can be used to realize a desired numerator of the transfer function. In the case of band-pass realization, R_3, R_5, and R_A are not needed. This means from (2.48) that $\alpha = 0$. Note that R_4 helps to control the gain. In the case where arbitrary gain can be accepted, R_4 need not be used. In this simple case known as Deliyannis band-pass biquad [2.31] shown in Fig. 2.11b, the transfer function simplifies as

$$\frac{V_o}{V_i} = -\frac{s\left(\frac{C_2}{R_1\,(1-\beta)}\right)}{s^2\ C_2\ C_1 + s\left(\left(\frac{(C_1+C_2)}{R_2}\right) - \frac{\beta C_2}{(1-\beta)R_1}\right) + \frac{1}{R_1\,R_2}} \tag{2.51}$$

Note that the pole-frequency is independent of β and β can be used to control the Q. Tradeoff between the spread of passive components (capacitors and resistors) and sensitivity can be achieved by proper choice of β and component values.

Denoting for simplicity $C_1 = C$, $C_2 = c^2C$, $R_1 = R$, and $R_2 = r^2R$, from the denominator of (2.51) we can obtain

$$\omega_o = \frac{1}{rcCR} \tag{2.52a}$$

and

$$Q_p = \frac{rc}{1 + c^2 - \frac{\beta}{(1-\beta)}\ r^2\ c^2} \tag{2.52b}$$

Note that for the case of no positive feedback (i.e., $\beta = 0$) the value of r is minimum when $c = 1$ and is then $r = 2Q_p$. Evidently, the resistor spread is $4{Q_p}^2$

which is very large for large Q_p values. The natural question that arises is the choice of r, c, and β values to reduce the sensitivity to component values. The opamp finite gain A can be considered in the above expression for Q_p by substituting $\beta = \beta_o - \frac{1}{A}$ where β_o is the ideal positive feedback factor given as $R_C/(R_C + R_B)$. This can be verified to be true by the reader by writing the equation for the voltage V_P at the inverting input of the opamp. Thus, the sensitivity to amplifier finite gain A can be obtained as follows.

Denoting $K = \frac{\beta}{1-\beta}$, we have $S_\beta^K = \frac{1}{1-\beta}$. Then, $S_K^{Q_p} = Krc\,Q_p$ and noting that $S_A^\beta = \frac{1}{A\beta_o - 1}$, we have

$$S_A^{Q_p} = S_\beta^{Q_p} \cdot S_A^\beta = S_K^{Q_p} \cdot S_\beta^K \cdot S_A^\beta = \frac{rc\,Q_p\,\beta}{(1-\beta)^2} \frac{1}{(A\,\beta_o - 1)} = \frac{rc\,Q_p}{A\left(1 - \frac{A\beta_o - 1}{A}\right)^2} \tag{2.53}$$

Since A is very large, this expression tends to zero thus obscuring the effect of finite but large A and its variations. Moschytz [2.32, 2.33] introduced a figure of merit known as the *gain sensitivity product* (GSP) which is defined as

$$GSP = A\,S_A^{Q_p} \tag{2.54}$$

The result is that $S_A^{Q_p}$ multiplied by A will not tend to zero but to a finite value:

$$GSP = AS_A^{Q_p} = \frac{rc\,Q_p}{(1-\beta_o)^2} \tag{2.55a}$$

Note that $\beta_o \cong \frac{1+c^2}{1+c^2+r^2}$ which can be obtained by equating the denominator of (2.52b) to zero implying very large Q_p values. Using this expression in (2.55a), we obtain the GSP in terms of the values c, r, and Q_p. Since Q_p is given as a design parameter, r and c need to be chosen to reduce the GSP.

$$GSP = \frac{(1 + c^2 + r^2\ c^2)^2\ Q_p}{r^3\ c^3} \tag{2.55b}$$

In the case of no positive feedback, under the optimum condition $c = 1$, $r = 2$ Q_p, the GSP is $2{Q_p}^2$. The GSP in the case of existence of positive feedback can be optimized by differentiating (2.55b) with respect to r or c and finding when it is minimum. Differentiating (2. 55b) with respect to r, the GSP can be found to be minimum under the condition

$$r^2 = \frac{3(1 + c^2)}{c^2} \tag{2.56a}$$

and the value of the GSP is

$$\text{GSP}_{\min 1} = \frac{16\,Q_p\,\sqrt{1+c^2}}{3\sqrt{3}} \tag{2.56b}$$

In a similar manner, differentiating (2.55b) with respect to c, the GSP can be found to be minimum under the condition

$$c^2 = \frac{3}{\left(1+r^2\right)} \tag{2.57a}$$

and the value of the GSP is

$$\text{GSP}_{\min 2} = \frac{16\,Q_p\,\left(1+r^2\right)^{3/2}}{3\,r^3\,\sqrt{3}} \tag{2.57b}$$

As an illustration for $c = 1$ from (2.56a) and (2.56b), we have $r = \sqrt{6}$, $GSP_{\min 1} = \frac{16\,Q_p\,\sqrt{2}}{3\sqrt{3}} = 4.354\,Q_p$ and for $c = 1$ from (2.57a) and (2.57b), we have $r = \sqrt{2}$, $GSP_{\min 2} = \frac{8\,Q_p}{\sqrt{2}} = 5.656\,Q_p$. The values of β_o for both these cases are, respectively, $\beta_o = \frac{1-\frac{\sqrt{3}}{Q_p\,\sqrt{2}}}{4-\frac{\sqrt{3}}{Q_p\,\sqrt{2}}}$ and $\beta_o = \frac{1-\frac{1}{Q_p\,\sqrt{2}}}{2-\frac{1}{Q_p\,\sqrt{2}}}$. As an illustration for $Q_p = 10$, the various cases yield the GSP as (a) $\beta_o = 0$, GSP $= 200$, (b) $\beta_o = 0.2334$, GSP $= 43.54$, and (c) $\beta_o = 0.48167$, GSP $= 56.56$.

2.5.2 *Multiple Feedback-Type Low-Pass Filter Due to Friend*

The biquad described in the previous section cannot realize a low-pass transfer function. An alternative circuit due to Friend [2.29] is considered next. This circuit is shown in Fig. 2.12a and has a transfer function given by

$$\frac{V_o}{V_i} = -\frac{1}{(1-\beta)} \times \frac{1}{s^2\,C_1\,C_2\,R_1\,R_2 + s\left(C_2\,R_1\,R_2\left(\frac{1}{R_1}+\frac{1}{R_2}+\frac{1}{R_3}\right) - \frac{\beta}{(1-\beta)}C_1\,R_1\right) + \frac{R_1}{R_3} - \frac{\beta}{(1-\beta)}} \tag{2.58a}$$

Note that when positive feedback does not exist (i.e., $\beta = 0$ or the noninverting input of the opamp is grounded), the circuit reduces to that shown in Fig. 2.12b. It still realizes a low-pass filter transfer function at the output and in addition a band-pass transfer function at the internal node:

$$\frac{V_x}{V_i} = -\left(\frac{V_o}{V_i}\right) s\,C_2\,R_2 \quad \text{when } \beta = 0 \tag{2.58b}$$

This circuit can be interpreted as having a lossy simulated inductance-based tank circuit. The lossy inductance realized by the circuit within dotted lines is based on a Ford and Girling [2.34] configuration and realizes an inductance of value $C_2R_2R_3$ and is shunted by a resistance R_2 in parallel with R_3. In the circuit of Fig. 2.12b, the pole-frequency can be seen to be independent of R_1 and R_1 can be used to control the dc gain R_3/R_1:

$$\omega_p^2 = \frac{1}{C_1\, C_2\, R_2\, R_3}, \quad Q_p = \sqrt{\frac{C_1}{C_2}} \cdot \frac{R_1\sqrt{R_2\, R_3}}{R_1\, R_2 + R_2\, R_3 + R_1\, R_3} \tag{2.59}$$

The capacitor spread can be seen to be minimum when $R_1 = R_2 = R_3$, yielding $\frac{C_1}{C_2} = 9\, Q_p^2$.

In the case of positive feedback being used (i.e., $\beta \neq 0$), the circuit can be designed for chosen C_1, C_2, and β values so as to realize the desired gain, pole-frequency, and pole-Q. The value of R_2 can be estimated first and then R_1 and R_3 can be obtained:

$$R_2 = \frac{\frac{1}{Q_p} \pm \sqrt{\frac{1}{Q_p^2} - 4(H_o + 1)\left(\frac{C_2}{C_1} - \frac{\beta}{1-\beta}\right)}}{2(H_o + 1)\,\omega_p\, C_2} \tag{2.60a}$$

$$R_1 = \frac{1}{H_o\,(1-\beta)\,\omega_p^2\, C_1\, C_2\, R_2} \tag{2.60b}$$

and

$$R_3 = \frac{H_o\,(1-\beta)\,R_1}{1 + H_o\,\beta} \tag{2.60c}$$

where H_o is the dc gain of the low-pass filter given by

$$H_o = \frac{1}{(1-\beta)\left(\frac{R_1}{R_3}\right) - \beta} \tag{2.60d}$$

Among the two solutions possible for R_2, the choice of negative sign in (2.60a) yields a lower spread.

The circuits of Figs. 2.11a and 2.12 cannot realize a second-order all-pass transfer function. A solution is to use an alternative configuration due to Steffen [2.29], shown in Fig. 2.13. The transfer function of this circuit can be derived as

$$\frac{V_o}{V_i} = -\frac{s^2\, C_2\, C_1 + s\left(\frac{C_1 + C_2}{R_B} - \frac{C_1\, R_3}{R_2}\left(\frac{1}{R_4} + \frac{1}{R_5}\right)\right) + \left(\frac{1}{R_4} + \frac{1}{R_5}\right)\frac{1}{R_B}}{s^2\, C_2\, C_1 + s\left(\frac{C_1}{R_5} + \frac{C_1 + C_2}{R_B} - \frac{C_1\, R_3}{R_2\, R_4}\right) + \left(\frac{1}{R_4} + \frac{1}{R_5}\right)\frac{1}{R_B}} \tag{2.61}$$

The condition for realizing an all-pass transfer function is that the coefficient of the "s" term in the numerator must be equal and opposite in sign to that in the denominator yielding

$$2\left(\frac{C_1+C_2}{R_B}\right)-\frac{C_1\,R_3}{R_2}\left(\frac{2}{R_4}+\frac{1}{R_5}\right)+\frac{C_1}{R_5}=0 \tag{2.62}$$

Next, assuming that $C_1 = C_2 = C$ and with chosen value of G_2/G_3, we have

$$R_5=\frac{\mu\,Q_p}{2\,C_2\;\omega_p} \tag{2.63a}$$

where

$$\mu=1+\frac{R_3}{R_2}. \tag{2.63b}$$

Next, R_4 can be obtained as

$$\frac{1}{R_4}=\frac{-\,G_5\,(4-3\mu)\pm\sqrt{G_5^2\;(4-3\mu)^2-8(1-\mu)(4\,C_1\;C_2\;\omega_p^2+G_5^2\,(2-\mu))}}{4(1-\mu)} \tag{2.63c}$$

Finally, R_B can be evaluated from the expression for pole-frequency as

$$G_B=\frac{C_1\;C_2\;\omega_p^2}{(G_4+G_5)} \tag{2.63d}$$

Example 2.5 Using SPICE, taking into account the finite bandwidth of the opamp, plot the response of the band-pass filter of Fig. E.2.5. Evaluate the poles and plot the group delay versus frequency.

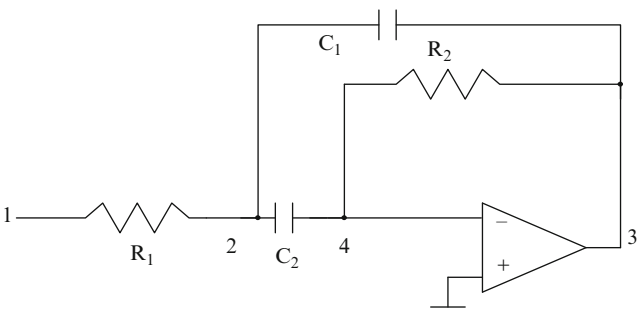

Fig. E.2.5a

This band-pass filter has a pole-frequency of 40 KHz and pole-Q of 20. The midband gain is 800. The effect of opamp finite bandwidth is to create a parasitic real pole and perturb the actual poles. The *.pz* command prints the poles and zeroes. The frequency response using ideal opamp and opamp with finite bandwidth 1 MHz are plotted in Fig. E.2.5b. The group delay is also plotted as a function of frequency by giving the *.plot gd(v(3))* command in Fig. E.2.5c.

```
*Multiple feedback SAB
R1 1 2 62.5
R2 4 3 100 K
C1 2 3 1590 pf
C2 2 4 1590 pf
E1 0 5 4 0 100,000
R4 5 6 1 k
C3 6 0 15.9 uf
E2 3 0 6 0 1
*Multiple feedback band-pass filter using ideal opamp
R11 1 7 62.5
R21 9 8 100 K
C11 7 8 1590 pf
C21 7 9 1590 pf
E3 0 8 9 0 10,000,000
vin 1 0 ac 1v
*.ac lin 1,000 10,000 100 K
.PZ 1 0 3 0 VOL PZ
pole(1) = –1.63576e + 07,0.000000e + 00
pole(2) = –3.62826e + 03,1.559514e + 05
pole(3) = –3.62826e + 03,–1.55951e + 05
zero(1) = 0.000000e + 00,0.000000e + 00
```

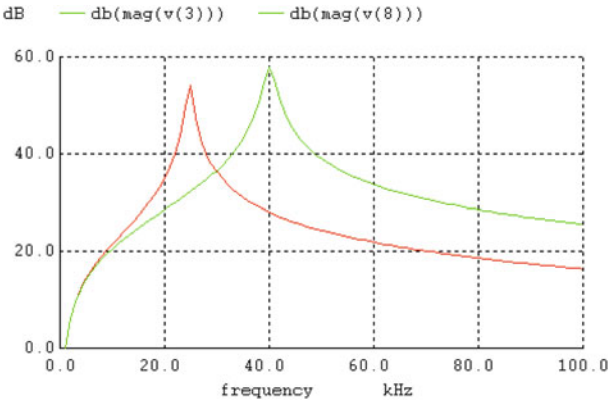

Fig. E.2.5b

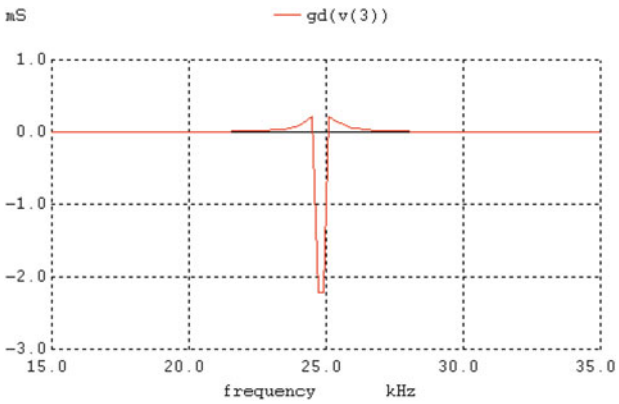

Fig. E.2.5c

The following describes a variable center frequency band-pass filter (by varying R5 for three values) with constant bandwidth and constant peak value considering an ideal opamp (see Fig. E.2.5d).

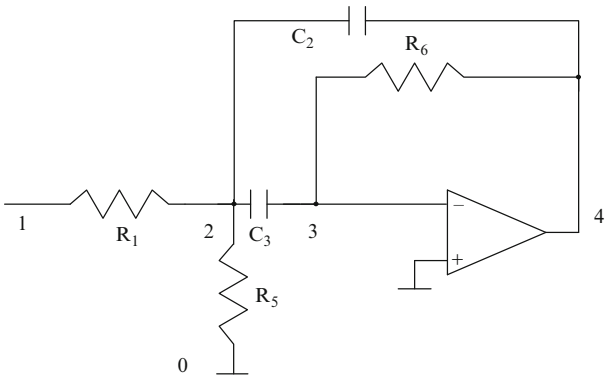

Fig. E.2.5d

```
* SA Bandpass
R1 1 2 3181.5
R5 2 0 15
C3 2 3 10000 pf
C2 2 4 10000 pf
R6 3 4 6363
E1 0 5 3 0 100,000
R4 5 6 1 k
C5 6 0 15.9 uf
E2 4 0 6 0 1
vin 1 0 ac 1v
*.ac dec 1,000 10 10,000 K
.control
destroy all
```

```
let ii = 0
while ii < 5
alter R5 = 15 + 20 * ii
ac dec 1,000 10 10,000 k
let ii = ii + 1
plot mag(ac1.v(4)) mag(ac3.v(4)) mag(ac5.v(4))
end
```

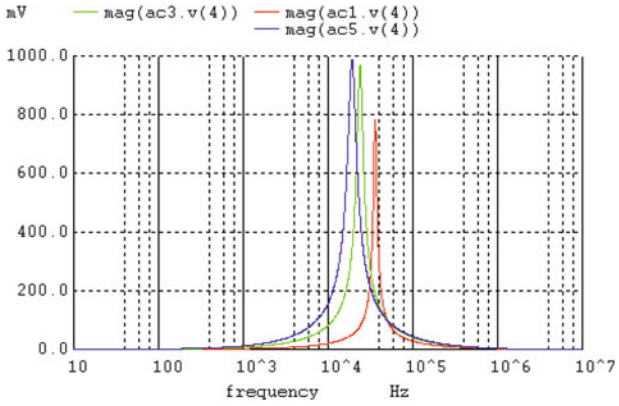

Fig. E.2.5e

Example 2.6 Find the magnitude and group delay of the transfer function of the MFB all-pass filter of Fig. E.2.6a. Find the response of the notch filter obtained using different feedforward gain defined by $R_4/(R_3 + R_4)$.

Note that the magnitude of an all-pass transfer function ideally should be flat (close to unity). The error is amplified and presented in Fig. E.2.6. The group delay response is shown in Fig E.2.6. The frequency response of the notch filter is shown in Fig. E.2.6d. (The same program with $R_3 = 2$K will realize a Notch filter (see

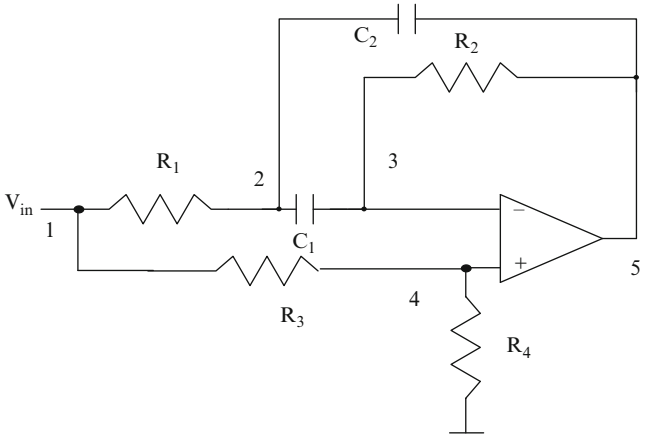

Fig. E.2.6a

Fig. E.2.6d)). Note that the opamp dc gain is very large, meaning that it is ideal. The reader is urged to find the responses with finite opamp bandwidth.

```
* Circuit MFB all-pass/Notch
R1 1 2 1 k
R2 3 5 400 k
C1 2 3 0.0001 uf
C2 2 5 0.0001 uf
R3 1 4 2k
R4 4 0 400 k
E1 6 0 4 3 10,000,000
R5 6 7 1 k
C3 7 0 15.9 uf
E2 5 0 7 0 1
vin 1 0 ac 1 v
.ac lin 99 1k 99 K
```

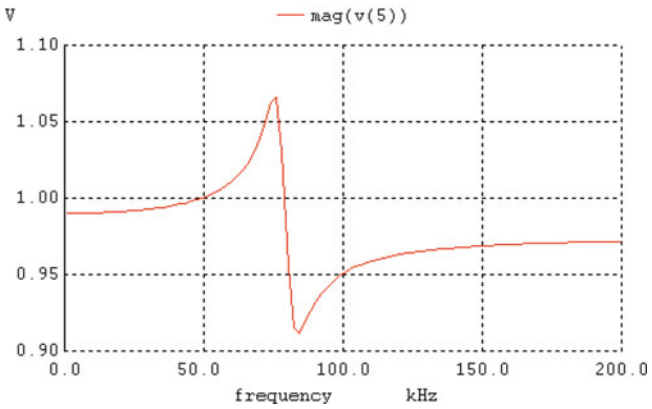

Fig. E.2.6b

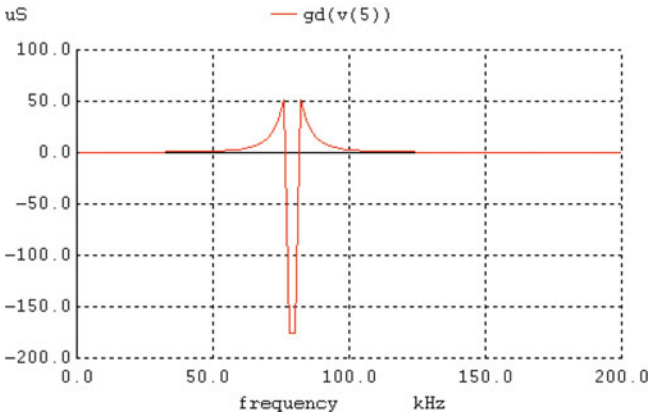

Fig. E.2.6c

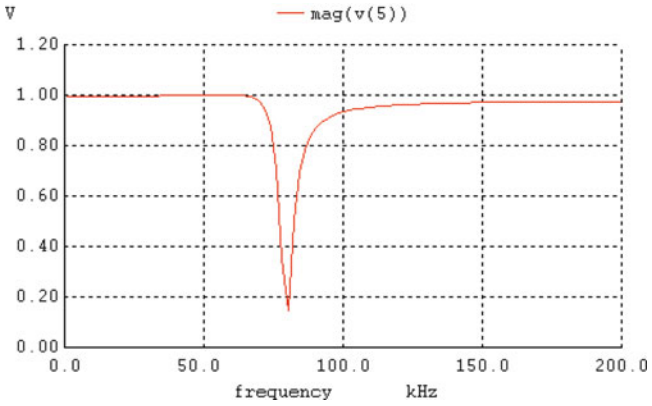

Fig. E.2.6d

2.5.3 Active Filters Using Single Fully Differential Amplifier

A very recent development is the easy availability of opamps with differential outputs. A typical filter using a current input that exploits this property [2.35, 2.36] is shown in Fig. 2.14a. Note that in this circuit, the noninverting input of the opamp is grounded. Moreover, in addition to the usual output of the opamp, an inverted output is also available which can be used to provide positive feedback. This technique eliminates the need for the two resistors providing positive feedback using resistors R_A and R_B; see, for example, Fig. 2.12a. For simplicity, an inverting block of gain -1 is shown in Fig. 2.14a. The input impedance realized by this block is as shown in Fig. 2.14b.

In the absence of feedback, the input impedance of the circuit is thus that of a lossy resonator (see block within dotted lines in Fig. 2.11b). At the resonance frequency, $\frac{1}{2\pi\sqrt{C_f\, R R_f\, C}}$, the input impedance is resistive $\left(\frac{R R_f}{R+R_f}\right)$. In the presence of C_{pf}, however, the input impedance comprises an additional capacitance C_{pf} and a negative resistance of value $-R\frac{C_f}{C_{pf}}$ as shown in Fig. 2.14b. Thus, the effect of positive feedback is to increase the effective capacitance from C to $C + C_{pf}$ and to decrease the damping. The input admittance is still that of a RLC tank circuit. For an appropriate choice of C_{pf} such that

$$-R\frac{C_f}{C_{pf}} + \left(\frac{R R_f}{R+R_f}\right) = 0 \quad \text{or} \quad C_{pf} = C_f\left(1 + \frac{R}{R_f}\right) \tag{2.64}$$

the resistance across the tank circuit can be completely cancelled thus realizing an oscillator with a frequency of oscillation given by

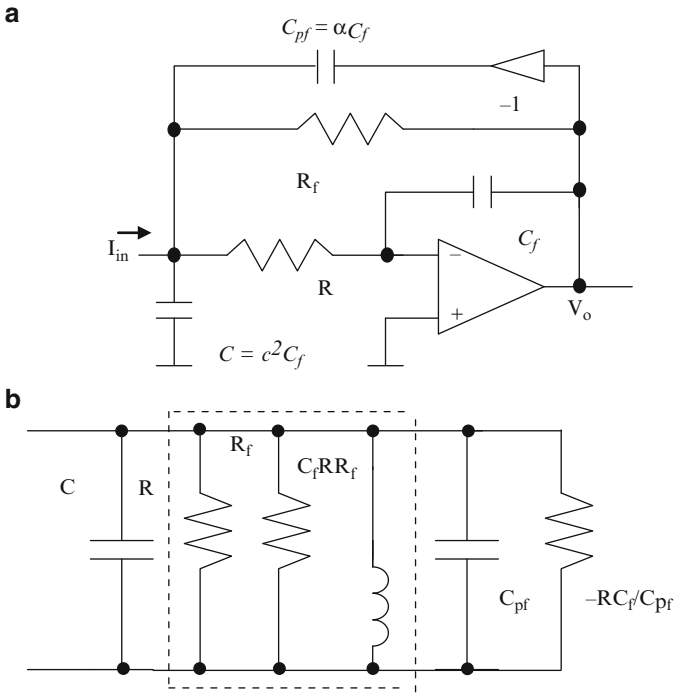

Fig. 2.14 (**a**) Multiple feedback filter using differential output opamp; (**b**) input impedance (Adapted from [2.35] ©IEEE 2008)

$$f_{osc} = \frac{1}{2\pi\sqrt{(C + C_{pf})\, C_f\, R\, R_f}} \tag{2.65}$$

The transfer function of the realized filter of Fig. 2.14a taking into account the finite gain of the opamp A can be obtained as

$$\frac{V_o}{I_{in}} = -\frac{R_f}{D(s)}$$

where

$$D(s) = s^2 R R_f \left(C + C_{pf}\right) C_f \left(1 + \frac{1}{A}\right) + s\left(C_f \left(R + R_f\right)\left(1 + \frac{1}{A}\right) - C_{pf}\, R_f + \frac{\left(C + C_{pf}\right) R_f}{A}\right) + \left(1 + \frac{1}{A}\right) \tag{2.66}$$

Considering first the case of an opamp with infinite gain, denoting $C = c^2 C_f$, $C_{pf} = \alpha C_f$, $R_f = r^2 R$, the pole-frequency ω_p, and the pole-Q Q_p can be written as follows.

$$\omega_p = \frac{1}{C_f R r \sqrt{c^2 + \alpha}} \tag{2.67a}$$

$$Q_p = \frac{r\sqrt{c^2 + \alpha}}{r^2(1-\alpha)+1} \tag{2.67b}$$

Note that α indicates the amount of positive feedback. Techniques for arriving at an optimum choice of the various degrees of freedom α, c, and r for given R and C values to arrive at a desirable solution to minimize the active and passive sensitivities or the spread in component values have been described in detail in [2.36].

It must have been noted that single-amplifier structures do not have flexibility in controlling the pole-frequency, gain, and pole-Q independently using separate noninteracting controls except in a few cases. Moreover, these generally have high sensitivities and require a large spread in component values. This is the reason for preferring multiple amplifier biquads.

2.6 Biquads Using Two Opamps

2.6.1 GIC-Based Biquads

A GIC (generalized impedance converter) [2.37] is shown in Fig. 2.15a. This circuit realizes an input impedance given by

$$Z_{in} = \frac{Z_1\, Z_3\, Z_5}{Z_2\, Z_4} \tag{2.68}$$

Note by virtue of the high gain of the opamps, all internal inverting and noninverting input nodes of the opamps are at the same voltage. It is interesting to see that a lossless grounded inductance can be realized when either Z_2 or Z_4 is a capacitor:

$$Z_{in} = \frac{sC_2R_1R_3R_5}{R_4} \text{ in the case } Z_2 = 1/sC_2 \text{ or } Z_{in} = \frac{sC_4R_1R_3R_5}{R_2} \text{ in the case } Z_4 = 1/sC_4$$

$$\begin{aligned} Z_{in} &= \frac{s\,C_2\,R_1\;R_3\;R_5}{R_4} \quad \text{in the case } Z_2 = 1/sC_2 \quad \text{or} \quad Z_{in} \\ &= \frac{s\,C_4\,R_1\;R_3\;R_5}{R_2} \quad \text{in the case } Z_4 = 1/sC_4 \end{aligned} \tag{2.69}$$

The value of the inductance can be changed by any one of the various resistors. They can be chosen equal for convenience as well.

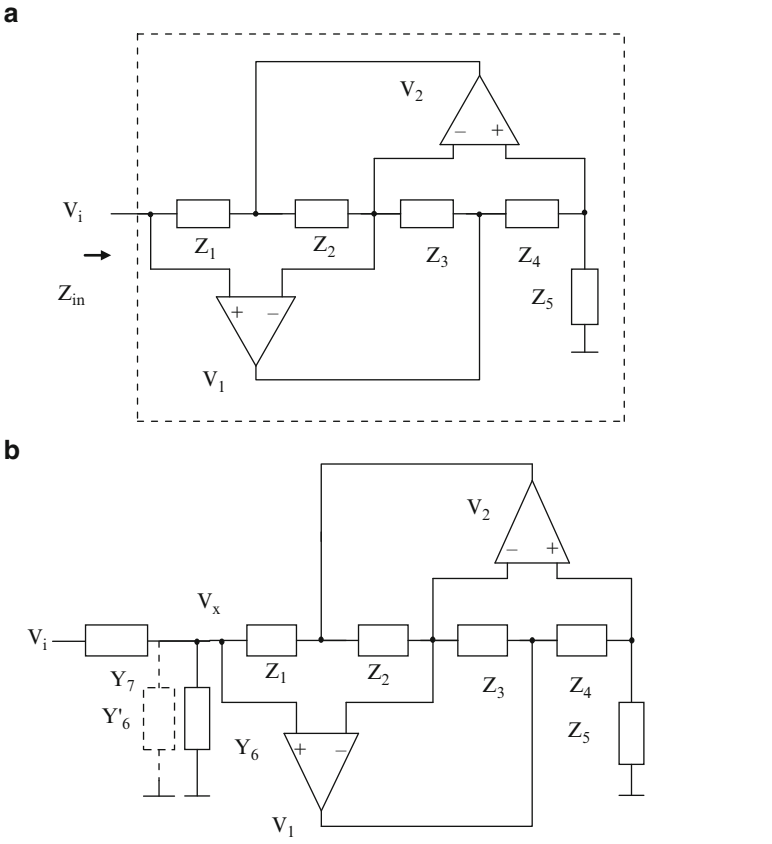

Fig. 2.15 (**a**) A Generalized impedance converter, and (**b**) application of (a) to realize a second-order filter

As an alternative, if both Z_2 and Z_4 are capacitors, a grounded frequency-dependent negative resistance can be obtained with input impedance of the form s^2D:

$$Z_{in} = s^2\ R_1\ R_3\ R_5\ C_2\ C_4 \tag{2.70}$$

For $s = j\omega$, evidently $Z_{in} = -\omega^2\ R_1\ R_3\ R_5\ C_2\ C_4$ which means that a negative resistance is realized (due to the negative sign) which is frequency-dependent due to the ω^2 term.

As yet another alternative, by choosing two of the impedances Z_1, Z_3, and Z_5 as capacitors, a grounded supercapacitance with impedance of the form $1/(s^2C)$ can be obtained. As an illustration, for $Z_1 = 1/sC_1$ and $Z_3 = 1/sC_3$, we have

$$Z_{in} = \frac{R_5}{s^2\ C_1\ C_3\ R_2\ R_4} \tag{2.71}$$

The application of these to realize high-order filters is shown later.

It is easy to build second-order filters based on classical RLC circuits based on the use of LC tank circuits. For example, a band-pass filter or a high-pass filter can be obtained as shown in Fig. 2.15b by choosing $Y_6 = sC_6$, $Y_7 = 1/R_7$, or $Y_6 = 1/R_6$, $Y_7 = sC_7$. In the case of a band-pass filter, the pole-Q can be controlled using R_7 whereas in the case of a high-pass filter, the pole-Q can be controlled by R_6.

The various transfer functions in the case of the choice of $Y_2 = sC_2$, are as follows.

$$\frac{V_x}{V_i} = \frac{s\,C_2\;Y_4\;Y_7}{s^2\;C_2\;Y_4\;C_6 + s\,C_2\;Y_4\;Y_7 + Y_1\;Y_3\;Y_5} \tag{2.72a}$$

$$\frac{V_1}{V_i} = \frac{(Y_4\;+Y_5)s\,C_2\;Y_7}{s^2\;C_2\;Y_4\;C_6 + s\,C_2\;Y_4\;Y_7 + Y_1\;Y_3\;Y_5} \tag{2.72b}$$

$$\frac{V_2}{V_i} = \frac{Y_7\,(s\,C_2\;Y_4 - Y_3\;Y_5)}{s^2\;C_2\;Y_4\;C_6 + s\,C_2\;Y_4\;Y_7 + Y_1\;Y_3\;Y_5} \tag{2.72c}$$

It may be noted that only the band-pass transfer function is available as V_x and V_1 outputs and the other transfer function is not useful.

In the case with $Z_4 = 1/sC_4$, we have

$$\frac{V_x}{V_i} = \frac{s\,C_4\;Y_2\;Y_7}{s^2\;C_4\;Y_2\;C_6 + s\,C_4\;Y_2\;Y_7 + Y_1\;Y_3\;Y_5} \tag{2.73a}$$

$$\frac{V_1}{V_i} = \frac{(sC_4\;+Y_5)\,Y_2\;Y_7}{s^2\;C_4\;Y_2\;C_6 + s\,C_4\;Y_2\;Y_7 + Y_1\;Y_3\;Y_5} \tag{2.73b}$$

$$\frac{V_2}{V_i} = \frac{Y_7\,(s\,C_2\;Y_4 - Y_3\;Y_5)}{s^2\;C_4\;Y_2\;C_6 + s\,C_4\;Y_2\;Y_7 + Y_1\;Y_3\;Y_5} \tag{2.73c}$$

Note that only (2.37a) realizes a useful transfer function.

The denominator of the transfer function of the general structure of Fig. 2.15b taking into account the finite bandwidth B of the opamp and assuming identical opamps is given as

$$D(s) = (Y_1\;Y_5\;Y_3 + Y_2\;Y_4\;Y_6) + (Y_1 + Y_6)(Y_3 + Y_2)(Y_4 + Y_5)\left(\frac{s}{B} + \frac{s^2}{B^2}\right) \tag{2.74}$$

For the choice $Y_2 = sC_2$, $Y_6 = sC_6$, and all other admittances as resistors, to realize a band-pass filter transfer function at V_A, (2.74) becomes

$$D(s) = s^4 \frac{C_6\, C_2}{B^2}(Y_4 + Y_5) + s^3\left(\frac{C_6\, C_2}{B}(Y_4 + Y_5) + \frac{(Y_4 + Y_5)(C_6\, Y_3 + C_2\, Y_1 + C_2\, Y_6) + Y_2\, Y_4\, Y_6}{B^2}\right) + s^2\left(C_2\, Y_4\, Y_6 + \frac{(Y_4 + Y_5)(Y_1 + Y_6)\, Y_3}{B^2} + \frac{(Y_4 + Y_5)(C_6\, Y_3 + C_2\, Y_1 + C_2\, Y_6)}{B}\right) + s\left(C_2\, Y_4\, Y_6 + \frac{(Y_4 + Y_5)(Y_1 + Y_6)\, Y_3}{B}\right) + Y_1\, Y_5\, Y_3 \tag{2.75}$$

The resulting modified pole-frequency can be calculated by looking at the s^0 and s^2 terms under the condition $Y_1 = Y_3 = Y_4 = Y_5 = 1/R$, $Y_2 = Y_6 = sC$, and $R_6 = RQ_p$.

$$\frac{\omega_o^2}{\hat{\omega}_o^2} = 1 + 2\left(2 + \frac{1}{Q_p}\right)\frac{\omega_p}{B} \tag{2.76}$$

Note that the results are same in the case $Y_4 = sC_4$ and $Y_1 = Y_3 = Y_2 = Y_5 = 1/\mathrm{R}$.

2.6.2 *Two-Amplifier Biquads Derived from Single-Amplifier Biquads*

The single opamp-based biquads described earlier have used noninverting input of the opamp as well. However, in order to reduce the effect of parasitic capacitances at the inverting input of the opamp, it is useful to derive filters using opamps with grounded noninverting input. Equivalent filter configurations can be derived based on the nodal voltage simulation technique [2.38]. In this technique, the equations at the internal nodes of the original circuit are realized in a different way so that the opamp noninverting inputs can be grounded.

As an illustration, consider the active RC filter of Fig. 2.12a redrawn in Fig. 2.16a. At node A, we have

$$\frac{V_x}{R_2} + V_o\, s\, C_2 = \beta\, V_o\left(\frac{1}{R_2} + s\, C_2\right) \tag{2.77}$$

which can be rewritten as

$$\frac{V_x}{R_2} + V_o\, s\, C_2\,(1 - \beta) - \left(\frac{\beta}{R_2}\right) V_o = 0 \tag{2.78}$$

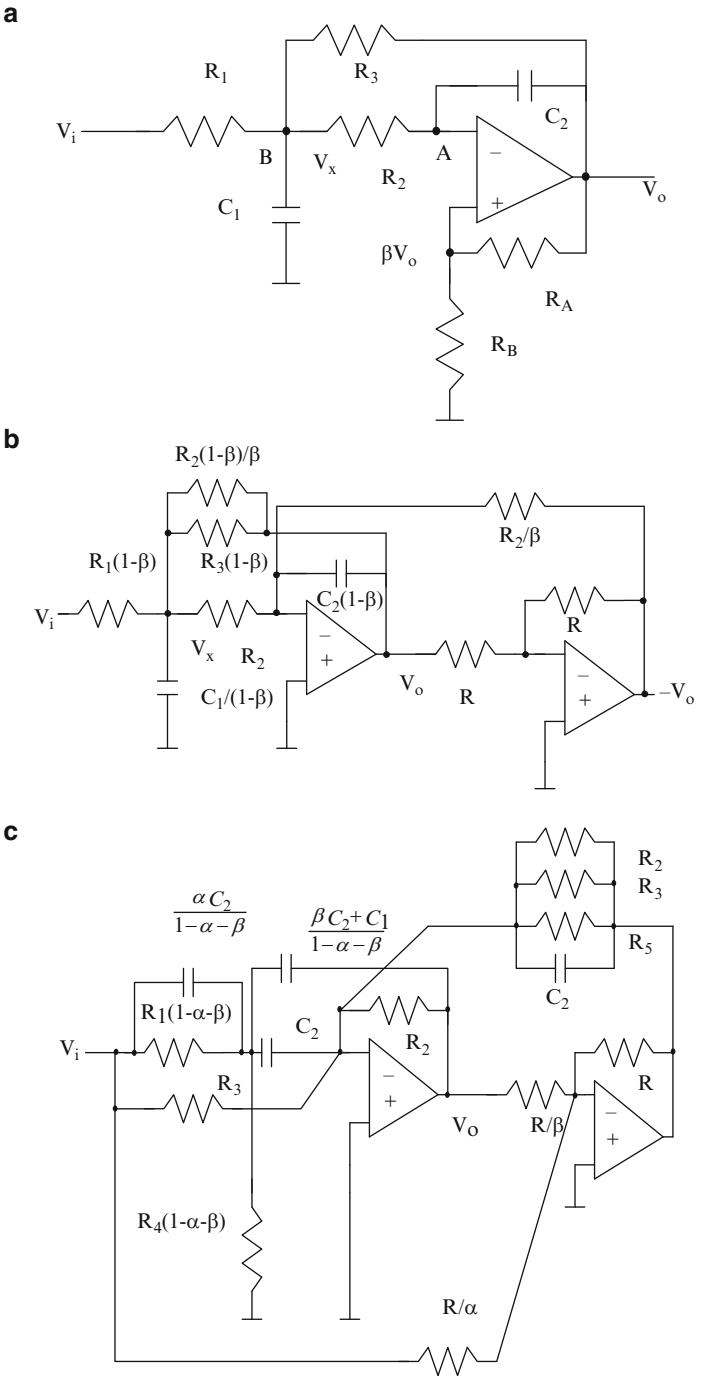

Fig. 2.16 (**a**) Multiple feedback-type low-pass biquad, (**b**) circuit derived using nodal voltage simulation, and (**c**) circuit derived from Friend's biquad (c Adapted from [2.38] ©IEE 1984)

This equation is implemented as shown in Fig. 2.15b using resistors R_2, capacitor $C_2(1-\beta)$, resistor R_2/β, and inverting amplifier of gain 1. Similarly, at node B, we have in the circuit of Fig. 2.15a

$$\frac{V_i}{R_1}+\frac{V_o}{R_3}+\frac{\beta V_o}{R_2}=V_x\left(\frac{1}{R_1}+\frac{1}{R_2}+\frac{1}{R_3}+sC_1\right) \tag{2.79a}$$

This can be rewritten first as

$$\frac{V_i-V_x}{R_1}+(V_o-V_x)\left(\frac{1}{R_3}+\frac{\beta}{R_2}\right)=V_x\left(\frac{1-\beta}{R_2}+sC_1\right) \tag{2.79b}$$

and next by dividing throughout by $(1-\beta)$ as

$$\begin{aligned}&\frac{V_i-V_x}{(1-\beta)R_1}+(V_o-V_x)\left(\frac{1}{R_3\,(1-\beta)}+\frac{\beta}{R_2\,(1-\beta)}\right)\\&\quad=V_x\left(\frac{1}{R_2}+\frac{sC_1}{(1-\beta)}\right)\end{aligned} \tag{2.79c}$$

in order to retain R_2 the same from V_x to virtual ground already present for realizing (2.79a) so that at node V_x, we obtain the same equation as in Fig. 2.16a. Note that all resistors and capacitors are realizable since $0<\beta<1$.

This technique was originally used for the Friend–Deliyannis biquad [2.29] of Fig. 2.11a which realizes exactly the same transfer function. The resulting two-amplifier circuit is presented in Fig. 2.16c for completeness. The circuit still has one internal node at which the parasitic capacitance can be absorbed by the capacitor C_2.

2.7 Biquads Using More Than Two Opamps

2.7.1 KHN Biquad

The well-known *Kerwin–Huelsman–Newcomb* (KHN) biquad [2.39] also known as the *state variable biquad* is presented in Fig. 2.17a. This circuit using three opamps realizes high-pass, band-pass, and low-pass transfer functions at the output terminals of the three opamps. The transfer functions of this circuit can be derived as follows.

$$\frac{V_{LP}}{V_i}=\frac{\frac{R_6\left(1+\frac{R_3}{R_4}\right)}{(R_5+R_6)}}{s^2\,C_1\,C_2\,R_1\,R_2+s\frac{C_1\,R_1\,R_5}{(R_5+R_6)}\left(1+\frac{R_3}{R_4}\right)+\frac{R_3}{R_4}} \tag{2.80a}$$

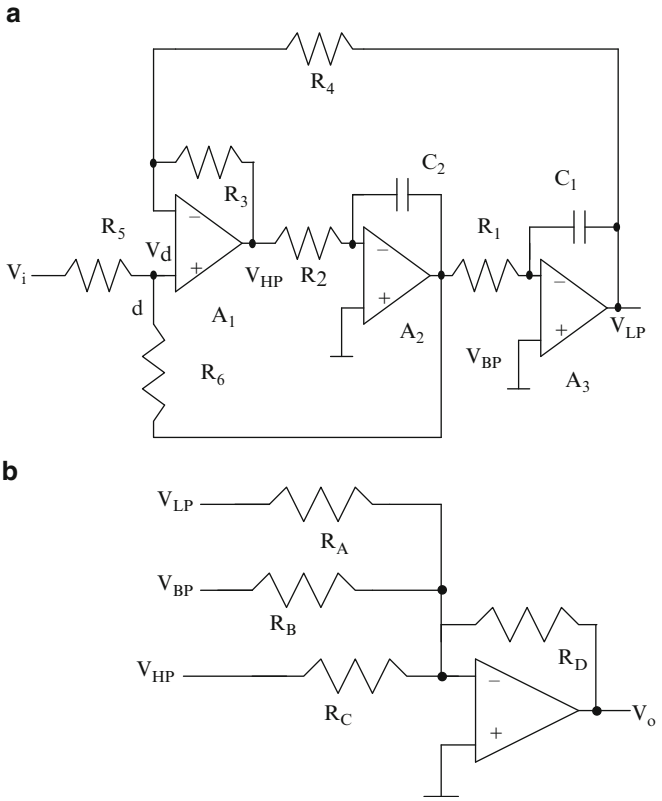

Fig. 2.17 (**a**) KHN Biquad, and (**b**) additional circuit to obtain a general biquadratic transfer function

$$V_{BP} = -\,s\,C_1\,R_1\,V_{LP} \tag{2.80b}$$

$$V_{HP} = s^2\,C_1\,R_1\,C_2\,R_2\,V_{LP} \tag{2.80c}$$

Evidently, all three transfer functions are available. The choice of components $R_1 = R_2 = R, C_1 = C_2 = C, R_4 = R_3$ simplifies these transfer functions as

$$\frac{V_{LP}}{V_i} = \frac{\dfrac{2R_6}{(R_5+R_6)}}{s^2\,C^2\,R^2 + s\dfrac{2CR\,R_5}{(R_5+R_6)} + 1}, \quad V_{BP} = -sCR\,V_{LP}, \quad V_{HP} = s^2\,C^2\,R^2\,V_{LP} \tag{2.81}$$

Evidently, the pole-frequency $\omega_p = 1/CR$ and the pole-Q is given by

$$Q_p = \frac{R_5+R_6}{2R_5} \quad \text{or} \quad \frac{R_6}{R_5} = 2\,Q_p - 1 \tag{2.82}$$

Thus, the circuit has low pole-Q sensitivities and low pole-frequency sensitivities and has the capability for orthogonal tuning of the pole-frequency and pole-Q. The dc gain of the low-pass filter can be seen to be $\left(2-\frac{1}{Q_p}\right)$ which cannot be independently controlled.

It is interesting to note that at node "d", a notch transfer function is realized [2.41]:

$$\frac{V_d}{V_i}=\frac{\frac{R_6}{(R_5+R_6)}\left(s^2\ C^2\ R^2+1\right)}{s^2\ C^2\ R^2+s\frac{2CR\,R_5}{(R_5+R_6)}+1} \tag{2.83}$$

The three outputs of the three opamps in the KHN biquad can be summed using an additional summing amplifier as shown in Fig. 2.17b. The resulting transfer function is given by

$$\frac{V_o}{V_i}=-\frac{s^2\ C^2\ R^2\frac{R_D}{R_C}-sCR\left(2-\frac{1}{Q_p}\right)\frac{R_D}{R_B}+\frac{R_D}{R_A}\left(2-\frac{1}{Q_p}\right)}{s^2\ C^2\ R^2+s\left(\frac{2CR\,R_5}{R_5+R_6}\right)+1} \tag{2.84}$$

Taking into account the finite gain bandwidth product of the three opamps, assuming identical opamps with $B_1=B_2=B_3=B$ and denoting $\tau=CR$, the denominator of the transfer function can be derived as

$$D(s)=2\,s^5\,\frac{\tau^2}{B^3}+s^4\left(\frac{5\tau^2}{B^2}+\frac{4\tau}{B^3}\right)+s^3\left(\frac{6\tau}{B^2}+\frac{4\tau^2}{B}+\frac{2}{B^3}\right)+s^2\left(\tau^2+\frac{1}{B^2}+\frac{2\tau}{B}+\frac{2\beta\tau}{B}\right)+s\left(\frac{2\beta}{B}+2\beta\tau\right)+1 \tag{2.85}$$

Thus the perturbed pole-frequency and pole-Q can be expressed as

$$\frac{\omega_p^2}{\hat{\omega}_p^2}=1+\frac{2\,\omega_p}{B}\left(1+\frac{1}{2\,Q_p}\right)+\frac{\omega_p^2}{B^2} \tag{2.86a}$$

and

$$\frac{\omega_p\ Q_p}{\hat{\omega}_p\ \hat{Q}_p}=1+\frac{\omega_p}{B}\left(1-4\,Q_p\right)-\frac{6\,\omega_p^2\ Q_p}{B^2}-2\,Q_p\left(\frac{\omega_p^3}{B^3}\right) \tag{2.86b}$$

In the KHN biquad, the front-end opamp uses both inputs of the opamps. Hence parasitic capacitance at the noninverting input may affect the frequency response. An alternative circuit known as the *Tow–Thomas biquad* is considered next.

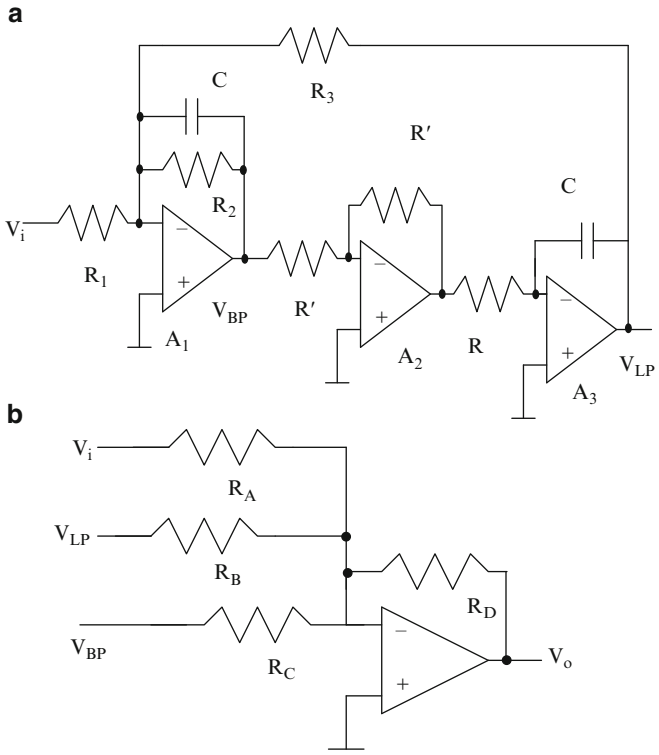

Fig. 2.18 (**a**) Tow–Thomas biquad, and (**b**) summing amplifier to realize a general biquadratic transfer function

2.7.2 Tow–Thomas Biquad

This circuit and the KHN biquad are known as *two-integrator loops*. Essentially, the Tow–Thomas biquad [2.23, 2.42] shown in Fig. 2.18a uses an inverting lossy integrator formed by R_1, R_2, R_3, C, and OA $A_1$and a noninverting lossless integrator formed by R', R, C, and OAs A_2 and A_3 in a feedback loop. The transfer functions of this circuit can be derived as

$$\frac{V_{LP}}{V_i} = -\frac{\frac{R}{R_1}}{s^2\, C^2\, R^2 + sC\frac{R^2}{R_2} + 1}, \quad V_{BP} = -sCR\, V_{LP} \tag{2.87}$$

under the condition $R_3 = R$. Note that an inverting low-pass transfer function is available at the output of opamp 2. Evidently the pole-Q is dependent on R_2/R_3 and the pole-frequency is dependent on R and C. The low-pass transfer function exhibits a dc gain of R/R_1 and the band-pass transfer function has a center frequency gain of R_2/R_1. This circuit evidently enjoys low sensitivities of pole-frequency and pole-Q to passive components.

It is possible to derive a general biquad by using an extra summing amplifier to combine the input and low-pass and band-pass outputs as shown in Fig. 2.18b. The transfer function of this circuit is given by

$$\frac{V_o}{V_i} = -\frac{s^2\, C^2\, R^2\, \frac{R_D}{R_A} + +sCR\left(\frac{R}{R_2}\frac{R_D}{R_A} - \frac{R_D}{R_C}\right) + \frac{R_D}{R_A} - \frac{R_D}{R_B}\frac{R}{R_1}}{s^2\, C^2\, R^2 + sC\frac{R^2}{R_2} + 1} \tag{2.88}$$

Taking into account the finite gain bandwidth product of the three opamps, assuming identical opamps with $B_1 = B_2 = B_3 = B$ and denoting $\tau = CR$, the denominator of the transfer function can be derived as

$$\begin{aligned} D(s) = {} & 2\,s^5\,\frac{\tau^2}{B^3} + s^4\left(\frac{2\tau}{B^3}\left(1 + \frac{1}{Q_p} + \frac{R}{R_1}\right) + \frac{5\tau^2}{B^2} + \frac{2\tau}{B^3}\right) \\ & + s^3\left(\frac{4\tau^2}{B} + \frac{2\tau}{B^2\,Q_p} + \frac{3\tau}{B^2}\left(2 + \frac{1}{Q_p} + \frac{R}{R_1}\right) + \frac{2}{B^3}\left(1 + \frac{1}{Q_p} + \frac{R}{R_1}\right)\right) \\ & + s^2\left(\tau^2 + \frac{\tau}{B}\left(2 + \frac{1}{Q_p} + \frac{R}{R_1}\right) + \frac{2}{B^2\,Q_p} + \frac{3\tau}{B\,Q_p} + \frac{1}{B^2}\left(1 + \frac{1}{Q_p} + \frac{R}{R_1}\right)\right) \\ & + s\left(\frac{1}{B\,Q_p} + \frac{\tau}{Q_p}\right) + 1 \end{aligned} \tag{2.89}$$

Thus the perturbed pole-frequency and pole-Q can be expressed as

$$\frac{\omega_p^2}{\hat{\omega}_p^2} = 1 + \frac{\omega_p}{B}\left(2 + \frac{4}{Q_p} + \frac{R}{R_1}\right) + \frac{\omega_p^2}{B^2}\left(1 + \frac{3}{Q_p} + \frac{R}{R_1}\right) \tag{2.90a}$$

and

$$\begin{aligned} \frac{\omega_p\, Q_p}{\hat{\omega}_p\, \hat{Q}_p} = {} & 1 + \frac{\omega_p}{B}\left(1 - 4\,Q_p\right) - \frac{\omega_p^2\, Q_p}{B^2}\left(6 + \frac{5}{Q_p} + \frac{3R}{R_1}\right) - 2\,Q_p\left(\frac{\omega_p^3}{B^3}\right) \\ & \times \left(1 + \frac{1}{Q_p} + \frac{R}{R_1}\right) \end{aligned} \tag{2.90b}$$

Example 2.7 Plot the low-pass and band-pass transfer functions of the Tow–Thomas biquad shown in Fig. E.2.7. using a nonideal macromodel of the opamp. The biquad is designed for a pole-frequency = 100 KHz, midband gain of band-pass response, and pole-Q of 40.

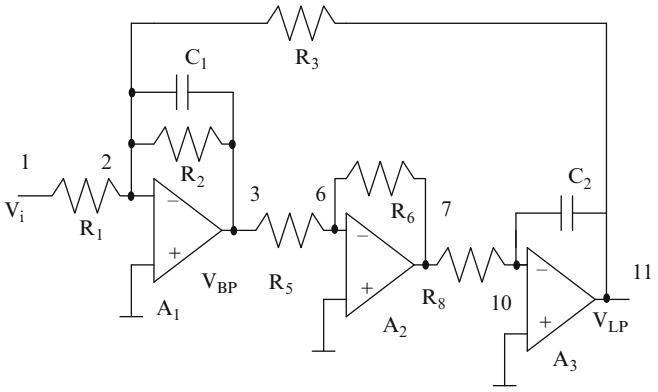

Fig. E.2.7

The two transfer functions can be seen to have slightly different peaks so that scaling will be necessary to equalize the outputs. The pole-frequency evidently has decreased due to the finite bandwidth of the opamps.

```
*Tow–Thomas biquad
R1 1 2 10 K
R2 2 3 400 K
C1 2 3 159 pf
R3 2 11 10 K
E1 0 4 2 0 100,000
R4 4 5 1 k
C3 5 0 15.9 uf
E2 3 0 5 0 1
R5 3 6 10 K
R6 6 7 10 K
E3 0 8 6 0 100,000
R7 8 9 1 k
C4 9 0 15.9 uf
E4 7 0 9 0 1
R8 7 10 10 K
C2 10 11 159 pf
E5 0 12 10 0 100,000
R9 12 13 1 k
C5 13 0 15.9 uf
E6 11 0 13 0 1
vin 1 0 ac 1v
.ac dec 1000 1 1,500 k
```

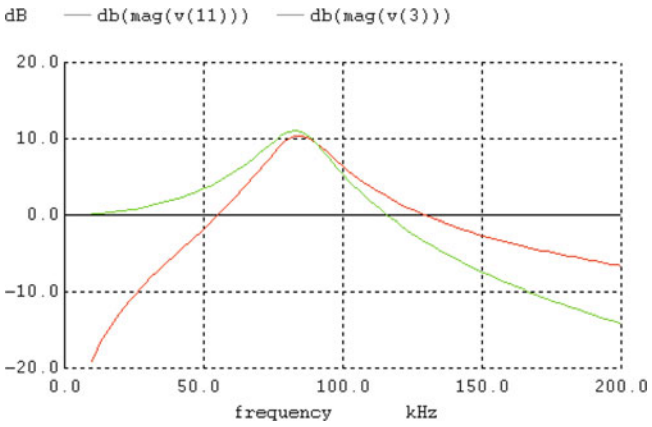

(**a**) With 1 MHz bandwidth opamps

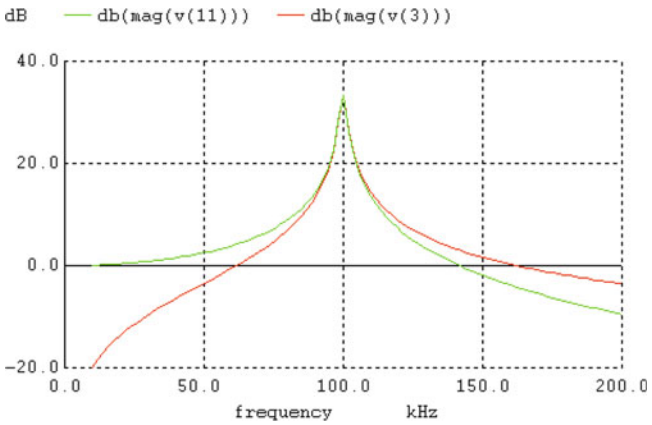

(**b**) With opamp bandwidth 100 MHz

2.7.3 Akerberg–Mossberg Biquad

Akerberg and Mossberg [2.24] suggested an active compensation technique without using any additional components. The noninverting integrator realization based on this approach has already been described in Fig. 2.4d. The denominator of the transfer function of this biquad shown in Fig. 2.19 can be derived as

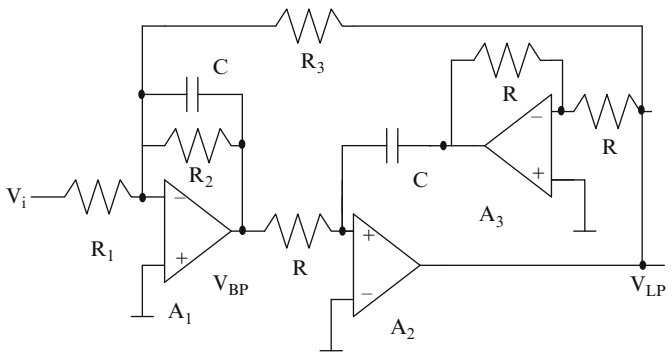

Fig. 2.19 Akerberg–Mossberg biquad

$$D(s) = s^5\left(\frac{2\tau^2}{B^3}\right) + s^4\left(\frac{2\tau}{B^3\,Q_p} + \frac{6\tau}{B^3} + + \frac{3\tau^2}{B^2}\right) + s^3\left(\frac{4}{B^3} + \frac{5\tau}{B^2} + \frac{2}{B^3\,Q_p} + \frac{3\tau}{B^2\,Q_p} + \frac{2\tau^2}{B}\right) + s^2\left(\frac{2}{B^2} + \frac{3\tau}{B} + \frac{3}{B^2\,Q_p} + \frac{2\tau}{B\,Q_p} + \tau^2\right) + s\left(\frac{1}{B\,Q_p} + \frac{\tau}{Q_p} + \frac{2}{B}\right) + 1 \tag{2.91}$$

Thus the perturbed pole-frequency and pole-Q can be expressed as

$$\frac{\omega_p^2}{\hat{\omega}_p^2} = 1 + \frac{\omega_p}{B}\left(3 + \frac{2}{Q_p}\right) + \frac{\omega_p^2}{B^2}\left(2 + \frac{3}{Q_p}\right) \tag{2.92a}$$

and

$$\frac{\omega_p\,Q_p}{\hat{\omega}_p\,\hat{Q}_p} = 1 + \frac{\omega_p}{B} - \frac{\omega_p^2\,(5\,Q_p + 3)}{B^2} - (2 + 4\,Q_p)\left(\frac{\omega_p^3}{B^3}\right) \tag{2.92b}$$

It may be seen by comparing (2.92) with (2.90) that the pole-Q variation is much smaller than in the Tow–Thomas biquad.

2.7.4 Scaling for Optimal Dynamic Range

A good design practice in both KHN and Tow–Thomas biquads is to choose equal time constants for both integrators for high pole-Q designs. This choice has the advantage that the maxima of all the outputs of the opamps tend to be the same for

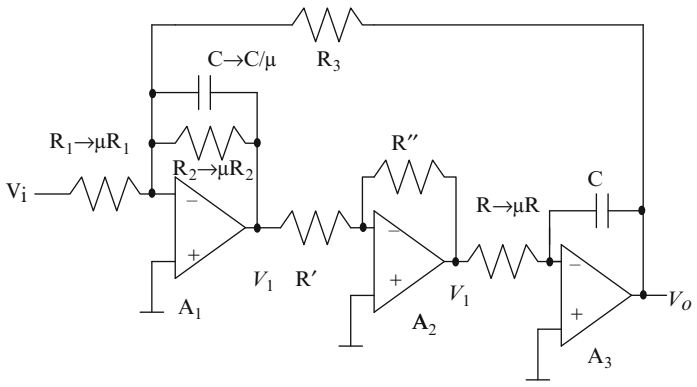

Fig. 2.20 Procedure for scaling for optimal dynamic range in Tow–Thomas biquad

high pole-Q designs. For low pole-Q designs, however, it is necessary to find the maximum of the transfer functions at all three outputs of the three opamps (in the case of the Tow–Thomas biquad only two) and then they need to be scaled to bring these maxima to the maximum of the actual given transfer function. This procedure is known as *scaling for optimal dynamic range*. The advantage of this step is explained next using Fig. 2.20.

Consider that we are interested in the desired output V_o. Its maximum value (i.e., $|V_o(j\omega)|_{\max}$) can be estimated. Similarly, the output V_1 and $-V_1$ will have a maximum value $|V_1(j\omega)|_{\max}$ which may occur at a different frequency. It may happen that these two maxima are widely different in magnitudes. The purpose of dynamic range scaling is to equalize these maxima by introducing a scaling factor μ such that $\mu|V_1(j\omega)|_{\max} = |V_o(j\omega)|_{\max}$. This ensures that the input signal can be increased safely and either V_o or V_1 saturate at the same input level. This scaling to change V_1 to μV_1 can be accomplished by changing R_2 and C in the feedback path of opamp A_1 to μR_2 and C/μ. Since the gain of the stage using resistors R' and R'' is unity, these can be retained as they are. Since the output V_1 has changed, the loop gain can be kept constant by changing R to μR in the third stage. The maxima of the second-order transfer function can be obtained through closed-form formulae [2.40] presented in Appendix B or by plotting to find out the maximum.

2.7.5 *Variants of Tow–Thomas and KHN Biquads*

Several alternative forms of TT and KHN biquads can be derived by using the nodal voltage simulation technique [2.41] from the single amplifier multiple-feedback low-pass filter of Fig. 2.16a. Note that earlier, circuits using only the inverting input of the opamp were derived. On the other hand, in these circuits (see, e.g., Fig. 2.16c), an internal node still existed where parasitic capacitances were present.

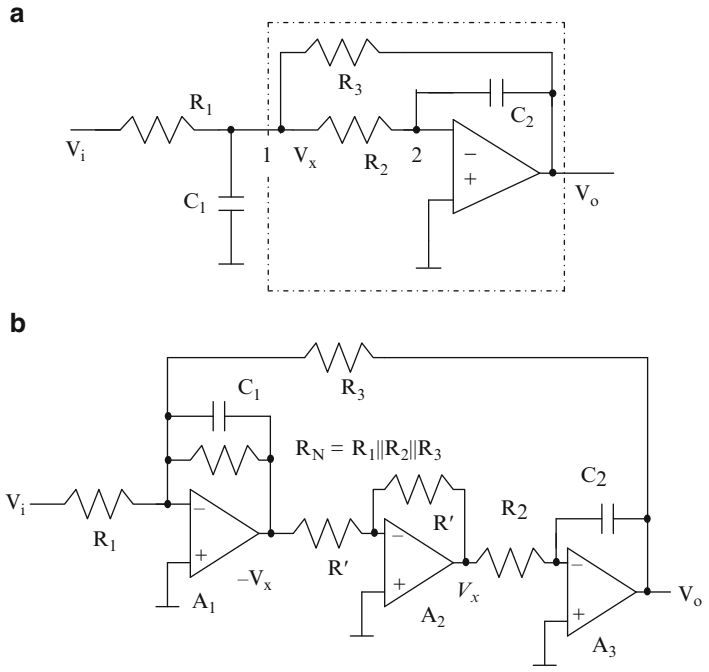

Fig. 2.21 (**a**) Multiple-feedback low-pass filter, and (**b**) circuit derived from (a) using nodal voltage simulation (Adapted from [2.41] ©IEEE 1985)

These internal nodes also can be eliminated by applying the nodal voltage simulation technique described next.

Consider the multiple feedback active RC filter of Fig. 2.21a. By writing nodal equations at nodes 1 and 2, the circuit of Fig. 2.21b can be constructed. Note that $-V_x$ is realized first and then using an inverting amplifier of unity gain, V_x is realized. The circuit used to realize V_o from V_x is preserved. Thus the nodal voltages are preserved in the new circuit. The similarity of the circuit of Fig. 2.21b to the Tow–Thomas biquad can be observed except that the damping (pole-Q determining) resistor is dependent on three resistors R_1, R_2, and R_3 in which place a single resistor R_N can be used to control the pole-Q.

We next consider the circuit of Fig. 2.22a, which is Fig. 2.12a redrawn for convenience. The equivalent circuit shown in Fig. 2.22b can be derived easily. Note that this circuit uses four opamps. The circuit cannot, however, realize a band-pass transfer function at node x similar to that in Fig. 2.22a. The transfer function of the circuit of Fig. 2.22b without considering the relationship of component values to those in the circuit of Fig. 2.22a can be seen to be

$$\frac{V_o}{V_i} = \frac{-1/R_1}{s^2\, C_1\, C_2\, R_4 + s\left(\frac{C_2\, R_4}{R_6} - \frac{C_1\, R_4}{R_5}\right) + \left(\frac{1}{R_7} - \frac{R_4}{R_5\, R_6}\right)} \tag{2.93}$$

Under the condition $C_1 = C_2 = C$, $R_7 = R_4 = R$, and $R_6 = Q_o R_4$, $R_5 = R_4/m$, we have

$$Q_p = \frac{\sqrt{(Q_o - m)\,Q_o}}{1 - m\,Q_o} \quad \text{and} \quad \omega_p = \omega_o \sqrt{1 - \frac{m}{Q_o}} \tag{2.94a}$$

The pole-Q sensitivities are as follows.

$$S_m^{Q_p} = -\frac{m}{2(Q_o - m)} + \frac{Q_p}{\sqrt{1 - \frac{m}{Q_o}}} \tag{2.94b}$$

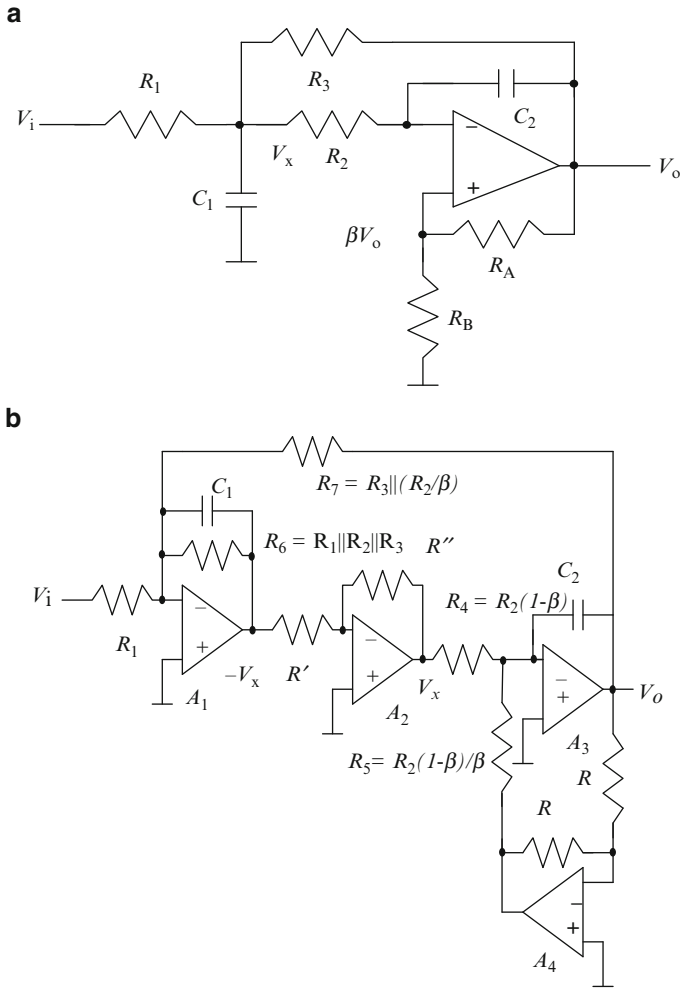

Fig. 2.22 (**a**) A multiple-feedback low-pass filter with positive feedback, (**b**) circuit obtained by nodal voltage simulation, (**c**) modification of (b), and (**d**) modification of (c) ((*b–d*) Adapted from [2.41] ©IEEE 1985)

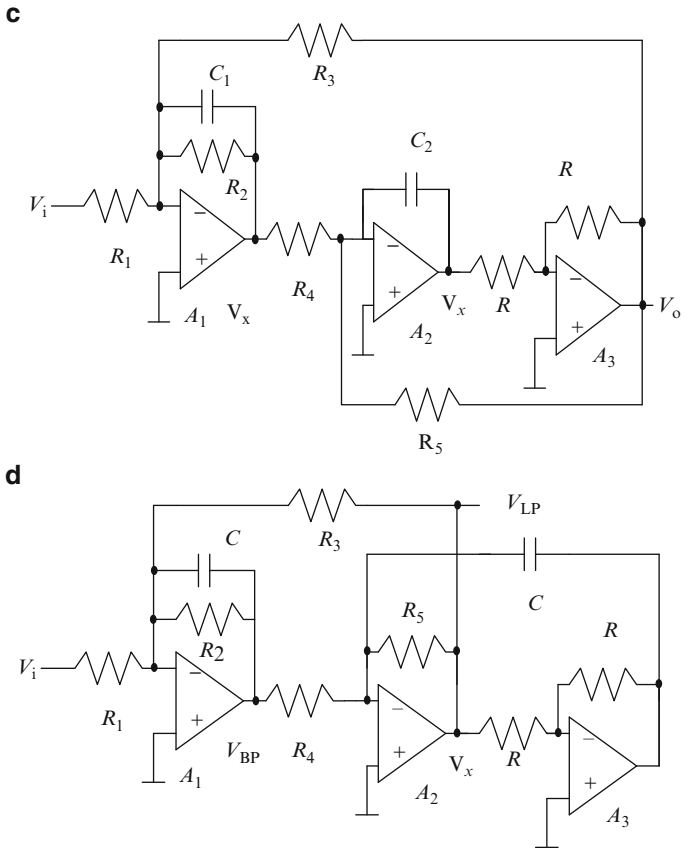

Fig. 2.22 (continued)

Thus, the Q_p-sensitivities can be large for finite m.

The circuit of Fig. 2.22b can be simplified as shown in Fig. 2.22c needing only three opamps. This circuit has same design equations as that of Fig. 2.22b. We next observe that the circuit of Fig. 2.22c can be rearranged to obtain another circuit shown in Fig. 2.22d which realizes effectively a noninverting integrator akin to the Akerberg–Mossberg biquad. Note, however, the advantage is the reduction in the spread of component values while achieving phase compensation. It is important to note that the polarity of the opamp input terminals is different in the Akerberg–Mossberg biquad.

In order to reduce the capacitor spread, a negative resistance realized using opamp A_2, resistors $(\alpha - 1)R, R$, and R_F can be shunted to ground at the V_x terminal as shown in Fig. 2.23a [2.43]. The corresponding circuit obtained by nodal voltage simulation is as shown in Fig. 2.23b. The transfer function of this circuit can be obtained as

$$\frac{V_o}{V_i} = \frac{-1/R_1}{s^2\, C_1\, C_2\, R_2 + s\, C_2\, R_2 \left(\frac{1}{R_N} - \frac{1}{R_5}\right) + \frac{1}{R_3}} \tag{2.95}$$

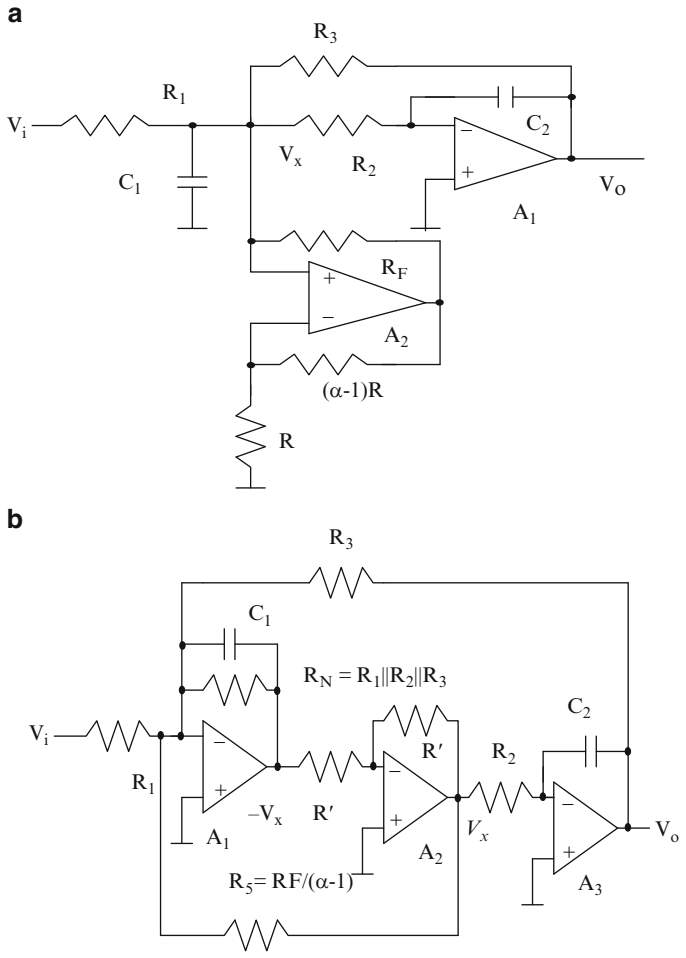

Fig. 2.23 (**a**) A multiple-feedback active RC filter using negative resistance for Q-enhancement, and (**b**) circuit obtained from (a) using nodal voltage simulation (Adapted from [2.41] ©IEEE 1985)

Thus although the pole-frequency is the same as that without the use of negative resistance, pole-Q is affected by R_5. For the choice $C_1 = C_2 = C$, $R_3 = R_2 = R$, we have $S_{R_5}^{Q_p} = -\frac{Q_p R_2}{R_5}$ and $S_{R_N}^{Q_p} = \frac{Q_p R_2}{R_N}$ which can be large and $S_{R_2}^{Q_p} = -1$.

Nodal voltage simulation technique can be applied to the KHN biquad redrawn in Fig. 2.24a as well since it uses one opamp where both input terminals are used. The circuit of Fig. 2.24b is the exact equivalent of the KHN biquad and needs four opamps and has the four transfer functions LP, BP, HP, and band-reject types at the outputs of the four opamps. Two rearrangements of this circuit are shown in Fig. 2.24c, d that do not change the internal transfer functions but change the sign

of the LP transfer function. In the circuit of Fig. 2.24c, the integrator and amplifier positions are changed. It uses a differential integrator formed by opamps A_2 and A_3, resistors R around A_2, resistors R_4, R_7 (=R_2), and capacitor C_2, and a noninverting integrator formed by resistors R around opamp A_5, and R_1,C_1 around OA A_4. Note that the high-pass transfer function is not realized. On the other hand, in the circuit of Fig. 2.24d, both feedback loops feed to the input opamp A_1. The circuit uses two noninverting integrators. Note that the circuit of Fig. 2.24d only realizes HP, BP, and LP transfer functions. These modifications have been used in deriving SC (switched-capacitor) filters.

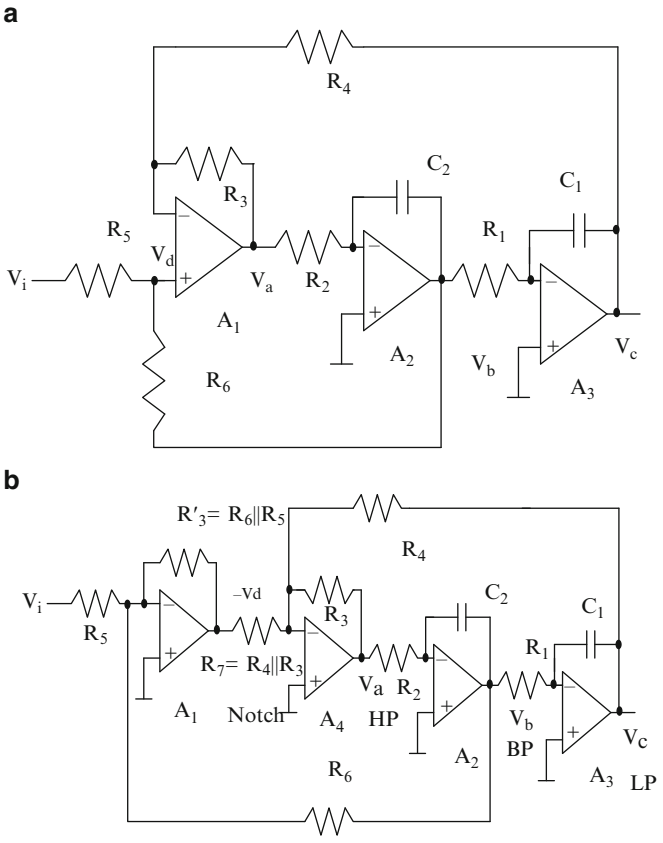

Fig. 2.24 (**a**) KHN biquad, (**b**) circuit obtained by nodal voltage simulation of (a), (**c**) modification of (b), and (**d**) another modification which feeds both outputs to the first opamp suitable for deriving SC filters (Adapted from [2.41] ©IEEE 1985)

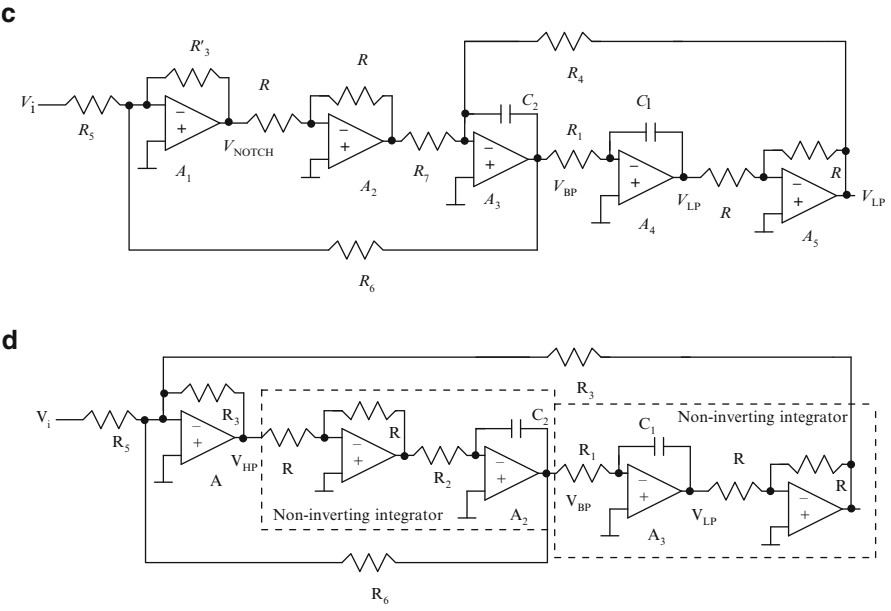

Fig. 2.24 (continued)

2.7.6 *Tarmy–Ghausi–Moschytz Three Opamp Biquad and Its Variations*

This is an interesting biquad [2.44, 2.45] which uses two first-order all-pass networks in a negative feedback loop. In this circuit, shown in Fig. 2.25a, the OA A_2 resistors R', R, and C (and similarly the OA A_3 resistors R', R, and C) realize a first-order all-pass transfer function H(s) given by

$$H(s) = \frac{1 - sCR}{1 + sCR} \tag{2.96}$$

The transfer function of this circuit can be derived as

$$\frac{V_o}{V_i} = -\frac{R_3}{R_1\left(1 + \frac{R_3}{R_2}\right)} \frac{\left(s^2\ C^2\ R^2 + 2sCR + 1\right)}{\left(s^2\ C^2\ R^2 + s\frac{2CR\left(\frac{R_3}{R_2} - 1\right)}{\left(1 + \frac{R_3}{R_2}\right)} + 1\right)} \tag{2.97}$$

Even though there are real zeroes, these do not affect the transfer function much. The pole-frequency and pole-Q can be derived as $\omega_p = \frac{1}{CR}$ and $Q_p = \frac{\left(1 + \frac{R_3}{R_2}\right)}{2\left(\frac{R_3}{R_2} - 1\right)}$.

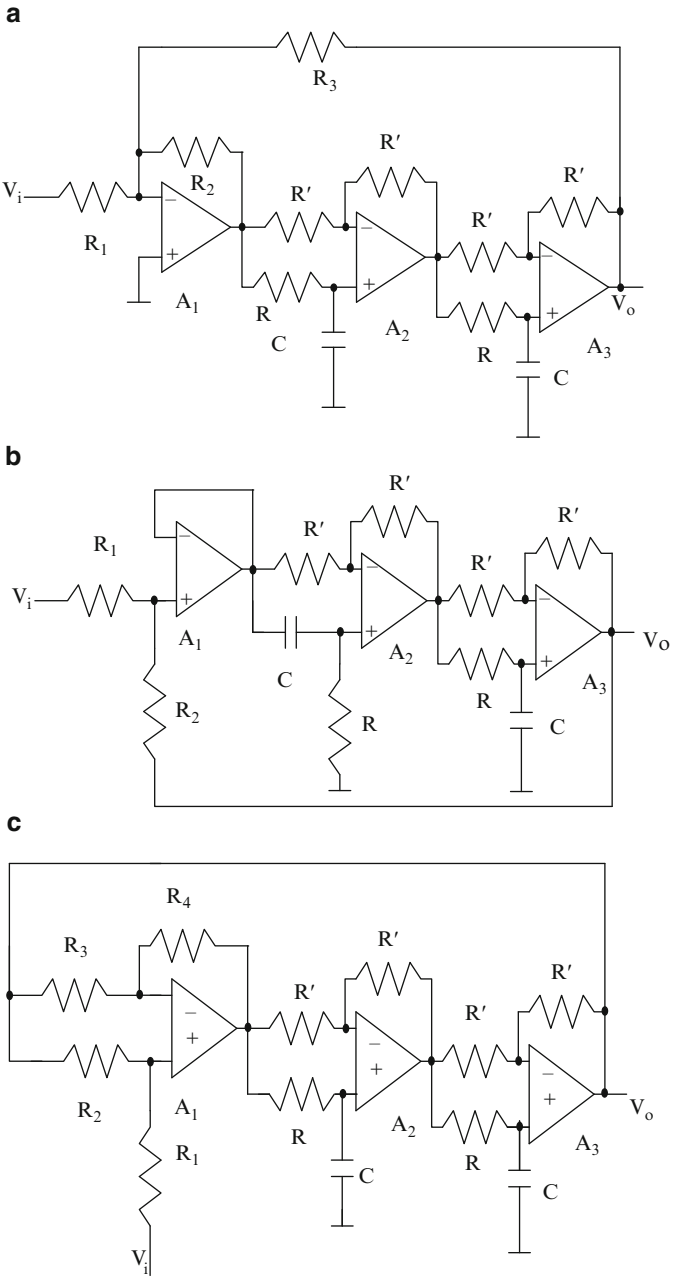

Fig. 2.25 (**a**) Tarmy–Ghausi band-pass filter modification due to Moschytz, (**b**) and (**c**) modifications of (a) to decrease the pole-Q sensitivity

The mid-band gain (i.e., gain at ω_p) is $\frac{R_3}{R_1}\frac{(2Q_p-1)}{2}$. Note that the sensitivity of Q_p to R_3/R_2 is large:

$$S_{\frac{R_3}{R_2}}^{Q_p} = -Q_p + \frac{1}{4Q_p} \tag{2.98}$$

Several interesting solutions [2.46, 2.47] have been suggested in the literature to reduce the pole-Q sensitivity. These use different techniques of implementation of the feedback loop while retaining the two first-order all-pass filters.

In the circuit of Fig. 2.25b, note that one inverting first-order all-pass filter and one noninverting first-order all-pass filter are used. The transfer function of this circuit can be derived as

$$\frac{V_o}{V_i} = -\frac{R_2}{(2R_1+R_2)}\frac{\left(s^2\ C^2\ R^2 - 2sCR + 1\right)}{\left(s^2\ C^2\ R^2 + s\frac{2CR}{(2R_1+R_2)} + 1\right)} \tag{2.99a}$$

The resulting pole-Q is given as

$$Q_p = \frac{R_1}{R_2} + \frac{1}{2} \tag{2.99b}$$

and the midband gain is unity. Thus, it is seen that the sensitivity of pole-Q is reduced considerably. In the alternative circuit shown in Fig. 2.25c, the realized transfer function is

$$\frac{V_o}{V_i} = \frac{\left(s^2\ C^2\ R^2 - 2sCR + 1\right)}{\left(s^2\ C^2\ R^2 + s\frac{2CR(2R_3\ R_1 + R_2\ R_3 - R_4\ R_2)}{R_2\ (R_3+R_4)} + 1\right)} \tag{2.100}$$

The resulting pole-Q under the condition $R_3 = R_4$ is given as

$$Q_p = \frac{R_2}{2R_1} \tag{2.101}$$

Thus, in this case as well, the Q-sensitivity is considerably reduced.

2.8 Second-Order Active Filters Using Amplifier Pole and One Capacitor

2.8.1 Using Single Capacitor

We consider a differentiator circuit shown in Fig. 2.26a. The transfer function of this circuit considering a nonideal opamp is given by

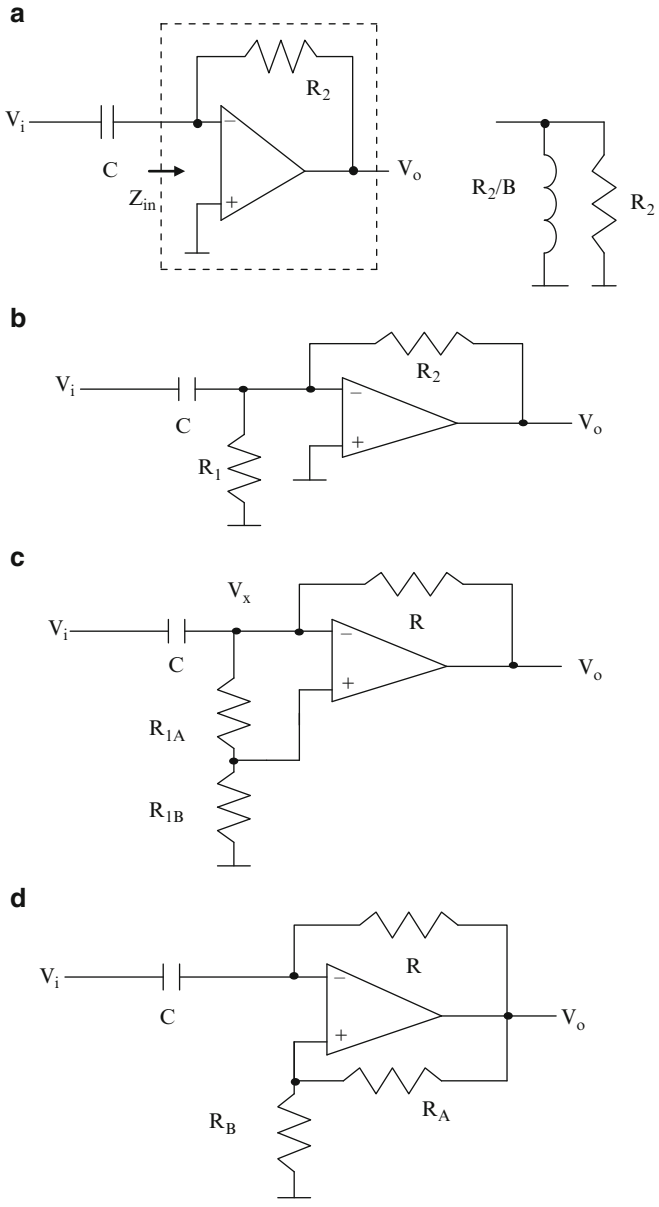

Fig. 2.26 (**a**) An active RC differentiator behaving as a second-order band-pass filter, (**b**) modification of (a) to realize variable pole-Q, (**c**) modification of (b) to change pole-frequency, (**d**) modification of (a) using positive feedback, (**e**) Rao and Srinivasan's low-pass/band-pass filter, (**f**) simplification of (e) to realize a low-pass/band-pass filter, and (**g**) a simplification of (e) to realize a notch filter (b Adapted from [2.48] © IEEE1977, d,e Adapted from [2.49] ©IEEE 1979, f, g adapted from [2.52] ©IEEE 1979)

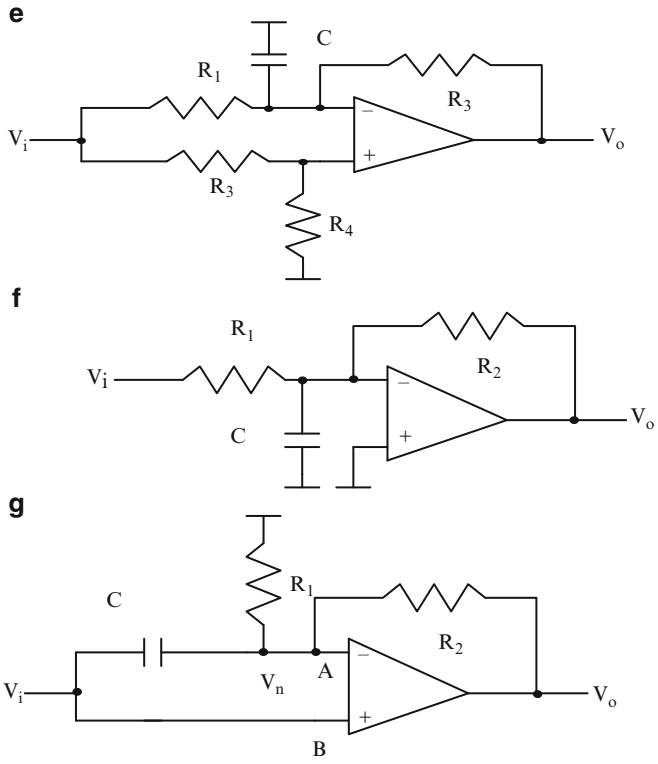

Fig. 2.26 (continued)

$$\frac{V_o}{V_i} = -\frac{-sB}{\left(s^2 + \frac{s}{CR_2} + \frac{B}{CR_2}\right)} \tag{2.102}$$

This is a band-pass transfer function with the pole-frequency being $\omega_p = \sqrt{\frac{B}{CR_2}}$ and $Q_p = \sqrt{BCR_2}$. Interestingly maximum $\omega_p Q_p = B$ thus showing that a band-pass filter with large pole-frequencies can be realized with moderate Q. It is interesting to note that a high-pass transfer function is realized at the inverting input of the OA. It may be appreciated that in effect the opamp with feedback resistor R_2 realizes a grounded inductor of value R_2/B shunted by a resistance R_2 as shown in Fig. 2.26a. Note that the addition of a resistance [2.48] as shown in Fig. 2.26b facilitates changing the pole-Q without changing the pole-frequency. The resulting transfer function of this circuit is given as

$$\frac{V_o}{V_i} = -\frac{-sB}{\left(s^2 + \frac{s}{C}\left(\frac{1}{R_1} + \frac{1}{R_2}\right) + \frac{B}{CR_2}\right)} \tag{2.103}$$

Thus, the pole-Q can be controlled by R_1. Note, however, that the resulting ω_p $Q_p = \frac{BR_1}{R_1+R_2}$ is less than B. The pole-frequency of the filter can be controlled by using a potential divider formed by resistors R_{1A} and R_{1B} in place of the resistor R_1 in Fig. 2.26b as shown in Fig. 2.26c. Note that the opamp is characterized in this case by the equation $V_o = -V_x\beta B/s$ effectively showing that the bandwidth has become βB where $\beta = \frac{R_{1A}}{R_{1A}+R_{1B}}$. Note, however, that modified bandwidth βB is less than the actual bandwidth B.

The realizable pole-Q can be enhanced using positive feedback [2.49] as shown in Fig. 2.26d. This circuit realizes a transfer function given by

$$\frac{V_o}{V_i} = -\frac{-sB}{\left(s^2 + s\left(\frac{1}{CR} - \beta B\right) + \frac{(1-\beta)B}{CR}\right)} \tag{2.104}$$

where $\beta = \frac{R_B}{R_A+R_B}$.

Interestingly, arbitrary pole-Q can be realized but the pole-frequency is also dependent on β. The circuit will realize a sinusoidal oscillator when $\beta = \frac{1}{BCR}$. The resulting frequency of oscillation is given as $B\sqrt{\beta(1-\beta)}$ showing that the maximum frequency of oscillation is $B/2$ when $\beta = 1/2$. The use of a positive feedback factor β larger than $1/BCR$ will lead to a relaxation oscillator. Most textbooks describe this circuit as a relaxation oscillator that can generate square and triangular waveforms [2.50].

Another interesting filter based on opamp pole [2.51] is presented in Fig. 2.26e. Note that this circuit realizes a transfer function given by

$$\frac{V_o}{V_i} = -\frac{s\beta B + \frac{B}{C}\left(\frac{\beta-1}{R_1} + \frac{\beta}{R_2}\right)}{\left(s^2 + \frac{s}{C}\left(\frac{1}{R_1} + \frac{1}{R_2}\right) + \frac{B}{CR_2}\right)} \tag{2.105}$$

where $\beta = \frac{R_4}{R_3+R_4}$. Note that under the condition $\beta = \frac{R_2}{R_1+R_2}$, a band-pass transfer function is realized. When $\beta = 0$ (see Fig. 2.26f), a low-pass transfer function is realized [2.52] as can be easily guessed by noting that the opamp with feedback resistance R_2 realizes a lossy grounded inductance that together with resistor R_1 (as shown before; see Fig. 2.26a) and capacitor C forms a RLC tank circuit. When $\beta = 1$ (in which case $R_4 = \infty$ and $R_3 = 0$; see Fig. 2.26g), a notch transfer function is realized [2.52] at the inverting input of the OA suggesting that a floating inductance is realized between A and B terminals with a parasitic resistance as shown in the equivalent circuit in Fig. 2.26g. At the output of OA A_1, a low-pass transfer function is realized:

$$\frac{V_n}{V_i} = -\frac{s^2 + \frac{B}{CR_2}}{\left(s^2 + \frac{s}{C}\left(\frac{1}{R_1} + \frac{1}{R_2}\right) + \frac{B}{CR_2}\right)} \tag{2.106a}$$

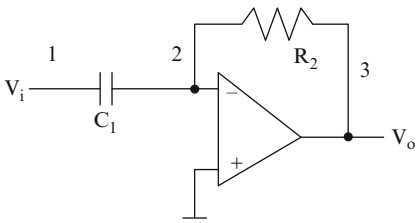

Fig. E.2.8

$$\frac{V_o}{V_i} = -\frac{\frac{B}{C}\left(\frac{1}{R_1}+\frac{1}{R_2}\right)}{\left(s^2+\frac{s}{C}\left(\frac{1}{R_1}+\frac{1}{R_2}\right)+\frac{B}{CR_2}\right)} \tag{2.106b}$$

Example 2.8 Determine the frequency response at the output and inverting input of the opamp of the differentiator using a nonideal opamp with finite bandwidth of 1 MHz (Fig. E.2.8).

It can be seen that the differentiator circuit behaves as a band-pass filter and at virtual ground node, a high-pass response can be seen. The midband gain of the band-pass response is $BCR = 628$ and pole-frequency is 40 KHz.

```
*Nonideal differentiator
C1 1 2 0.1 uf
R1 2 3 1 K
E1 0 4 2 0 100,000
R3 4 5 1 k
C3 5 0 15.90 uf
E2 3 0 5 0 1
vin 1 0 ac 1 v
.ac dec 10 1 1,000 K
```

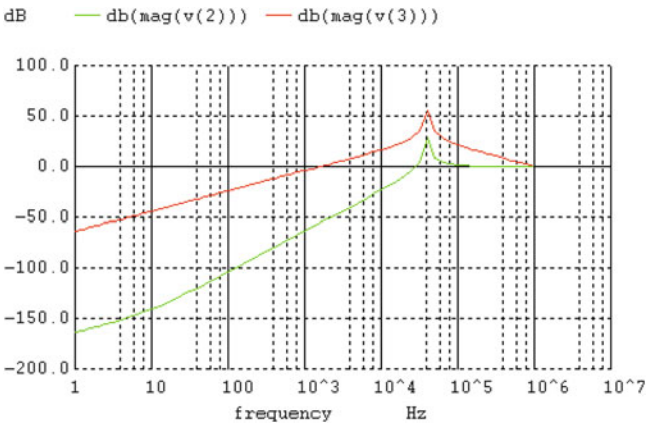

Example 2.9 Determine the frequency response at the output and inverting input of the opamp of the active-G_m-RC filter of Fig. 2.26f using a nonideal opamp with finite bandwidth of 1 MHz.

It can be seen that a low-pass response is realized at the output of the opamp and a band-pass response at the inverting input of the opamp. The pole-frequency is 91.84 Hz.

```
*Low-pass filter using amplifier pole
vin 1 0 ac 1 v
R1 1 2 18.86 K
C1 2 0 0.001 uf
R2 2 3 18.86 K
E1 0 4 2 0 100,000
R3 4 5 1 K
C3 5 0 15.90 uf
E2 3 0 5 0 1
.ac dec 10 1 1,000 K
```

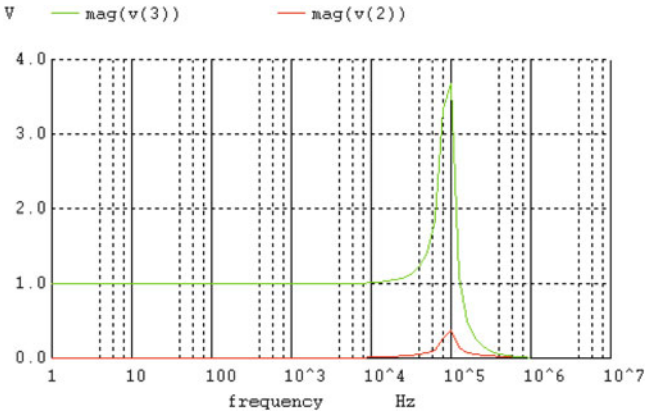

2.8.2 *Second-Order Filters Using Only Resistors and Amplifier Poles*

The capacitors can be eliminated altogether in active filters by using the poles of two opamps and only resistors. This is feasible by recognizing the fact that the opamp basically is an integrator and hence two-integrator loops can be built to realize biquadratic transfer functions. The simplest two-integrator loop using opamps and resistors is shown in Fig. 2.27a. The transfer function of this circuit is given by

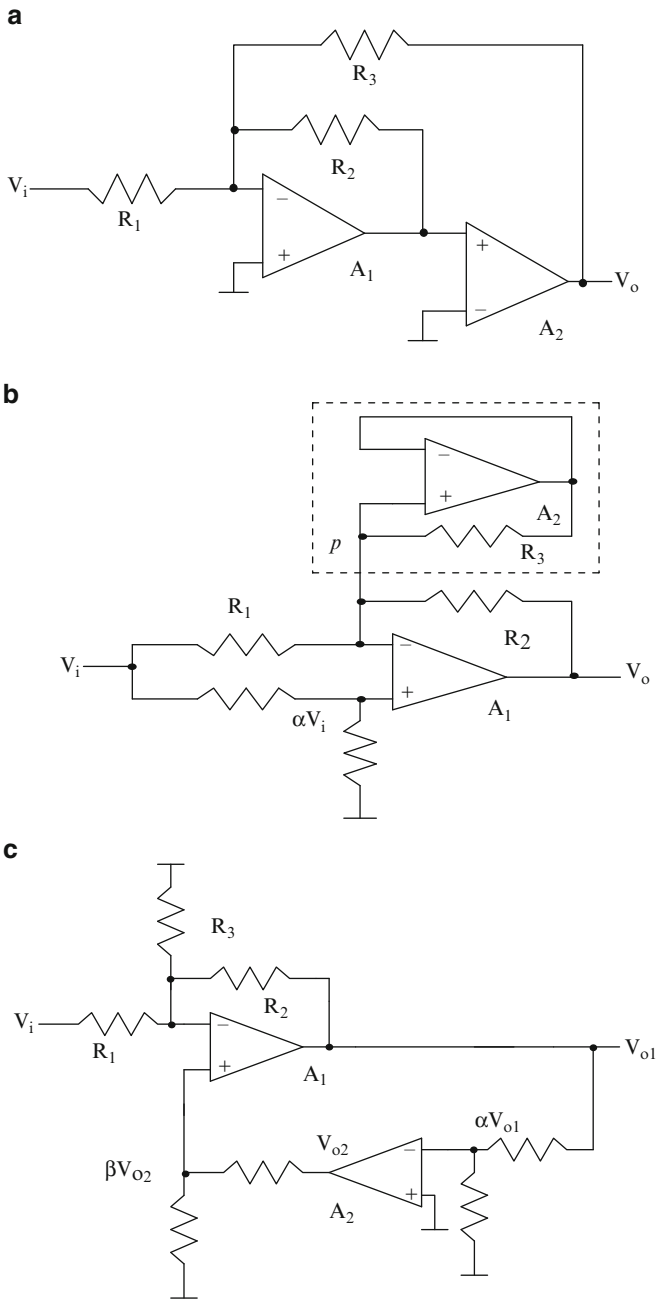

Fig. 2.27 Active R-filters: (**a**) based on two-integrator loop, (**b**) Ananda–Mohan structure based on Rao–Srinivasan filter of Fig. 3.25e, (**c**) Mitra–Aatre structure. Active R filters due to (**d**) and (**e**) Rao and Srinivasan [2.55] and (**f**) Schaumann [2.56] (**b**) Adapted from [2.53] ©IEE 1980, (**c**) Adapted from [2.54] ©IEEE 1976, (**d**,**e**) Adapted from [2.55] ©IEE 1974, (**f**) Adapted from [2.56] ©IEE 1974)

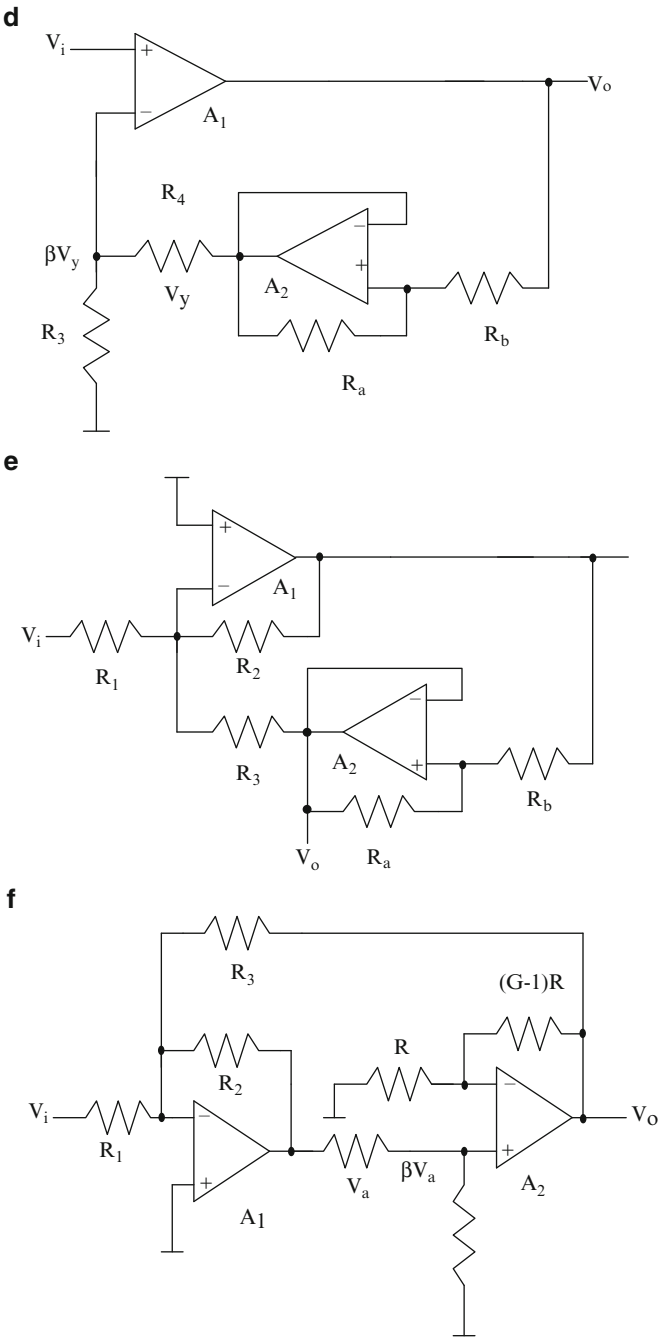

Fig. 2.27 (continued)

$$\frac{V_n}{V_i} = -\frac{-\frac{R_3}{R_1}}{\left(\frac{s^2}{B_1 B_2}\left(\frac{R_3}{R_1}+\frac{R_3}{R_2}+1\right)+\frac{s}{B_2}\left(\frac{R_3}{R_2}\right)+1\right)} \tag{2.107a}$$

and

$$\frac{V_a}{V_o} = -\frac{s}{B_2} \tag{2.107b}$$

Thus the dc gain is given by R_3/R_1 and independent control of pole-frequency and pole-Q is not possible. A band-pass transfer function is also available (see (2.107b)).

Another active R filter can be obtained from the low-pass filter derived from the Rao and Srinivasan filter using the opamp pole and one capacitor as shown in Fig. 2.26e [2.51] by replacing the capacitor C with a lossy simulated capacitor using the amplifier pole [2.53]. The resulting circuit is shown in Fig. 2.27b. Note that the OA A_2 and resistor R_3 will yield an input impedance at the terminal p given by

$$Z_{in} = R_3 + \frac{B_2\ R_3}{s} \tag{2.108}$$

The resulting transfer functions of the circuit at both outputs of the opamps are given by

$$\frac{V_o}{V_i} = -\frac{\left(\frac{1-\alpha}{R_1}-\frac{\alpha}{R_2}-\frac{\alpha}{R_4}\right)+\frac{s}{B_2}\left(\frac{1-\alpha}{R_1}-\frac{\alpha}{R_2}-\frac{\alpha}{R_3}-\frac{\alpha}{R_4}\right)}{\left(\frac{s^2}{B_1 B_2}\left(\frac{1}{R_1}+\frac{1}{R_2}+\frac{1}{R_3}+\frac{1}{R_4}\right)+s\left(\frac{1}{B_1}\left(\frac{1}{R_1}+\frac{1}{R_2}+\frac{1}{R_4}\right)+\frac{1}{B_2 R_2}\right)+\frac{1}{R_2}\right)} \tag{2.109a}$$

and

$$\frac{V_x}{V_i} = -\frac{\frac{s}{B_1 R_1}+\frac{\alpha}{R_2}}{\left(\frac{s^2}{B_1 B_2}\left(\frac{1}{R_1}+\frac{1}{R_2}+\frac{1}{R_3}+\frac{1}{R_4}\right)+s\left(\frac{1}{B_1}\left(\frac{1}{R_1}+\frac{1}{R_2}+\frac{1}{R_4}\right)+\frac{1}{B_2 R_2}\right)+\frac{1}{R_2}\right)} \tag{2.109b}$$

Evidently, a band-pass transfer function and a low-pass filter transfer function can be realized at V_o when

$$\frac{1-\alpha}{R_1} = \frac{\alpha}{R_2}+\frac{\alpha}{R_4} \tag{2.110a}$$

$$\frac{1-\alpha}{R_1} = \frac{\alpha}{R_2}+\frac{\alpha}{R_3}+\frac{\alpha}{R_4} \tag{2.110b}$$

Note also that V_x realizes a band-pass transfer function when $\alpha = 0$.

Mitra and Aatre [2.54] have described an active-R filter using opamps as shown in Fig. 2.27c. The transfer function of this circuit can be derived as

$$\frac{V_{o1}}{V_i} = \frac{-\frac{sB_1}{R_1}}{s^2\left(\frac{1}{R_1}+\frac{1}{R_2}+\frac{1}{R_3}\right)+\frac{sB_1}{R_3}+\alpha\beta B_1\, B_2\left(\frac{1}{R_1}+\frac{1}{R_2}+\frac{1}{R_3}\right)} \tag{2.111}$$

This realizes a band-pass transfer function with a center frequency gain R_2/R_1, and pole-frequency and pole-Q given as

$$\omega_p = \sqrt{\alpha\beta B_1\, B_2} \tag{2.112a}$$

$$Q_p = \sqrt{\frac{\alpha\beta B_2}{B_1}}\left(\frac{R_2}{R_1}+\frac{R_2}{R_3}+1\right) \tag{2.112b}$$

Thus the pole-Q is controlled by ratios of resistors and ratios of bandwidths of the opamps and the pole-frequency is dependent on opamp bandwidths. The maximum pole-frequency is evidently B where $B_1 = B_2 = B$ and $\alpha = \beta = 1$. Note that either α or β will be sufficient so that two resistors can be saved.

Rao and Srinivasan [2.55] have described an active R filter using two opamps which is presented in Fig. 2.27d. This uses the capacitor simulation circuit described earlier (see Fig. 2.27b). The transfer function of this circuit can be derived as

$$\frac{V_o}{V_i} = \left(\frac{1}{\beta}\right)\left(\frac{1+K\left(\frac{s}{B_2}\right)}{1+\frac{s}{\beta B_1}+\frac{Ks^2}{\beta B_1\, B_2}}\right) \tag{2.113}$$

where $K = 1+\frac{R_b}{R_a}$ and $\beta = \frac{R_3}{R_3+R_4}$.

For high pole-Q designs, (2.113) realizes a band-pass response. Note also that V_y is a low-pass transfer function:

$$\frac{V_y}{V_i} = \left(\frac{1}{\beta}\right)\left(\frac{1}{1+\frac{s}{\beta B_1}+\frac{Ks^2}{\beta B_1\, B_2}}\right) \tag{2.114}$$

Rao and Srinivasan have also suggested another circuit [2.55] shown in Fig. 2.27e for realizing a low-pass transfer function:

$$\frac{V_o}{V_i} = \left(\frac{-\frac{1}{R_1}}{\frac{1}{R_2}+\frac{1}{R_3}+s\left(\frac{K}{B_2R_2}+\frac{1}{B_1}\left(\frac{1}{R_1}+\frac{1}{R_2}+\frac{1}{R_3}\right)\right)+\frac{s^2}{KB_1\, B_2}\left(\frac{1}{R_1}+\frac{1}{R_2}+\frac{1}{R_3}\right)}\right) \tag{2.115}$$

Schaumann [2.56] has proposed another active R filter which is presented in Fig. 2.27f whose transfer functions are given by

$$\frac{V_a}{V_i} = \left(\frac{\frac{1}{R_1}\left(\frac{s}{B_2} + \frac{1}{G}\right)}{\frac{1}{GR_2} + \frac{\beta}{R_3} + s\left(\frac{1}{B_2 R_2} + \frac{1}{GB_1}\left(\frac{1}{R_1} + \frac{1}{R_2} + \frac{1}{R_3}\right)\right) + \frac{s^2}{B_1 B_2}\left(\frac{1}{R_1} + \frac{1}{R_2} + \frac{1}{R_3}\right)} \right) \tag{2.116a}$$

and

$$\frac{V_o}{V_i} = \left(\frac{\frac{1}{\beta R_1}}{\frac{1}{GR_2} + \frac{\beta}{R_3} + s\left(\frac{1}{B_2 R_2} + \frac{1}{GB_1}\left(\frac{1}{R_1} + \frac{1}{R_2} + \frac{1}{R_3}\right)\right) + \frac{s^2}{B_1 B_2}\left(\frac{1}{R_1} + \frac{1}{R_2} + \frac{1}{R_3}\right)} \right) \tag{2.116b}$$

Note that although V_o/V_i is a useful transfer function, V_a/V_i is not a useful transfer function. Schaumann suggests tuning the circuit for pole-Q, gain, and pole-frequency using R_3, R_1, and β, respectively.

The various configurations of active R filters have shown that ratios of resistors or ratios of bandwidths of opamps can control the gain and pole-Q whereas the pole-frequency is still dependent on absolute values of bandwidths of both opamps which vary with temperature and power supply voltage. Hence active R filter designers have suggested the concept of master–slave tuning which laid the foundation of continuous-time filter tuning. This topic is discussed at a later stage in this book.

Example 2.10 Determine the frequency response at the output and inverting input of the opamp of the active-R filter using two nonideal opamps. Study the effect of an opamp second pole also (Fig. E.2.10).

Note that the opamp second pole is modeled by R_5 and C_4 for one opamp and by R_7 and C_6 for another opamp. The effect of the second pole at 1.5 MHz is to cause Q-enhancement and a shift in the peak frequency. The filter has a radian pole-frequency of $B/\sqrt{3}$. The band-pass midband gain is 1. The pole-Q is $\sqrt{3}$.

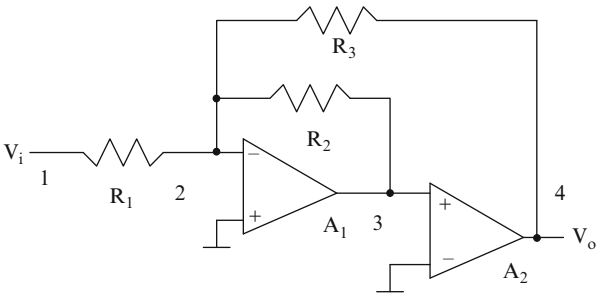

Fig. E.2.10

*Active R filter
R1 1 2 1 k
R2 2 3 1 k
R3 2 4 1 k
E1 0 5 2 0 100,000
R4 5 6 1 k
C3 6 0 15.90 uf
E2 3 0 6 0 1
E3 7 0 3 0 100,000
R5 7 8 1 K
C4 8 0 15.9 uf
E4 4 0 8 0 1
vin 1 0 ac 1 v
.ac dec 10 1 1,000 K

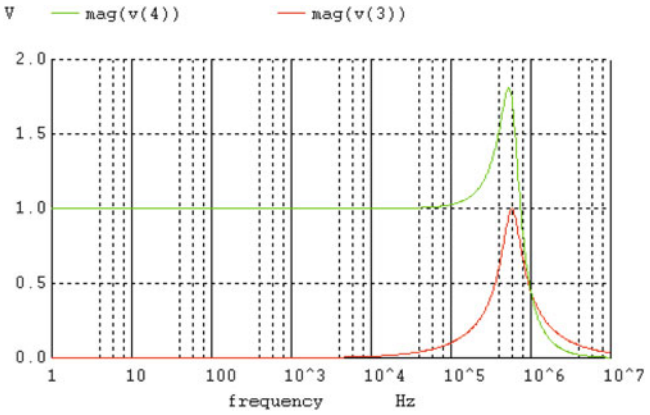

*Active R filter using second pole
R1 1 2 1 k
R2 2 3 1 k
R3 2 4 1 k
E1 0 5 2 0 100,000
R4 5 6 1 k
C3 6 0 15.90 uf
E2 9 0 6 0 1
R5 9 10 1 K
C4 10 0 106.15 pf
E3 3 0 10 0 1
E4 7 0 3 0 100,000
R6 7 8 1 k
C5 8 0 15.9 uf
E5 11 0 8 0 1
R7 11 12 1 k

```
C6 12 0 106.15 pf
E6 4 0 12 0 1
vin 1 0 ac 1 v
.ac dec 10 1 1,000 K
```

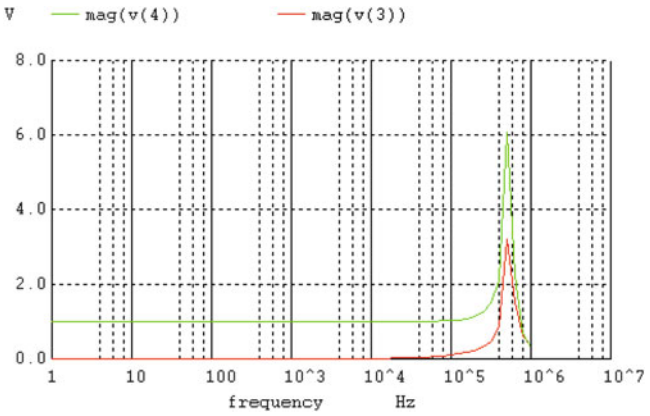

2.9 Active Filters Based on RLC Ladder Filters

Thus far, we have considered the design of active RC filters using the cascade technique. The advantage of this technique is that proven and high-performance biquads can be chosen to realize the high-order filters. But this technique has the drawback that there is no interaction between the various biquads. Thus, the individual biquad performance gets transferred to the output of the high-order filter. On the other hand, doubly terminated passive ladder filters using inductances, capacitances, and resistors have been found to exhibit very low sensitivity due to the coupling that exists among all the components in the ladder filters. Any variation in any one component will propagate to the source end as well as termination end and the resulting frequency response has very low sensitivity. This fact has been pointed out by Orchard [2.57] in his famous argument.

Consider, for instance, a high-order filter with equiripple pass-band. This implies that there are several points of inflection in the pass-band. At these critical frequencies, the derivative of the transfer function is zero. Thus, it follows that the sensitivity to any component at these frequencies is zero. Therefore by having several frequencies at which sensitivity of the transfer function is zero, in between these frequencies also, sensitivity tends to be low. This has been extensively verified by simulation for the past few decades. Hence, active filters based on RLC prototype ladder filters tend to lead to low-sensitivity designs.

Thus low-sensitivity active RC filters can be derived by imitating the RLC ladder filters. There are other techniques of high-order filter design that are not

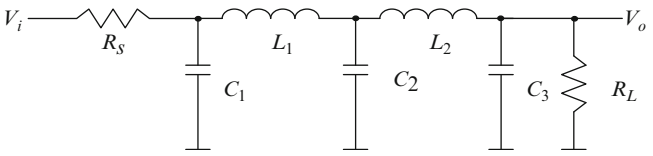

Fig. 2.28 A RLC prototype fifth-order low-pass ladder filter

based on simulation of RLC ladders. These are based on multiloop feedback technique. Both these topics are covered in the next two sections.

Active filters can be derived from RLC filters using two methods. In one method, for example, the inductors in the RLC low-pass filter prototype of Fig. 2.28 are replaced by active simulated inductances. This technique is known as the *component simulation technique*. In the second option, the *internal working* of the prototype RLC is filter is mimicked. By this, we mean that the nodal voltage equations are realized as being the same. This technique is known as the *operational simulation technique*.

Even though the component simulation technique is feasible, it will usually lead to a large number of components for realizing a floating inductor especially as compared to the operational simulation method.

2.9.1 Component Simulation Technique

In order to realize the circuit of Fig. 2.28 evidently one needs floating inductors. In a previous section, grounded inductance simulation based on GIC was described (see Fig. 2.15a). Other alternatives also exist. Consider another grounded inductance realization circuit shown in Fig. 2.29a [2.58]. The grounded inductance needs to have an input impedance of sL. The basic principle of inductance simulation is shown in Fig. 2.29b. The following equation describing the current through an inductor and the voltage across it can be written to mimic an inductor:

$$I_{in} = \frac{V_i}{sL} = \frac{V_i - V_o}{R_1} \tag{2.117}$$

Thus, we have to realize V_o from V_i such that

$$\frac{V_o}{V_i} = 1 - \frac{R_1}{sL} = 2 - \left(1 + \frac{R_1}{sL}\right) \tag{2.118}$$

so that a resistance inserted between V_i and V_o simulates an inductance.

We need to generate a voltage V_o from the input voltage V_i. The gain of 2 is achieved by using a noninverting amplifier formed by opamp A_2 and two resistors R'. The transfer function $\left(1 + \frac{1}{sCR_2}\right)$ is obtained by using the subcircuit shown in

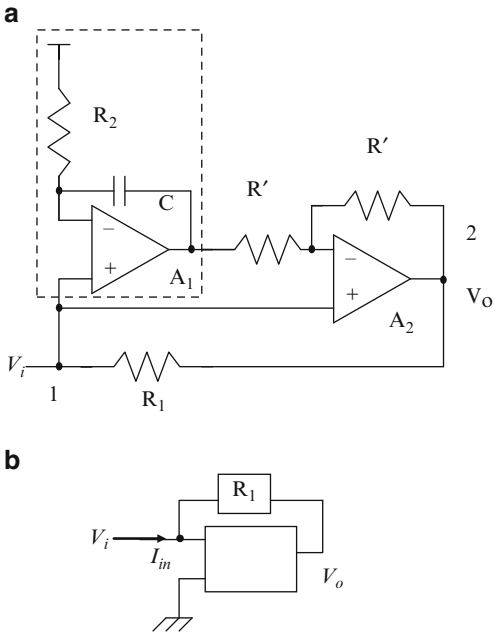

Fig. 2.29 (**a**) A grounded inductance simulator, and (**b**) the basic principle of grounded inductance simulation (Adapted from [2.58] ©IEEE 1967)

Fig. 2.29a in dotted lines and the needed inversion is carried out by the opamp A_2. It should be noted that the block used to realize the voltage transfer function $(1 - (R_1/sL))$ must have high input impedance. The inductance realized is given by CR_1R_2.

For the realization of floating inductance, it is required to augment the circuit of grounded inductance shown in Fig. 2.29b, by lifting the grounded terminal off the ground and connecting another similar circuit back to back as shown in Fig. 2.30a. The active RC implementation is as shown in Fig. 2.30b. Note that $(V_a - V_b)$ is available across the resistance R which is integrated using capacitors C and opamps A_1 and A_2. These outputs of the integrators are added appropriately with the terminal voltages V_a and V_b to realize V_x and V_y such that

$$V_y = V_b + \frac{V_a - V_b}{sCR} \tag{2.119a}$$

and

$$V_x = V_a + \frac{V_b - V_a}{sCR} \tag{2.119b}$$

Thus, the currents flowing into the terminal A and B are $\frac{V_a - V_x}{R}$ and $\frac{V_b - V_y}{R}$ which correspond to a floating inductance of value CR^2. Note that the circuit needs two capacitors and $R_1 = R_2 = R$.

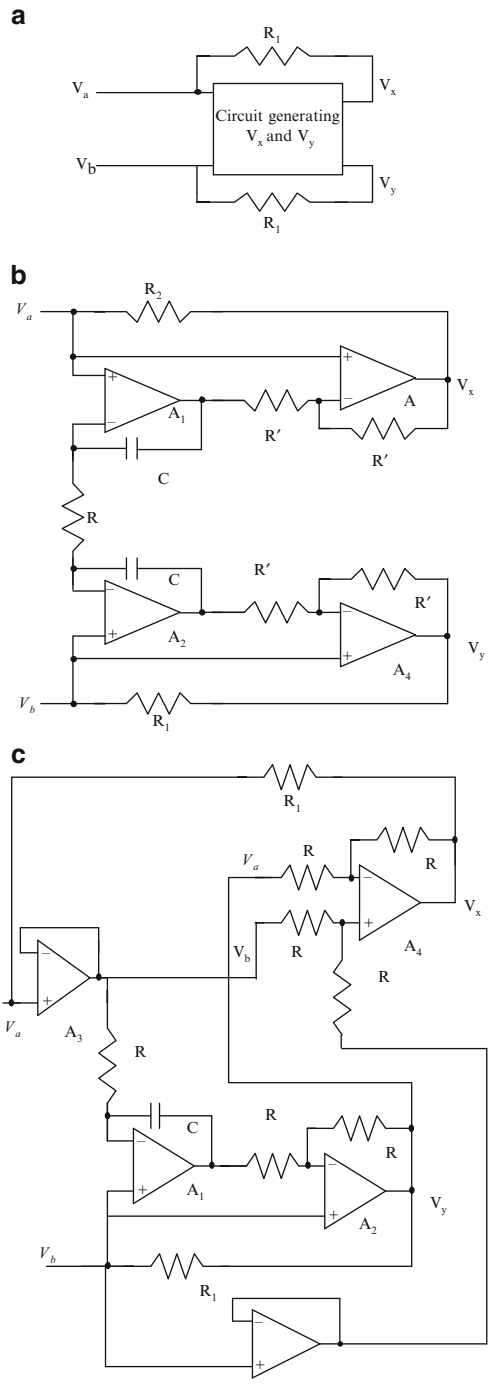

Fig. 2.30 (**a**) A floating inductance simulation scheme based on the grounded inductance of Fig. 2.29a, (**b**) conceptual model ((b) Adapted from [2.58] ©IEEE 1967) of floating inductance realization, and (**c**) another floating inductance simulation circuit

A modified circuit that needs only one capacitor is shown in Fig. 2.30c. Note that the buffer-connected opamps A_3 and A_5 are needed to isolate loading of the V_a and V_b terminal by the resistor R. In the conceptual model of floating inductance realization shown in Fig. 2.30a, it can be seen that

$$\frac{V_a - V_x}{R} = \frac{V_y^{'} - V_b}{R} \tag{2.119c}$$

or alternatively, we have

$$V_x = V_a + V_b - V_y \tag{2.119d}$$

Hence V_y can be realized using the modified grounded inductance circuit as shown in Fig. 2.30c and using an additional OA A_4 and four equal resistors, V_x can be realized. It may be noted the circuits of Fig. 2.30b, c rely on matching of components for exact floating inductance realization.

All-pole high-pass filters can be easily realized using the grounded inductances described above. Floating inductances can be avoided in the design of all-pole low-pass filters using the concept of FDNR which is considered next.

2.9.2 FDNR-Based Filters

Bruton [2.59] has introduced the concept of *frequency-dependent negative resistance* (FDNR) in order to facilitate easy realization of low-pass active RC ladder filters. Consider once again the prototype of Fig. 2.31a. Bruton suggested dividing all the impedances by s so that the transfer function remains unchanged. Then the following equivalences will occur.

R changes to $\frac{R}{s}$ (a capacitor of value 1/R)

$\frac{1}{sC}$ changes to $\frac{1}{s^2 C}$ (a frequency-dependent negative resistance $D \equiv -1/(\omega^2 C)$)

sL changes to L, a resistance.

Thus, floating inductances are transformed to floating resistances and resistors are transformed to capacitors and capacitors are transformed to grounded FDNRs as shown in Fig. 2.31b. The impedance $-1/(\omega^2 C)$ is real and negative and hence is a negative resistance, however, it is frequency-dependent due to the ω^2 term. Fortunately, grounded FDNR can be easily realized using a GIC (generalized impedance converter) studied in Fig. 2.15a. Note, however, that unlike the RLC prototype, the low-pass filter does not have a dc response as needed for a low-pass filter, since input is fed through a series capacitor. This situation can be remedied by shunting the input and load capacitors by resistances which, of course, changes the frequency response slightly.

Note, however, that this technique is applicable only for low-pass ladder filters. The FDNR is also known as supercapacitance.

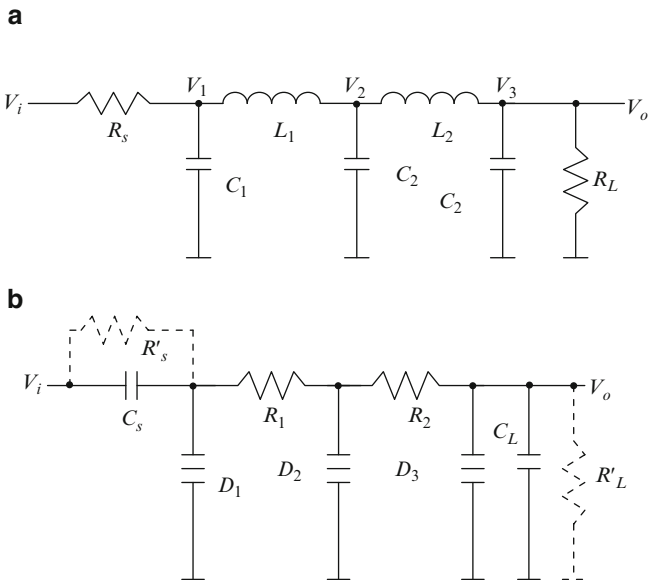

Fig. 2.31 (**a**) A fifth-order low-pass ladder filter prototype, and (**b**) a grounded FDNR-based circuit derived from (a)

2.9.3 Active RC Ladder Filters Based on Operational Simulation

2.9.3.1 Low-Pass Ladder Filters

In this technique, the nodal voltage equations are realized. As an illustration, consider the RLC low-pass all-pole ladder filter prototype shown in Fig. 2.32a. One can easily write the nodal voltage equations at nodes 1, 2, and 3 as follows.

$$\frac{V_i - V_1}{R_s} + I_1 = s C_1 V_1 \tag{2.120a}$$

$$I_1 = \frac{V_2 - V_1}{s L_1} \tag{2.120b}$$

$$I_2 = \frac{V_2 - V_3}{s L_2} \tag{2.120c}$$

$$-(I_1 + I_2) = \frac{V_2}{s C_2} \tag{2.120d}$$

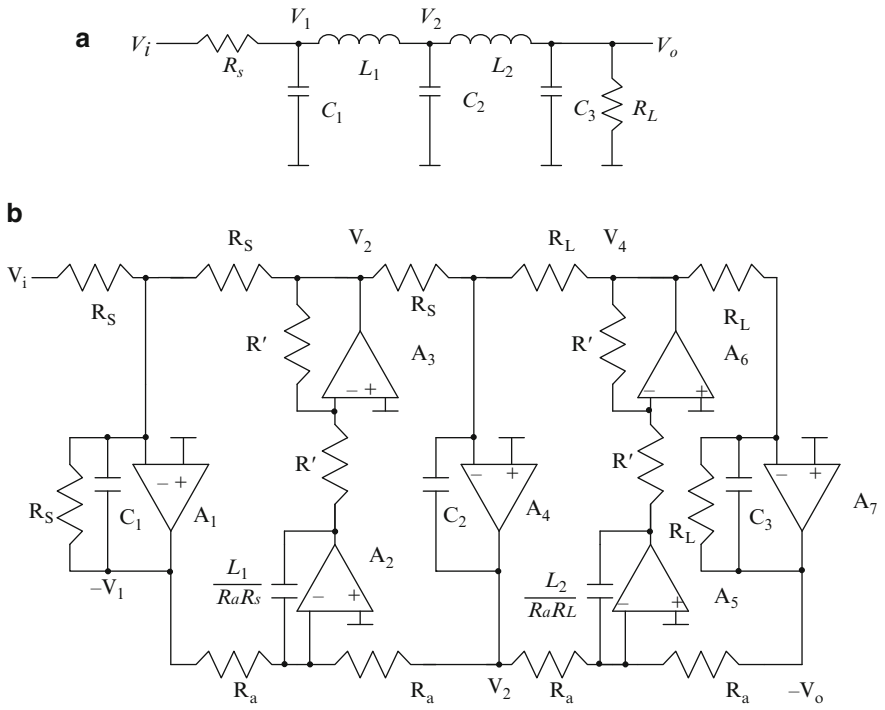

Fig. 2.32 (**a**) A passive RLC ladder prototype, and (**b**) a leap-frog active ladder filter derived from (a)

$$I_2 - V_o\, s\, C_3 = \frac{V_o}{R_L} \tag{2.120e}$$

Note that by considering $-V_1$, V_2 and $-V_0$ are realized at the outputs of the OAs, these equations can be easily realized as shown in the complete circuit of Fig. 2.32b. Note that the currents through the inductors I_1 and I_2 are also realized at the outputs of OAs A_3 and A_6 as I_1R and I_2R using noninverting integrators formed by (A_2 and A_3) and (A_5 and A_6) and associated resistors and capacitors, respectively. All the equations (2.120) can be realized using integrators. The termination resistances R_s and R_L will form part of the damped integrators as shown. The inductance and capacitance values in the prototype directly correspond to the integrating capacitors. The elegance of obtaining the circuit from the prototype of Fig. 2.32a has been noted.

Note that in a good design, there is an additional scaling step for optimal dynamic range. This requires that the currents through the inductors and voltages across the capacitors (i.e., the state variables realized at the output terminals of the various opamps) need to be analyzed to find their maximum value across the complete frequency range and then these voltages would be scaled to be equal.

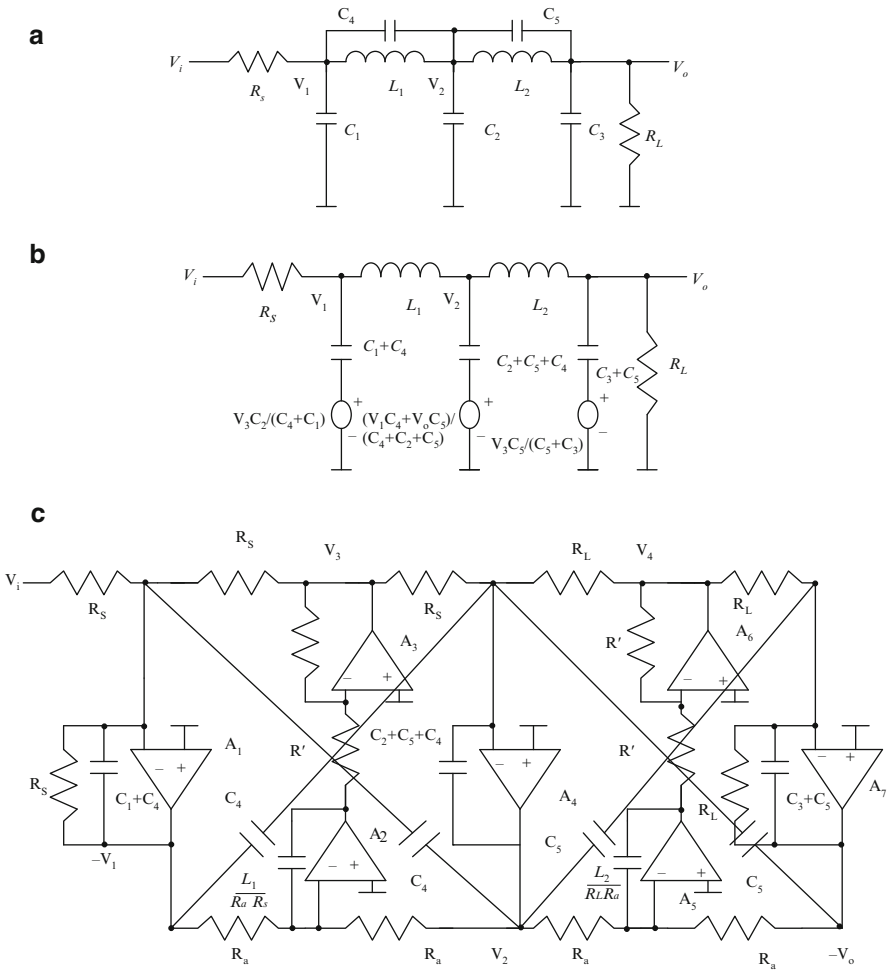

Fig. 2.33 (**a**) A passive RLC fifth-order elliptic low-pass ladder filter prototype, (**b**) an equivalent of (a), and (**c**) leap-frog active ladder filter derived from (b)

The scaling procedure has been illustrated in Fig. 2.20 for the case of the Tow–Thomas biquad which in fact is based on an operational simulation of a second-order singly terminated filter (R_s or $R_L = 0$).

For several years, the operational simulation of low-pass elliptic filters was not easy. However, during the course of research on SC filters, Allstot, Brodersen, and Gray [2.60] suggested an ingenious technique of realizing low-pass elliptic filters. This approach is considered briefly next. In this method, the nodal equations at nodes V_1, V_2, and V_3 in the prototype filter of Fig. 2.33a are rewritten so that by augmenting additional components, the low-pass filter structure can still be used. The circuit of Fig. 2.33b can be seen to be the exact equivalent of the prototype fifth-order elliptic low-pass filter circuit of Fig. 2.33a, wherein new voltage sources

are introduced. Also, note that the original grounded capacitor values C_1, C_2, and C_3 are increased. This circuit can be realized by the active RC filter of Fig. 2.33c in which the two pairs of cross-coupling capacitors facilitate the realization of the two pairs of transmission zeroes. Note that for each floating capacitor in the prototype, we have used two cross-coupling capacitors. However, it has been shown by Allstot, Brodersen, and Gray [2.60] that the mismatch of these capacitors does not affect the frequency response of the realized filter.

Example 2.11 Plot the frequency response of (a) the third-order elliptic ladder filter using SPICE and (b) leap-frog simulation of this filter considering the opamps to be nonideal. (c) Use an Akerberg–Mossberg type integrator for the middle integrator and evaluate the behavior.

```
*Third Order RLC Elliptic filter
Rs 1 22 1,000
RL 23 0 1,000
C21 22 0 1,203 pf
L21 22 23 962 uh
C22 22 23 201 pf
C23 23 0 1,203 pf
```

The operational simulation yields the active RC filter of Fig. E.2.11a. It can be seen that there is undesirable peaking at the pass-band edge and the transmission zero is obscured. The use of the Akerberg–Mossberg type of noninverting integrator improves the frequency response as shown (see Fig. E.2.11b).

```
* Third order leap-frog ladder filter
R1 1 2 1 K
R7 8 2 1 k
```

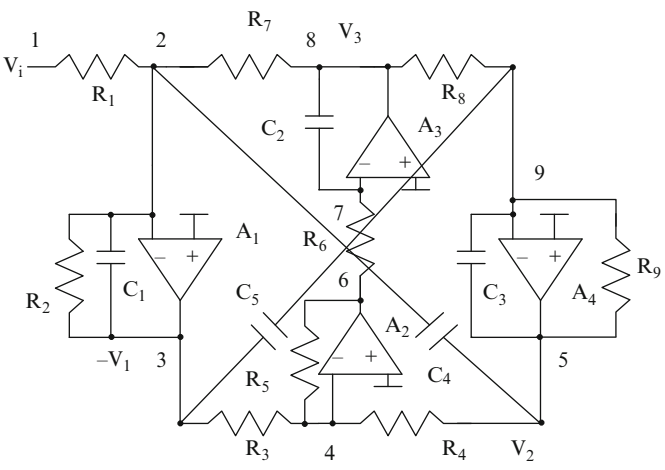

Fig. E.2.11a

R2 2 3 1 k
C1 2 3 1,404 pf
C2 8 7 962 pf
R6 6 7 1 k
R5 4 6 1 k
R3 3 4 1 k
R4 4 5 1 k
R8 8 9 1 k
R9 9 5 1 K
C3 9 5 1,404 pf
C4 2 5 201 pf
C5 3 9 201 pf
E1 0 10 2 0 100,000
R10 10 11 1 k
C6 11 0 15.9 uf
E2 3 0 11 0 1
E3 0 12 4 0 100,000
R11 12 13 1 k
C7 13 0 15.9 uf
E4 6 0 13 0 1
E5 0 14 7 0 100,000
R12 14 15 1 k
C8 15 0 15.9 uf
E6 8 0 15 0 1
E7 0 16 9 0 100,000
R13 16 17 1 k
C9 17 0 15.9 uf
E8 5 0 17 0 1
vin 1 0 ac 1 v
.ac dec 10 1 1,000 k

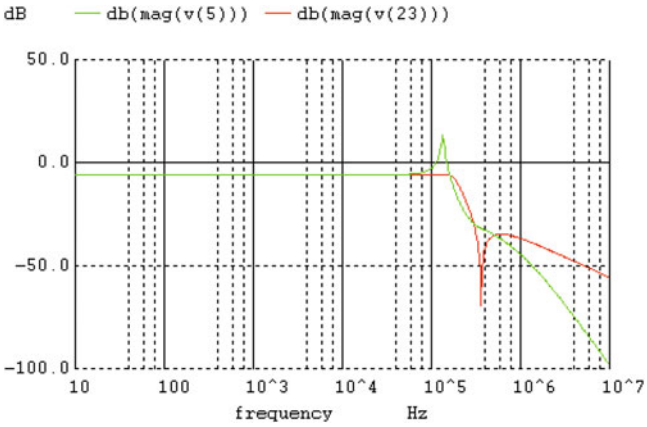

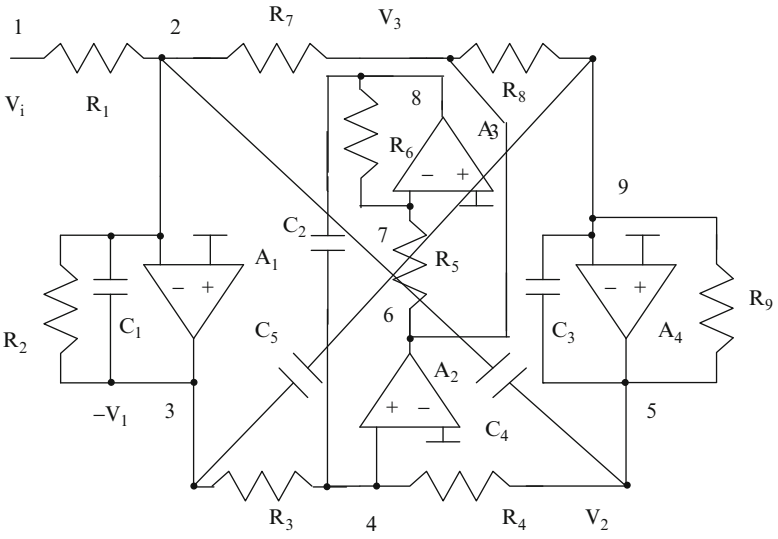

Fig. E.2.11b

* Third order leap-frog ladder filter Akerberg–Mossberg
R1 1 2 1 K
R7 6 2 1 k
R2 2 3 1 k
C1 2 3 1,404 pf
C2 4 8 962 pf
R5 6 7 1 k
R6 7 8 1 k
R3 3 4 1 k
R4 4 5 1 k
R8 6 9 1 k
R9 9 5 1 K
C3 9 5 1,404 pf
C4 2 5 201 pf
C5 3 9 201 pf
E1 0 10 2 0 100,000
R10 10 11 1 k
C6 11 0 15.9 uf
E2 3 0 11 0 1
E3 12 0 4 0 100,000
R11 12 13 1 k
C7 13 0 15.9 uf
E4 6 0 13 0 1
E5 0 14 7 0 100,000
R12 14 15 1 k

```
C8 15 0 15.9 uf
E6 8 0 15 0 1
E7 0 16 9 0 100,000
R13 16 17 1 k
C9 17 0 15.9 uf
E8 5 0 17 0 1
vin 1 0 ac 1 v
.ac dec 10 1 1,000 k
```

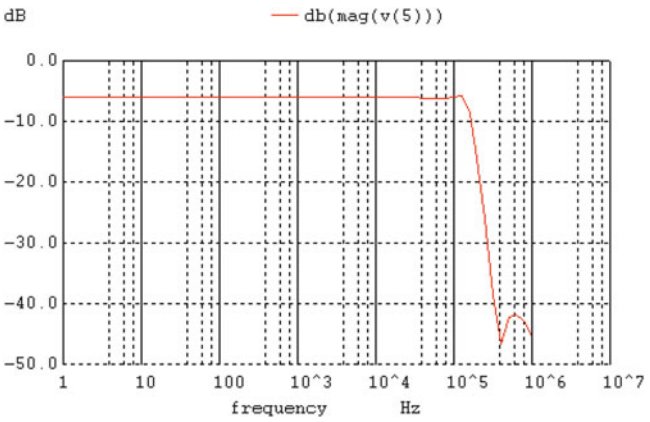

2.9.3.2 Band-Pass Filters

It may be pointed out that using low-pass to band-pass transformation, from the low-pass all-pole filter structure of Fig. 2.32a, we can obtain the band-pass filters. Note that LP to BP transformation transforms a lossless integrator to a resonator with infinite Q whereas a damped integrator is converted to a resonator with finite Q. The LP to BP transformation is given as $s \rightarrow \frac{s^2+\omega_o^2}{Bs}$ where the cutoff frequency of the prototype low-pass filter is 1 rad/s, ω_o is the desired center frequency of the band-pass filter, and B is the 3-dB bandwidth of the desired band-pass filter. Note that this transformation yields geometrically symmetric responses which means that there are two frequencies ω_1, ω_2 corresponding to a given gain such that $\omega_o = \sqrt{\omega_1\ \omega_2}$. Using the LP to BP transformation, an integrator and first-order low-pass filter will yield, respectively,

$$\frac{1}{s} \rightarrow \frac{Bs}{s^2+\omega_o^2} \text{ and } \frac{a}{s+a} \rightarrow \frac{aBs}{s^2+aBs+\omega_o^2}$$

For operational simulation of BP filters from the LC prototype, the signs of the integrators in the low-pass prototype need to be preserved. Moreover, the

summation of the inputs as needed in a low-pass filter needs to be done in the case of a band-pass filter as well.

The nodal voltages V_1 and V_3 can be expressed first from the prototype of Fig. 2.34a as follows.

$$\frac{V_i}{R_s} - V_1\left(\frac{1}{R_s} + s(C_1 + C_2)\right) + V_3\, s\, C_2 + \frac{(V_3 - V_1)}{s\, L_2} = 0 \tag{2.121a}$$

$$V_1\, s\, C_2 - V_3\, s(C_2 + C_3) - \frac{V_3}{R_L} + \frac{V_1 - V_3}{s\, L_2} = 0 \tag{2.121b}$$

By substituting for s, the LP to BP transformation $\frac{\left(s^2 + \omega_o^2\right)}{Bs}$, we obtain the following two equations after little manipulation:

$$\frac{s\, V_i\, B}{(C_1 + C_2)R_s} - V_1\left(s^2 + \frac{sB}{(C_1 + C_2)R_s} + \omega_o^2\right) + V_3\left(s^2 + \omega_o^2\right)\frac{C_2}{(C_1 + C_2)} + \frac{(V_3 - V_1)\, s^2\, B^2}{(C_1 + C_2)\left(s^2 + \omega_o^2\right) L_2} = 0 \tag{2.122a}$$

$$V_1\left(s^2 + \omega_o^2\right)\frac{C_2}{(C_2 + C_3)} - V_3\left(s^2 + \frac{sB}{(C_2 + C_3)R_L} + \omega_o^2\right) + \frac{(V_1 - V_3)\, s^2\, B^2}{(C_2 + C_3)\left(s^2 + \omega_o^2\right) L_2} = 0 \tag{2.122b}$$

These equations can be implemented by the block diagram of Fig. 2.34b. Any well-known biquad can be employed in the band-pass filter realization. The use of the Tow–Thomas biquad for this purpose is shown in Fig. 2.34c in the complete sixth-order band-pass filter derived from a third-order all-pole low-pass prototype active RC filter. Note that the low-pass prototype can be scaled first for optimal dynamic range and the resulting LP prototype circuit can be used directly to obtain the band-pass filter that will yield an optimal dynamic range solution at the nodes of the corresponding third-order prototype. However, for high pole-Q designs, within the three two-integrator loops, scaling needs to be done by choosing equal time constants for the integrators.

2.9.4 *Operational Simulation of High-Pass Filters: Yoshihoro's Technique*

The techniques presented above do not work easily for realizing high-pass filters. Some solutions have been suggested in the literature but they are very complex. The reader is referred to Brackett and Sedra [2.1] for more information. Yoshihoro's nodal voltage simulation technique [2.61] can be used to realize

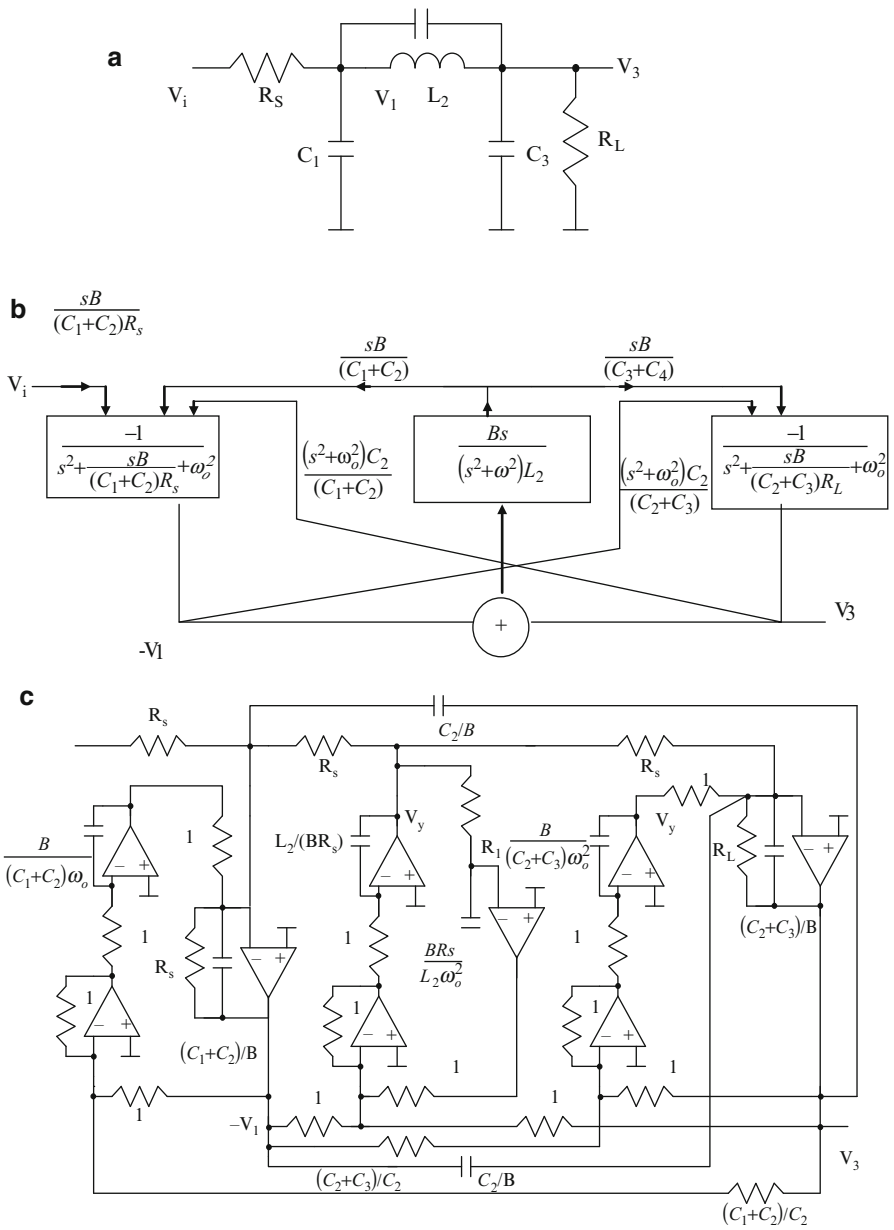

Fig. 2.34 (**a**) A third-order all-pole low-pass filter, (**b**) block diagram obtained by LP to BP transformation from (**a**), and (**c**) complete sixth-order band-pass active RC filter obtained from (**b**) (b Adapted from [2.63] ©IEE 1980)

high-pass filters based on RLC ladder filters [2.62]. Consider the prototype third-order elliptic high-pass shown in Fig. 2.35a. The equations for the node voltages V_x and V_o can be easily written in terms of the neighboring node voltages as follows by simple analysis.

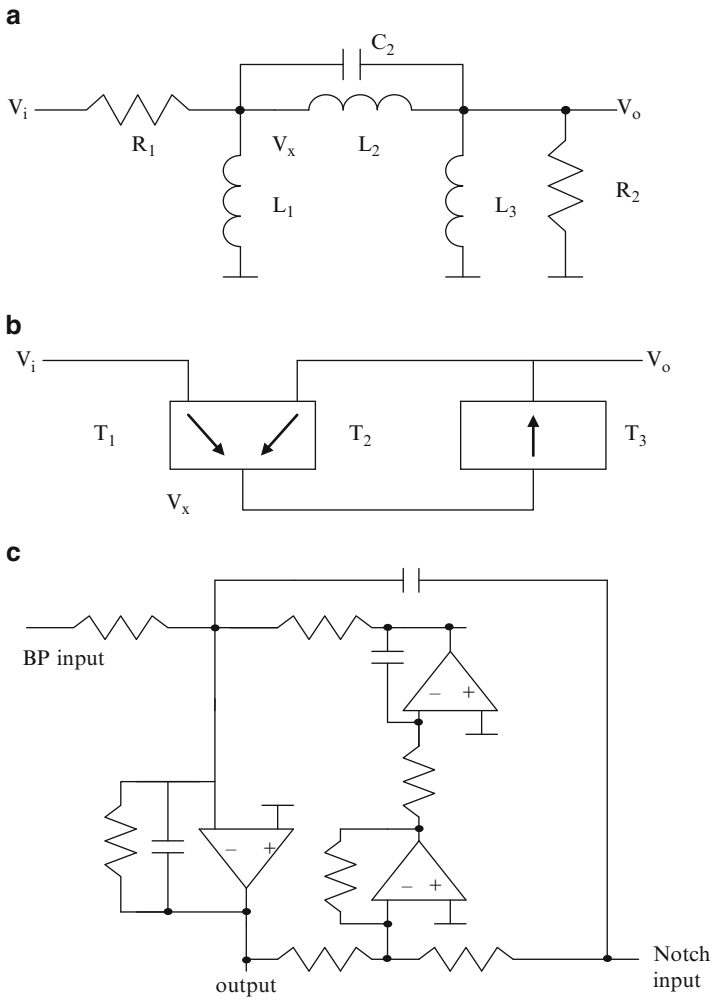

Fig. 2.35 (**a**) A third-order elliptic high-pass filter, (**b**) block diagram of filter obtained using Yoshihoro's technique, (**c**) second-order active RC BP/notch filter that can be used in (b), (**d**) complete high-pass filter, and (**e**) equivalent model of (d) (Adapted from [2.62] ©IEE 1988)

d

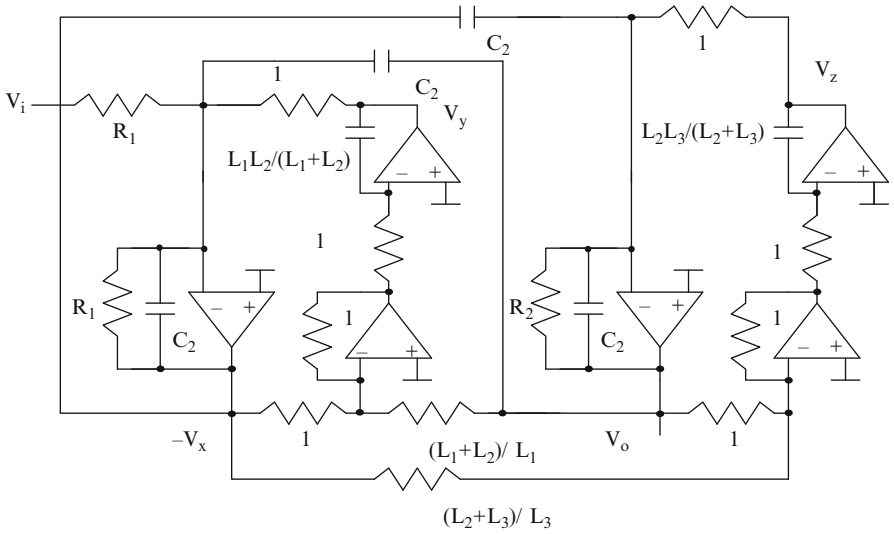

e

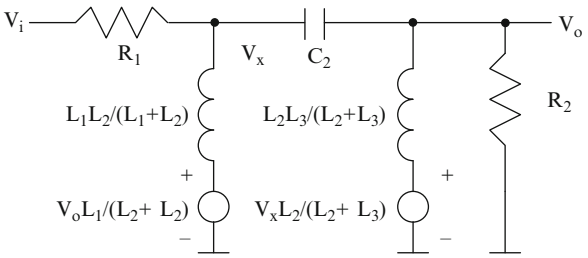

Fig. 2.35 (continued)

$$V_x = V_i \left(\frac{\frac{s}{C_2 R_1}}{s^2 + \frac{s}{C_2 R_1} + \frac{1}{C_2}\left(\frac{1}{L_1} + \frac{1}{L_2}\right)} \right) + V_o \left(\frac{s^2 + \frac{1}{L_2 C_2}}{s^2 + \frac{s}{C_2 R_1} + \frac{1}{C_2}\left(\frac{1}{L_1} + \frac{1}{L_2}\right)} \right)$$
$$= V_i T_1 + V_o T_2 \tag{2.123a}$$

$$V_0 = V_x \left(\frac{s^2 + \frac{1}{L_2 C_2}}{s^2 + \frac{s}{C_2 R_2} + \frac{1}{C_2}\left(\frac{1}{L_2} + \frac{1}{L_3}\right)} \right) = V_x T_3 \tag{2.123b}$$

Thus these two equations enable us to construct the block diagram of Fig. 2.35b where T_1, T_2, and T_3 are biquadratic transfer functions. Note also that T_1 and T_2 share the same denominator. The Tow–Thomas biquad circuit with appropriate

feedforward branches as shown in Fig. 2.35c can realize a band-pass and notch transfer function at the same output terminal, however, with a negative sign (i.e., $-V_x$ is realized). A similar circuit with only the input to realize a notch transfer function, can be used to realize (2.123b). Since this transfer function also is an inverting type, the desired V_o will be realized. Interconnection of these two second-order filters will realize the complete band-pass filter as shown in Fig. 2.35d. Note that as compared to the low-pass elliptic filter, two opamps forming a noninverting integrator are additionally needed. The equivalent circuit realized can be drawn as shown in Fig. 2.35e.

Note that in the case of all-pole high-pass filters, the inductor L_2 will be absent and hence, the resistors $(L_1 + L_2)/L_1$ and $(L_2 + L_3)/L_3$ are not needed (they do not exist) and the capacitor values $L_1L_2/(L_1 + L_2)$ and $L_2L_3(L_2 + L_3)$ become L_1 and L_3, respectively. The voltages V_y and V_z correspond to the currents through the shunt inductors in the equivalent circuit of Fig. 2.35e which need to be estimated to determine their peak values to facilitate scaling for optimal dynamic range.

2.9.5 *Operational Simulation of General-Parameter Ladder Filters*

Note that Yoshihoro's method can easily be used for general-parameter ladder filters as well [2.63]. Note that these general-parameter filters are not derived from the low-pass prototypes using frequency transformation. As an illustration, consider the twelfth-order band-pass filter of Fig. 2.36a. The block diagram shown in Fig. 2.36b can be easily obtained. The various band-pass and notch transfer functions are as follows.

Biquad 1:

$$T_{i1} = \left(\frac{\frac{s}{C_2 R_s}}{s^2 + \frac{s}{C_2 R_s} + \frac{1}{C_2}\left(\frac{1}{L_1} + \frac{1}{L_2}\right)} \right) \tag{2.124a}$$

$$T_{31} = \left(\frac{s^2 + \frac{1}{L_2 C_2}}{s^2 + \frac{s}{C_2 R_s} + \frac{1}{C_2}\left(\frac{1}{L_1} + \frac{1}{L_2}\right)} \right) \tag{2.124b}$$

Biquad 2:

$$T_{13} = \left(\frac{C_2}{C_2 + C_3 + C_4} \frac{s^2 + \frac{1}{L_2 C_2}}{s^2 + \frac{1}{(C_2 + C_3 + C_4)}\left(\frac{1}{L_2} + \frac{1}{L_4}\right)} \right) \tag{2.124c}$$

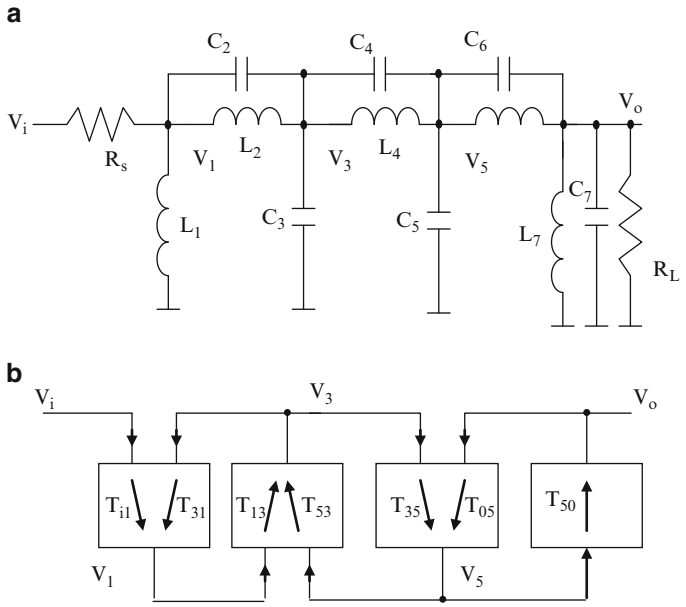

Fig. 2.36 (**a**) A general-parameter filter prototype, (**b**) block diagram of the filter obtained from (a) using Yoshihoro's method (Adapted from [2.63] ©IEEE 1980)

$$T_{53} = \left(\frac{C_4}{C_2 + C_3 + C_4} \frac{s^2 + \frac{1}{L_4\, C_4}}{s^2 + \frac{1}{(C_2 + C_3 + C_4)} \left(\frac{1}{L_2} + \frac{1}{L_4} \right)} \right) \tag{2.124d}$$

Biquad 3:

$$T_{35} = \left(\frac{C_4}{C_4 + C_5 + C_6} \frac{s^2 + \frac{1}{L_4\, C_4}}{s^2 + \frac{1}{(C_4 + C_5 + C_6)} \left(\frac{1}{L_4} + \frac{1}{L_6} \right)} \right) \tag{2.124e}$$

$$T_{05} = \left(\frac{C_6}{C_4 + C_5 + C_6} \frac{s^2 + \frac{1}{L_6\, C_6}}{s^2 + \frac{1}{(C_4 + C_5 + C_6)} \left(\frac{1}{L_4} + \frac{1}{L_6} \right)} \right) \tag{2.124f}$$

Biquad 4:

$$T_{50} = \left(\frac{C_6}{C_6 + C_7} \frac{s^2 + \frac{1}{L_6\, C_6}}{s^2 + s \frac{1}{(C_6 + C_7) R_L} + \frac{1}{(C_6 + C_7)} \left(\frac{1}{L_6} + \frac{1}{L_7} \right)} \right) \tag{2.124g}$$

Since only band-pass and notch transfer functions are needed, the biquad of Fig. 2.35c can be used to obtain the complete circuit. Note that scaling can be done easily by knowing the maxima of all the voltages at various nodes in the prototype circuit. There is no need to compute the various inductor currents.

2.10 Multiloop Feedback-Based Active RC Filters

We next consider another technique for realizing high-order filters with low sensitivity. This is known as multiple-loop feedback [2.64]. There are various options available for the filter designer choosing this technique. These are discussed next.

2.10.1 FLF (Follow-the-Leader Feedback)

The follow-the-leader feedback structure is shown in Fig. 2.37a. This structure is designed to realize a low-pass prototype transfer function at output V_o. Usually, for convenience all the blocks $T_1 - T_n$ can be chosen to be identical. Using LP to BP transformation, a $2n$th-order band-pass filter can be realized. The multipliers β_i and summer are realized using one opamp and various resistors. The various q_is can be positive or negative depending on the required transfer function. The transfer function of this circuit can be derived as

$$\frac{V_o}{V_i} = -\frac{p_1\,(\beta_1 + \beta_2\,T_1 + \beta_3\,T_1\,T_2 + \beta_4\,T_1\,T_2\,T_3)}{1 + q_1\,T_1 + q_2\,T_1\,T_2 + T_1\,T_2\,T_3\,q_3} \tag{2.125}$$

Considering a first-order low-pass filter with transfer function $\frac{a}{s+a}$ to be used for all T_is, the denominator of the transfer function can be seen to be (after multiplying with $(s + a)^3$)

$$D(s) = s^3 + s^2\,a(3 + q_1) + s\,a^2\,(3 + 2\,q_1 + q_2) + a^3\,(1 + q_1 + q_2 + q_3) \tag{2.126}$$

From the desired denominator of the transfer function, the various q_i values and a need to be determined. The next step is to determine various β_i values to obtain the desired transfer function by matching the coefficients of s, s^2, and s^3 terms in the numerator. In the third-order case, the equations obtained are linear and can be solved for q_1, q_2, and q_3 choosing a. Solutions that give positive values for various q_i are preferable to avoid additional opamps. The value of a can be chosen so that q_1 is positive and iteratively, q_2 and q_3 values can be calculated by matching the coefficients. Note that all the blocks can also have different transfer functions.

The individual blocks are of second-order band-pass type after LP → BP transformation and have the same center frequency ω_o. Their transfer function with pole-frequency normalized ω_o to unity is given by

$$T_i(s) = H_i \frac{\left(\frac{s}{Q_i}\right)}{s^2 + \frac{s}{Q_i} + 1} \tag{2.127}$$

where H_i is the midband gain.

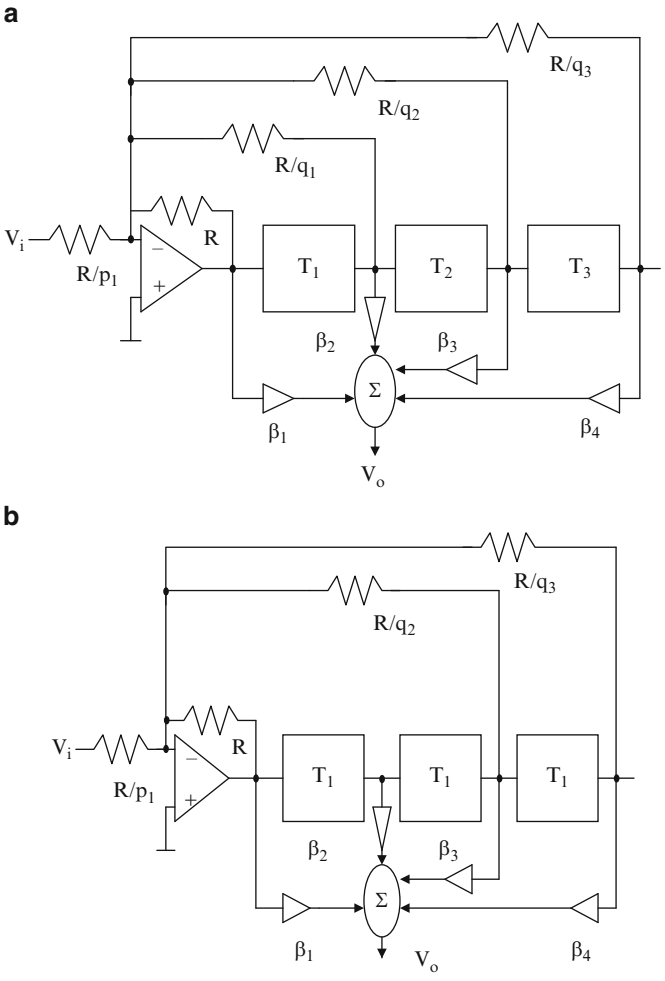

Fig. 2.37 Multiple-loop feedback structures of various types: (**a**) FLF, (**b**) PRB, (**c**) SCF, (**d**) MLF, (**e**) IFLF, and (**f**) MSF ((**d–f**) Adapted from [2.64] ©IEEE 1979)

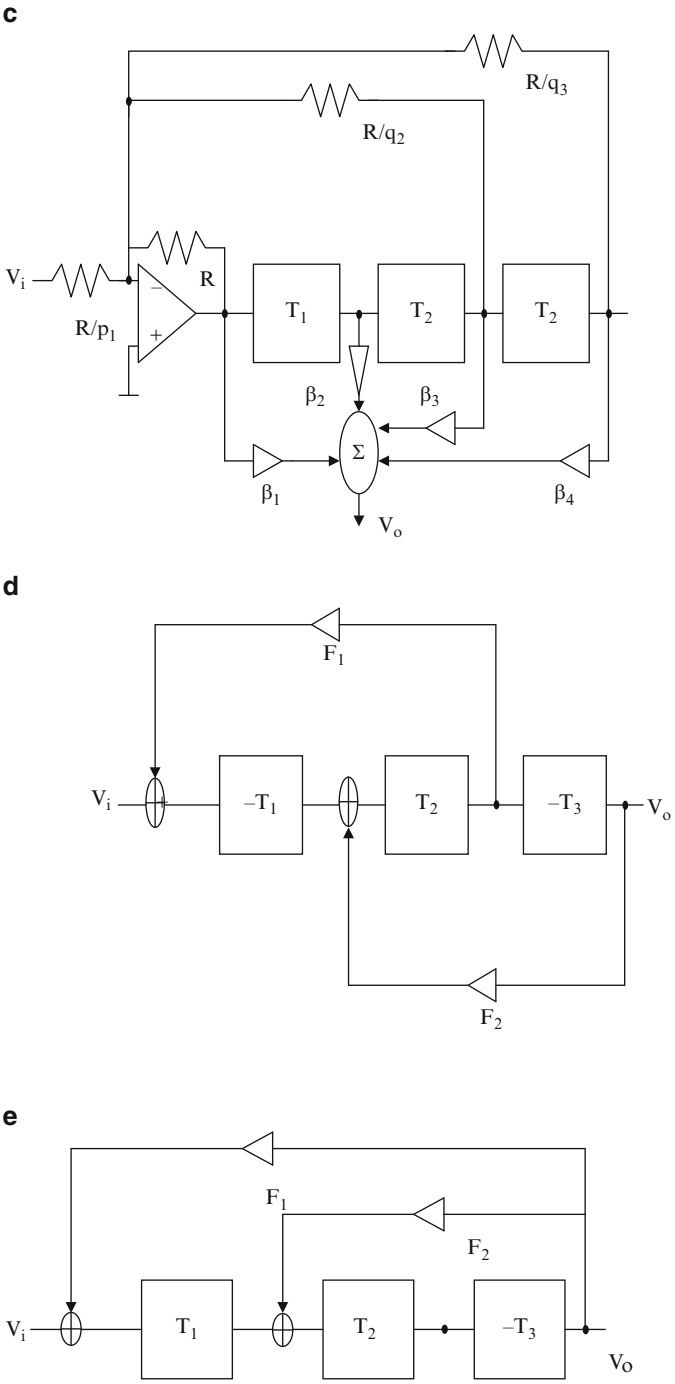

Fig. 2.37 (continued)

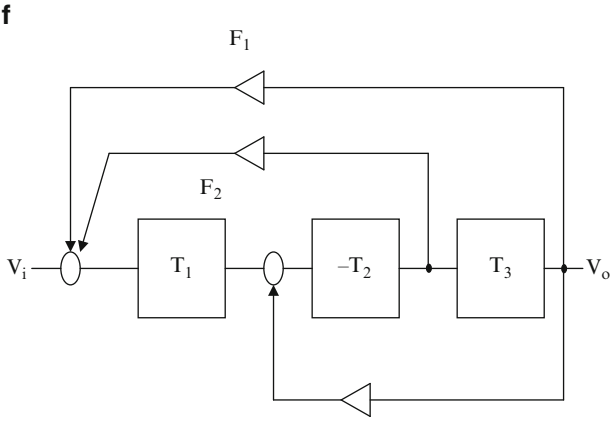

Fig. 2.37 (continued)

2.10.2 PRB (Primary Resonator Block) Structure

The PRB (primary resonator block) shown in Fig. 2.37b is a special case of FLF and is obtained by deleting the first feedback loop, that is, by making $q_1 = 0$. Note also that all blocks are identical in this case. For the third-order case, from (2.126), we obtain the denominator of the transfer function as

$$D(s) = s^3 + 3a\,s^2 + s\,a^2\,(3 + q_2) + a^3\,(1 + q_2 + q_3) \tag{2.128}$$

Thus, a can be obtained from the desired denominator of the transfer function directly and using this value, q_2 and q_3 can be determined. This structure is easier to design. Note that the use of identical blocks reduces the engineering effort such as the design of the filter and enhances reproducibility. The circuit cannot be scaled for optimal dynamic range since all blocks have the same gain H_i. As an illustration for the realization of the third-order Butterworth transfer function whose denominator is $s^3 + 2s^2 + 2s + 1$, the design values are $a = 2/3$, $q_2 = 3/2$, and $q_3 = 7/8$.

2.10.3 SCF (Shifted Companion Form) Structure

We next consider another multiloop feedback technique as shown in Fig. 2.37c. Note that this structure is a modification of FLF obtained by removing the first feedback loop and making all the blocks $T_2, T_3, \ldots, T_{n-1}, T_n$ identical whereas T_1 is

different. Denoting the gain of the block T_1 as H_1 and that of the other blocks as H_2, the resulting denominator of the transfer function is given as

$$D(s) = s^3 + 3a\,s^2 + s\,a^2\,(3 + q_2\,H_1\,H_2) + a^3\,(1 + q_2\,H_1\,H_2 + q_3\,H_1\,H_2^2) \tag{2.129}$$

A comparison of (2.128) and (2.129) shows that although the a value is the same, $q_2H_1H_2$ and $q_3H_1H_2^2$ can be determined iteratively. The additional degrees of freedom in H_1 and H_2 can help to optimize the dynamic range.

2.10.4 Multiloop Feedback (MLF) Structure

The multiloop feedback (MLF) structure shown in Fig. 2.37d is similar to the leap-frog structure. However, note that in the leap-frog structure, the intermediate blocks have an infinite Q-factor and terminating blocks have a finite pole-Q. On the other hand, in a MLF structure, the individual blocks can have finite pole-Qs. This may be a benefit in practical situations where nonidealities of active or passive devices make the circuit Q finite. Note that the feedforward portion is not shown in Fig. 2.37d.

2.10.5 IFLF (Inverse Follow-the-Leader Feedback) Structure

In the IFLF (inverse follow-the-leader feedback) structure of Fig. 2.37e, the output is weighted and fed to the inputs of various blocks. The transfer function of this circuit can be seen to be

$$\frac{V_o}{V_i} = -\frac{T_3}{1 + F_2\,T_2\,T_3 + F_1\,T_1\,T_2\,T_3} \tag{2.130}$$

Note that this transfer function is similar to that of the FLF structure given in (2.125) with $q_1 = 0$.

2.10.6 MSF (Minimum Sensitivity Feedback) Structure

We finally consider a generalized version known as MSF (minimum sensitivity feedback) shown in Fig. 2.37f from which all other configurations can be derived. The transfer function of this circuit is given as

$$\frac{V_o}{V_i} = -\frac{T_1\ T_2\ T_3}{1 + F_2\ T_1\ T_2 + F_3\ T_2\ T_3 + F_1\ T_1\ T_2\ T_3} \tag{2.131}$$

Laker, Schaumann, and Ghausi [2.64] have thoroughly investigated all these structures given in Fig. 2.37a–f. Their recommended design procedure is to choose all the center frequencies the same. The gains and Q_is can, however, be different and chosen a priori. Then, the feedback coefficients are selected to minimize the sensitivity of the realized filters. The sensitivity can be considered to be of two parts: one due to the individual T_i block and another due to the feedback. Their sensitivity evaluation considered the passive sensitivities only. They have also assumed that statistical correlation among components exists only within a section.

The PRB type, FLF, and IFLF types do not need any sensitivity optimization. Only MSF-type filters need optimization. In these, the high-Q sections are not necessarily most critical. Optimized LF and MLF active filters yield the lowest sensitivities in the pass-band. Optimized FLF active filters generally yield lower sensitivities than LF designs at the band edges and in the stop-band. The typical results for a three-section Butterworth band-pass filter are presented in Fig. 2.38. It can be seen that the RLC filter exhibits good performance and cascade design is poorest among these. Among others, FLF gives the best performance. The reader is referred to [2.64] for an exhaustive discussion on the design of multiloop feedback filters.

2.11 Noise in Active RC Filters

The dynamic range of active RC filters is limited by the noise in active RC filters. The noise arises because of two sources: (a) resistor noise (also called *inherent noise* excluding noise of resistors used for canceling dc offset), and (b) noise due to opamp. The opamp noise can be modeled by an input referred noise voltage source and noise current source as shown in Fig. 2.39b whereas a resistor noise can be modeled as shown in (a). The contribution due to the noise current source is dependent on the resistances in the active RC filter whereas the noise voltage source is independent of the resistances. The noise voltage and current sources are specified by the noise power spectral density expressed as voltage square/Hertz and current square/Hertz. Thus, depending on the frequency band of measurement, these will be weighted to obtain the total noise by adding them since they are uncorrelated. The resistor noise of a resistor R is modeled by a noise voltage source e_{nr} in series with an ideal noise-free resistor R and the power spectral density is expressed as

$$e_{nr}^2 = 4kTRB \tag{2.132}$$

where k is Boltzmann's constant $1.3806503 \times 10^{-23}$ J/K and T is the absolute temperature in degrees with B the bandwidth of the measurement.

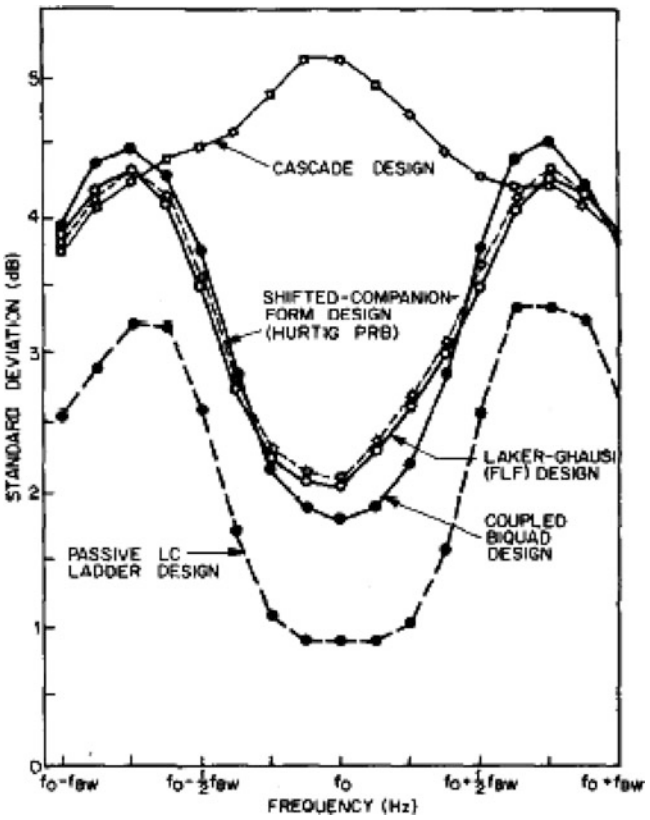

Fig. 2.38 Monte Carlo simulation results of sixth-order Butterworth (three-section) filters of different topologies with passive component tolerance assumed 1.732% (Adapted from [2.64] ©IEEE 1979)

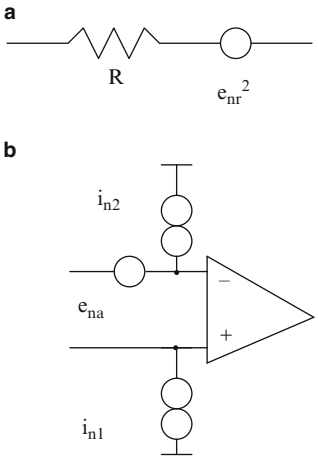

Fig. 2.39 Noise models (**a**) of a resistor, and (**b**) of an opamp

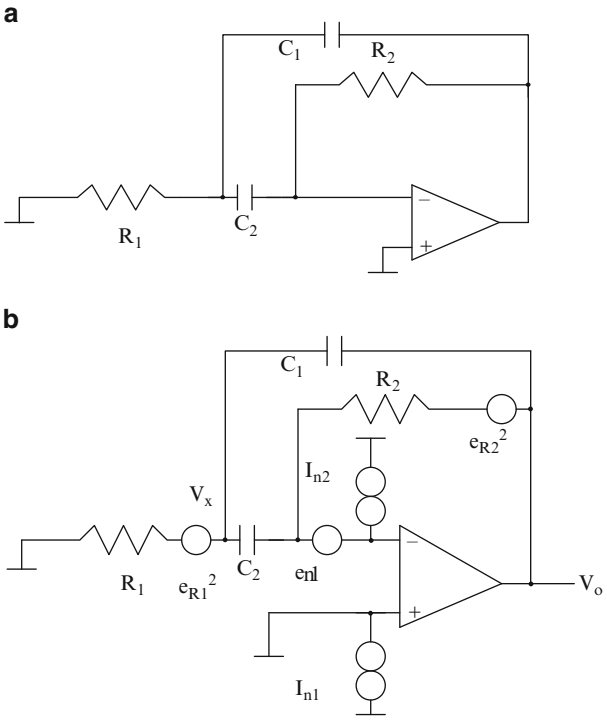

Fig. 2.40 (**a**) A multiple feedback active RC filter, and (**b**) circuit of (**a**) with various noise sources

The noise analysis of active devices and resistors can be carried out in one analysis and then estimated [2.65, 2.66]. As an illustration, consider the single amplifier band-pass filter of Fig. 2.40a. The noise equivalent circuit is as shown in Fig. 2.40b. Analyzing the circuit in the usual manner, considering the noise voltage source as a noise voltage and noise current source as a current without worrying about the fact that they are power spectral densities, first the node equations can be written as follows.

$$\frac{e_{R1}}{R_1} + V_o\, s\, C_1 + e_{n1}\, s\, C_2 = V_x \left(\frac{1}{R_1} + s(C_1 + C_2) \right) \tag{2.133a}$$

$$\frac{V_o + e_{R_2}}{R_2} + V_x\, s\, C_2 + I_{n2} = e_{n1} \left(\frac{1}{R_2} + s\, C_2 \right) \tag{2.133b}$$

Solving these two equations, we obtain

$$V_o = -\frac{\left(\begin{array}{l} \frac{e_{R1}\, s}{C_1 R_1} + e_{R_2} \left(\frac{1}{C_1 C_2 R_1 R_2} + \frac{s(C_1 + C_2)}{C_1 C_2 R_2} \right) \\ - e_{n1} \left(\frac{s}{C_1 R_1} + \frac{s(C_1 + C_2)}{C_1 C_2 R_2} + s^2 + \frac{1}{R_1 R_2 C_1 C_2} \right) + I_{n2} \left(\frac{1}{C_1 C_2 R_1} + \frac{s(C_1 + C_2)}{C_1 C_2} \right) \end{array} \right)}{s^2 + \frac{s(C_1 + C_2)}{R_2 C_1 C_2} + \frac{1}{R_1 R_2 C_1 C_2}} \tag{2.134a}$$

It can be seen that the four noise sources have different noise transfer functions. We next express (2.134a) as

$$V_o = -(e_{R1}\, H_1(s) + e_{R2}\, H_2(s) + e_{n1}\, H_3(s) + I_{n2}\, H_4(s)) \tag{2.134b}$$

Note that $H_1(s)$, $H_2(s)$, and $H_3(s)$ are dimensionless whereas $H_4(s)$ corresponds to a resistance. The total output noise e_{nt} can be found as

$$e_{nt}^2 = \left(\begin{array}{l} e_{R1}^2 \displaystyle\int_0^\infty |H_1(j\omega)|^2 d\omega + e_{R2}^2 \int_0^\infty |H_2(j\omega)|^2 d\omega + e_{n1}^2 \int_0^\infty |H_3(j\omega)|^2 d\omega \\ + I_{n2}^2 \displaystyle\int_0^\infty |H_4(j\omega)|^2\, d\omega \end{array} \right) \tag{2.135}$$

Bruton, Trofimenkoff, and Treleaven [2.65, 2.66] have given closed-form expressions for these integrals for general biquadratic transfer functions. The low-pass and band-pass transfer functions have simple solutions:

$$\int_0^\infty \left| \frac{s\,\omega_p}{s^2 + s\frac{\omega_p}{Q_p} + \omega_p^2} \right|_{s=j\omega}^2 d\omega = \frac{Q_p\,\pi\,\omega_p}{2} \tag{2.136a}$$

$$\int_0^\infty \left| \frac{\omega_p^2}{s^2 + s\frac{\omega_p}{Q_p} + \omega_p^2} \right|_{s=j\omega}^2 d\omega = \frac{Q_p\,\pi\,\omega_p}{2} \tag{2.136b}$$

Applying these relationships, corresponding to a general biquadratic transfer function given as

$$H(s) = \frac{a\,s^2 + bs + c}{s^2 + s\left(\frac{\omega_p}{Q_p}\right) + \omega_p^2} \tag{2.137}$$

we obtain the noise spectral density as

$$|H_1(j\omega)|^2 = a^2 + \frac{\omega^2\ \omega_p^2 \left(\frac{b^2 - 2ac}{\omega_p^2} - \frac{a^2}{Q_p^2} + 2\,a^2 \right)}{D} + \frac{\omega_p^4 \left(\frac{c^2}{\omega_p^4} - a^2 \right)}{D} \tag{2.138}$$

where

$$D = \omega^4 + \omega^2 \left(\frac{\omega_p^2}{Q_p^2} - 2\,\omega_p^2 \right) + \omega_p^4 \tag{2.139}$$

Hence, (2.138) can be written as

$$|H_1(j\omega)|^2 = a^2 + \left(\frac{b^2 - 2ac}{\omega_p^2} - \frac{a^2}{Q_p^2} + 2a^2\right)|H_{BP}(j\omega)|^2 + \left(\frac{c^2}{\omega_p^4} - a^2\right)|H_{LP}(j\omega)|^2$$
$$= a^2 B_x + \left(\frac{b^2 - 2ac}{\omega_p^2} - \frac{a^2}{Q_p^2} + a^2 + \frac{c^2}{\omega_p^4}\right)|H_{BP}(j\omega)|^2 \tag{2.140}$$

where B_x is the measurement bandwidth since from (2.136a) and (2.136b), $\int_0^\infty |H_{LP}(j\omega)|^2 d\omega$ and $\int_0^\infty |H_{BP}(j\omega)|^2 d\omega$ are the same. Thus from (2.140), it follows that

$$|H_1(j\omega)|^2 = a^2 B_x + \left(\frac{b^2 - 2ac}{\omega_p^2} - \frac{a^2}{Q_p^2} + a^2 + \frac{c^2}{\omega_p^4}\right)\frac{Q_p \pi \omega_p}{2} \tag{2.141}$$

As an illustration, for the high-pass case ($b = c = 0$), we have

$$|H_1(j\omega)|^2 = a^2 B + \left(-\frac{a^2}{Q_p^2} + a^2\right)\frac{Q_p \pi \omega_p}{2} \tag{2.142}$$

For the noise source e_{R2}, matching the noise transfer function (2.134a) with (2.137), we note that $a = 0, b = \frac{C_1 + C_2}{C_1 C_2 R_2}, c = \frac{1}{C_1 C_2 R_1 R_2}$ and from the general formula (2.141), we obtain the noise as $e_{R_2}^2 \left(1 + \frac{(C_1 + C_2)^2 R_1}{C_1 C_2 R_2}\right)|H_{LP}(j\omega)|^2$. In a similar manner, we obtain the total noise of the circuit of Fig. 2.40a from (2.135) as

$$e_{tn}^2 = e_{R_1}^2 \frac{1}{\omega_p^2 C_1^2 R_1^2}|H_{LP}(j\omega)|^2 + e_{R_2}^2\left(1 + \frac{(C_1 + C_2)^2 R_1}{C_1 C_2 R_2}\right)|H_{LP}(j\omega)|^2$$
$$+ i_{n2}^2\left(R_2^2 + \frac{(C_1 + C_2)^2 R_1 R_2}{C_1 C_2}\right)|H_{LP}(j\omega)|^2$$
$$+ e_{n1}^2\left(B_x + |H_{LP}(j\omega)|^2\left(\frac{1}{\omega_p^2 C_1^2 R_1^2} + \frac{2}{\omega_p Q_p C_1 R_1}\right)\right) \tag{2.143}$$

Substituting for the integrals using (2.136), we have

$$e_{tn}^2 = \left(\begin{array}{l} e_{R_1}^2 \frac{1}{\omega_p^2 C_1^2 R_1^2} + e_{R_2}^2\left(1 + \frac{(C_1 + C_2)^2 R_1}{C_1 C_2 R_2}\right) + i_{n2}^2\left(R_2^2 + \frac{(C_1 + C_2)^2 R_1 R_2}{C_1 C_2}\right) \\ + e_{n1}^2\left(\frac{1}{\omega_p^2 C_1^2 R_1^2} + \frac{2}{\omega_p Q_p C_1 R_1}\right) \end{array}\right)\frac{Q_p \pi \omega_p}{2}$$
$$+ e_{n1}^2 B_x \tag{2.144}$$

It is seen that the active noise (decided by i_{n2} and e_{n1}) and passive noise (decided by e_{R1} and e_{R2}) are dependent on the resistor and capacitor values. These can be optimized by appropriate design.

In active RC filters, the active noise can be made low by using low-noise opamps so that the resistor noise is dominant.

Consider, for example, the case $C_1 = C_2$. Evidently, for this choice in the circuit of Fig. 2.40a, we have $Q_p = \frac{1}{2}\sqrt{\frac{R_2}{R_1}}$ and $\omega_p - = \frac{1}{2Q_p\ C_1\ R_1}$ yielding from (2.144),

$$e_{tn}^2 = \left(\frac{2kT}{\pi}\left(R_2\left(2+\frac{1}{Q_p^2}\right)\right) + i_{n2}^2\ R_2^2\left(1+\frac{1}{Q_p^2}\right) + e_{n1}^2\left(4Q_p^2+4\right)\right)\frac{Q_p\,\pi\,\omega_p}{2} + e_{n1}^2\ B_x \tag{2.145}$$

Generally i_{n1} and i_{n2} of the opamp will be very small, typically $0.1\text{pA}/\sqrt{Hz}$, and hence the term containing i_{n1} can be neglected. As an illustration, for realizing $Q_p = 5$ and a pole-frequency $f_p = 1{,}000$ Hz, we obtain $\frac{R_2}{R_1} = 100$. Next, choosing $R_1 = 1\ \text{K}\Omega$ and $R_2 = 100\ \text{K}\Omega$ and considering $C_1 = C_2 = C$, we have $C = 15{,}923$ pF. Considering a typical opamp with $e_{nI} = 15$ nV/√Hz, the total noise can be found from (2.145) as

$$e_{tn}^2 = (1155.673 + 26.53)\ 10^{-12}$$

where the first term is inherent noise (passive noise) and the second term is active noise. The rms noise can be found by finding the square root of ${e_{nt}}^2$ and is thus 34.38 μV. The active noise is more than the passive noise for this circuit.

For single-amplifier filters, Bachler and Guggenbuhl [2.67, 2.68] have suggested that the passive noise can be modeled by a noise voltage source at the inverting input of the opamp and the equivalent noise resistance can be estimated as $\text{Re}\left(\frac{1}{y_{22}}\right)$ where $\left(\frac{1}{y_{22}}\right)$ is the equivalent resistance at the inverting input of the opamp with the opamp disconnected and grounding the terminal connected to the opamp output terminal and input terminal of the filter (see Fig. 2.41a). As an illustration, for the circuit of Fig. 2.41a, we have

$$\text{Re}\left(\frac{1}{y_{22}}\right) = \frac{R_2\left(1+\omega^2\left(C_2^2\ R_1\ R_2 + 2R_1^2\ C_1\ C_2 + C_2^2\ R_1^2 + C_1^2\ R_1^2\right)\right)}{\left(1-\omega^2\ R_1\ R_2\ C_1\ C_2\right)^2 + \omega^2\ \left(C_1\ R_1 + C_2\ R_1\right)^2} \tag{2.146}$$

The noise can then be evaluated from the model shown in Fig. 2.41b. Note that e_{np} and e_{na} are the active and passive noise contributions which have the same transfer function that has already been derived in (2.134a) (see e_{n1} term). Note that the denominator in (2.146) cancels with the squared magnitude of the coefficient of the e_{n1} term in (2.134a) yielding the same result as before. The total passive noise

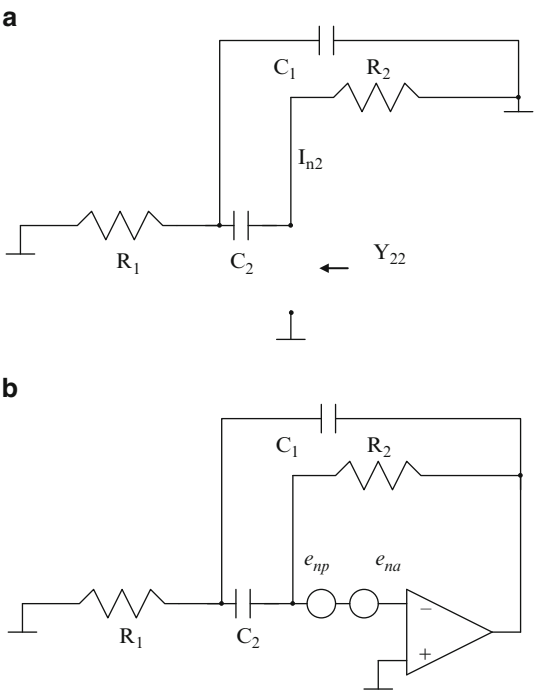

Fig. 2.41 (**a**) Circuit for estimation of passive noise of the active RC filter of Fig. 2.40b, (**b**) complete noise model

can be estimated by integrating $\frac{2kT}{\pi}\text{Re}\left(\frac{1}{y_{22}}\right)|H_n(j\omega)|^2$ where $H_n(s)$ is the transfer function of the noise source to the output of the filter. The same result can be obtained by combining the noise due to R_1 and R_2 in (2.144)

Bachler and Guggenbuhl [2.67, 2.68] have also pointed out that the noise transfer function is the same as GSP which is shown next. Considering the circuit of Fig. 2.42a, the transfer function can be written as

$$T = -\frac{t_{31}}{t_{32} + \frac{1}{A}} \tag{2.147}$$

where t_{31} is the transfer function of the three- terminal network at terminal 3 with input given at terminal 1. The GSP can then be derived as

$$GSP = A\, S_A^T = \frac{1}{t_{32} + \frac{1}{A}} \cong \frac{1}{t_{32}} \tag{2.148}$$

Next considering the noise source as shown in Fig. 2.42b, the transfer function is given as

$$\frac{V_0}{e_n} = \frac{1}{t_{32}} \tag{2.149}$$

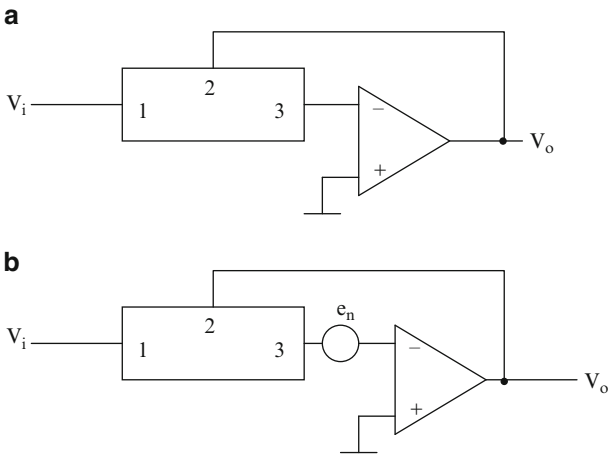

Fig. 2.42 (**a**) Circuit for estimating the GSP of an active RC circuit, and (**b**) circuit for noise estimation

From (2.148) and (2.149), we see that the GSP is the same as the noise transfer function. Note from (2.148) that the GSP is a function of frequency. It may be recalled that in our earlier definition of the GSP with respect to A, the finite gain of the opamp, the GSP was found to be dimensionless. Even though the GSP defined by (2.148) is frequency-dependent, it can be shown that the GSP value at the pole-frequency is equal to the GSP with respect to A (i.e., AS^{Q}_{A}). Thus minimizing the GSP by the proper choice of resistors and capacitor values (spreads) to reduce the active sensitivity will lead to minimization of active noise of an active RC filter, an interesting result. It is useful to note that since the passive noise is also dependent on $\mathrm{Re}\left(\frac{1}{y_{22}}\right)$, optimization of the GSP alone may not reduce passive noise.

The total noise of the filter is the sum of active and passive noise. Bachler and Guggenbuhl [2.67, 2.68] have shown that the total noise using the spread of components as a degree of freedom can be computed and optimized. This is similar to sensitivity optimization which has passive and active components. The reader is referred to their work for more information.

The application of minimization of the GSP to reduce noise has been extended to the minimization of distortion as well by Borys [2.73]. This aspect is considered next after studying distortion in active RC filters.

We consider SPICE-based estimation of noise of active RC filters in the next two examples.

Example 2.12 The noise voltage source will have thermal noise as well as $1/f$ noise components. These can be modeled using resistor and diode noise biased in the knee region. The amount of $1/f$ noise can be controlled by the value KF in the diode model. The biasing voltage can be defined, for example, as $V_1\ (= V_2) = 0.1$ V and a resistor R_{30} (and R_{31}) is used in series with the diode D_1 (and D_2) to generate wide-band noise. Two such independent circuits are used and the floating voltage

between these (nodes 59 and 61) is taken to remove the dc component. The noise statement has an ac reference point which in this case is one zero voltage source v_3 connected in series. The total noise as well as its various constituents such as diode resistance noise, $1/f$ noise, resistor noise, and the like, can be found by the command *print all*. The noise spectrum can be seen by the command *plot ylog onoise_spectrum*. Note also that input referred noise also can be obtained.

```
*opamp voltage noise generation
V3 58 0 ac 0
V1 58 65 dc 0.1
V2 60 0 0.1
D1 65 59 DIODE
R30 59 0 726.4
D2 60 61 DIODE
R31 61 0 726.4
E1 1 0 59 61 1

.MODEL DIODE D(AF=1.0,IS=0.001F,KF=1.667E-9)
.noise v(1) v3 dec 10 0.5 1000 1
```

```
*Opamp voltage noise generation
V3 58 0 ac 0
V1 58 65 dc 0.1
V2 60 0 0.1
D1 65 59 DIODE
R30 59 0 726.4
D2 60 61 DIODE
R31 61 0 726.4
E1 1 0 59 61 1

.MODEL DIODE D(AF=1.0,IS=0.001F,KF=1.667E-9)
.noise v(1) v3 dec 10 0.5 1000 1
```

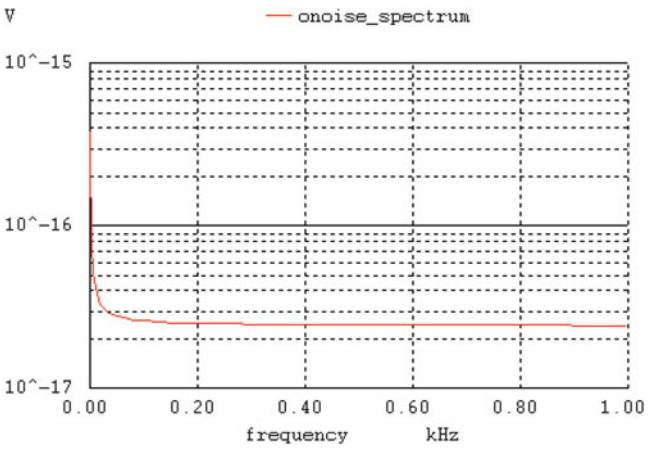

Circuit: *Opamp voltage noise generation
TEMP=27 deg C
Noise analysis ... 100%
WinSpice 3 -> print all
inoise_total = 2.534923e+06
inoise_total_d1 = 6.683765e+04
inoise_total_d1_1overf = 6.683765e+04
inoise_total_d1_id = 1.685981e-03
inoise_total_d1_rs = 0.000000e+00
inoise_total_d2 = 6.686825e+04
inoise_total_d2_1overf = 6.686825e+04
inoise_total_d2_id = 1.686753e-03
inoise_total_d2_rs = 0.000000e+00
inoise_total_r30 = 1.200609e+06
inoise_total_r31 = 1.200609e+06
onoise_total = 2.534923e-14
onoise_total_d1 = 6.683765e-16
onoise_total_d1_1overf = 6.683765e-16
onoise_total_d1_id = 1.685981e-23
onoise_total_d1_rs = 0.000000e+00
onoise_total_d2 = 6.686825e-16
onoise_total_d2_1overf = 6.686825e-16
onoise_total_d2_id = 1.686753e-23
onoise_total_d2_rs = 0.000000e+00
onoise_total_r30 = 1.200609e-14
onoise_total_r31 = 1.200609e-14

Example 2.13 The analysis of a multiple feedback band-pass filter using the opamp noise model obtained earlier is considered next. An offset compensating resistor R_3 is also used.

The complete noise model is in the subcircuit *noisyopamp*. Note that the opamp input terminals have noisy current sources which do not have a $1/f$ component and hence simple resistors can be used. The resistors R_{32} and R_{33} need to be in a closed circuit and hence zero voltage sources V17 and V18 are connected across them. The current sources are implemented by the statements FN1 in. 0 V18 1 and FN2 ninp 0 V17 1, respectively. As before the total output referred noise, input referred noise, and noise spectrum can be found as shown. The band-pass filtering of the noise spectrum is evident.

*Example MFB noise analysis
R1 1 2 62.5
R2 4 3 100 K
C1 2 3 1590 pf
C2 2 4 1590 pf
R3 71 0 62.5

```
Xopamp1 4 71 3 noisyopamp
.subckt noisyopamp 70 ninp out
V1 58 0 dc 0.1
V2 60 0 dc 0.1
D1 58 59 DIODE
R30 59 0 726.4
D2 60 61 DIODE
R31 61 0 726.4
E1 70 in. 59 61 1
V17 62 0 0
V18 63 0 0
R32 62 0 73.6
R33 63 0 73.6
FN1 in. 0 V18 1
FN2 ninp 0 V17 1

E2 15 0 ninp inp 100,000
R4 15 16 1 k
C3 16 0 15.9 uf
E3 out 0 16 0 1
.ends noisyopamp

vin 1 0 ac 0
.noise v(3) vin dec 10 0.5 300,000 1

.MODEL DIODE D(AF=1.0,IS=0.001F,KF=1.667E-9)
```

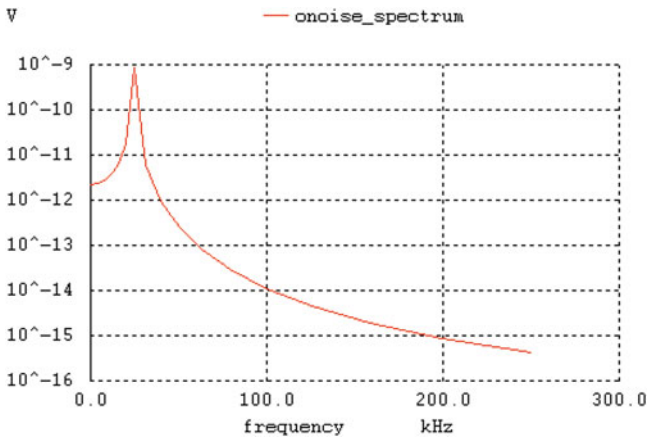

Circuit: *example MFB noise analysis

TEMP=27 deg C
Noise analysis . . . 100%
WinSpice 4 -> print all

inoise_total = 2.408588e+14
inoise_total_d:xopamp1:d1 = 2.305272e+08
inoise_total_d:xopamp1:d1_1overf = 2.305261e+08
inoise_total_d:xopamp1:d1_id = 1.118864e+03
inoise_total_d:xopamp1:d1_rs = 0.000000e+00
inoise_total_d:xopamp1:d2 = 2.305272e+08
inoise_total_d:xopamp1:d2_1overf = 2.305261e+08
inoise_total_d:xopamp1:d2_id = 1.118864e+03
inoise_total_d:xopamp1:d2_rs = 0.000000e+00
inoise_total_r1 = 6.830456e+10
inoise_total_r2 = 1.758265e+11
inoise_total_r3 = 6.852223e+10
inoise_total_r:xopamp1:r4 = 1.096356e+02
inoise_total_r:xopamp1:r30 = 7.963928e+11
inoise_total_r:xopamp1:r31 = 7.963928e+11
inoise_total_r:xopamp1:r32 = 5.818804e+10
inoise_total_r:xopamp1:r33 = 2.388947e+14
onoise_total = 2.408588e-06
onoise_total_d:xopamp1:d1 = 2.305272e-12
onoise_total_d:xopamp1:d1_1overf = 2.305261e-12
onoise_total_d:xopamp1:d1_id = 1.118864e-17
onoise_total_d:xopamp1:d1_rs = 0.000000e+00
onoise_total_d:xopamp1:d2 = 2.305272e-12
onoise_total_d:xopamp1:d2_1overf = 2.305261e-12
onoise_total_d:xopamp1:d2_id = 1.118864e-17
onoise_total_d:xopamp1:d2_rs = 0.000000e+00
onoise_total_r1 = 6.830456e-10
onoise_total_r2 = 1.758265e-09
onoise_total_r3 = 6.852223e-10
onoise_total_r:xopamp1:r4 = 1.096356e-18
onoise_total_r:xopamp1:r30 = 7.963928e-09
onoise_total_r:xopamp1:r31 = 7.963928e-09
onoise_total_r:xopamp1:r32 = 5.818804e-10
onoise_total_r:xopamp1:r33 = 2.388947e-06

2.12 Distortion in Active RC Filters

The large signal handling capability of active filters implies the use of components that collectively exhibit a linear behavior, even though the active components may be intrinsically nonlinear, such as bipolar transistors or MOS transistors. In a differential amplifier, the basic element in the opamp, the nonlinearity arises for two reasons: nonlinear V−I conversion of the input differential pair and the voltage dependence of the output impedance of the cascade devices.

If an opamp is overdriven by a large input signal, the output slews at some limiting rate determined by internal currents and capacitances. If an applied sinusoidal input signal causes the output to have the maximum slope greater than the slew rate of the opamp, the output will no longer be sinusoidal and will suffer distortion. There can be *slew-induced distortion* (SID) of amplitude in the open-loop mode of the amplifier operation but phase distortion may not exist. On the other hand, in the closed-loop mode, both will exist. Under typical operating conditions, the SID causes phase shift (phase lag) and an attenuation of the fundamental component of the input signal at the output. In active RC filters, the OA slew rate can cause distortion by creating harmonics and intermodulation products. Such degradation can lead to instability and this phenomenon is called "*jump resonance*." In such a situation, the filter will exhibit two modes of operation and will regeneratively switch back and forth between these two modes of operation.

The distortion increases with increasing input signal level between the input terminals of the opamp. The opamp input voltage, although small, will not be negligible as has been seen earlier due to the finite gain and bandwidth of the opamp. When this voltage reaches a certain threshold, nonlinearity increases. Hence, it is important to reduce the differential input voltage of the opamp to a small value. The distortion of the opamp can be considered to be at the output of the opamp (output referred distortion) or at the input of the opamp (input referred distortion). Thus the transfer function of distortion source to the opamp output in the latter case is same as that of noise as seen in Fig. 2.42b. Thus minimizing the GSP minimizes distortion and noise as well as sensitivity.

The effect of the output referred distortion can be evaluated by a figure of merit, the *distortion aggravation factor* (DAG) introduced by Billam [2.69]. Evidently, the transfer functions due to *input referred distortion* or *output referred distortion* are related by the frequency-dependent finite gain of the opamp.

Consider the Sallen and Key active RC filter schematic of Fig. 2.43 wherein the distortion is denoted by U_{in}. We evaluate DAG for this circuit as

$$DAG = \frac{V_o}{U_{in}} = \frac{s^2\ C_1\ C_2\ R_1\ R_2 + s(C_1\ R_1 + C_2\ (R_1 + R_2)) + 1}{s^2\ C_1\ C_2\ R_1\ R_2 + s(C_1\ R_1\ (1-K) + C_2\ (R_1 + R_2)) + 1} \tag{2.150}$$

Thus, DAG will be maximum at the pole-frequency ω_p given by

$$DAG_{MAX} = \frac{C_1\ R_1 + C_2\ (R_1 + R_2)}{C_1\ R_1\ (1-K) + C_2\ (R_1 + R_2)} \tag{2.151}$$

Evidently, DAG is $3Q_p$ at the resonant frequency and is maximum at this frequency for the choice $R_1 = R_2 = R$ and $C_1 = C_2 = C$ and $K = 3 - \frac{1}{Q_p}$. On the other hand, by choosing unequal resistor and capacitor values, DAG can be reduced. Defining $GSP = K\, S_K^Q$, we have from the denominator of (2.150),

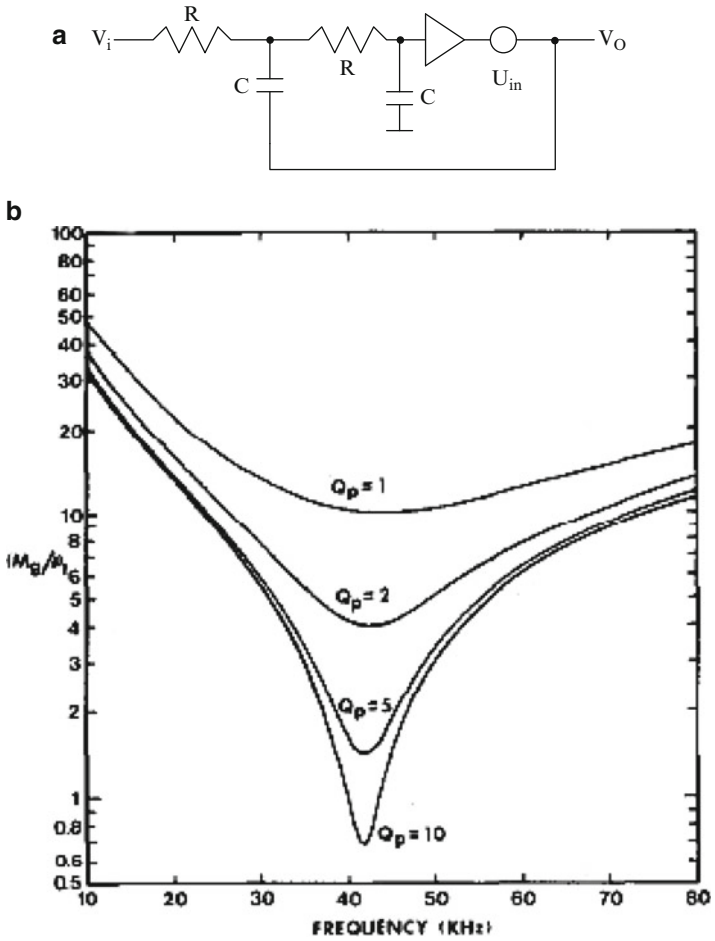

Fig. 2.43 (**a**) Sallen–Key active RC filter modeling input referred distortion, (**b**) plots of input signal versus frequency for the Sallen–Key active RC filter with Q as a parameter (pole-frequency 10 KHz $R_1 = R_2$ and $C_1 = C_2$ using 741 opamp). ((**b**) Adapted from [2.71] ©IEEE 1978)

$$GSP = \frac{K^2 C_1 R_1}{C_1 R_1 (1-K) + C_2 (R_1 + R_2)} \tag{2.152}$$

Thus, DAG and GSP are related as

$$DAG_{MAX} = GSP\left(\frac{C_1 R_1 + C_2 (R_1 + R_2)}{K^2 C_1 R_1}\right) \tag{2.153}$$

As an illustration, for $R_1 = R_2 = R$, $C_1 = C_2 = C$, we have $GSP = 9Q_p$ and $DAG = 3Q_p$. This can also be observed by noting that the GSP is the same as the noise transfer function. If distortion is also input referred, it is the same as the GSP.

It can be seen that Billam's technique [2.69] does not consider the nonidealities of the opamp. Allen [2.70, 2.71] has suggested taking the bandwidth of the amplifier into account, since due to the finite gain and bandwidth of the opamp, the differential input voltage at the opamp input terminals is finite and if it exceeds a particular threshold value δ, distortion sets in. As such, for a given input M_g, Allen suggests evaluating the resulting δ expressed as M_g/δ which reaches a minimum at a particular frequency. That minimum is less than δ. Note that the differential input voltage of the opamp is $V_o s/B$. We consider the Sallen–Key filter of Fig. 2.43a once again and evaluate the magnitude of M_g/δ as

$$\frac{M_g}{\delta} = \sqrt{\left(1 - \omega_n^2 + \frac{B_n}{3\,Q_p - 1}\right)^2 + \left(3\,\omega_n + \frac{B_n\,Q_p}{3\,Q_p - 1}\left(\omega_n - \frac{1}{\omega_n}\right)^2\right)^2} \qquad (2.154)$$

where $\omega_n = \frac{\omega}{\omega_p}$ and $B_n = \frac{B}{\omega_p}$

Typical curves for different pole-Qs are as shown in Fig. 2.43b for an example considering $f_p = 50$ KHz. Thus for a pole-Q of 10, the input voltage must be less than 140 mV assuming $\delta = 100$ mV for a typical bipolar opamp μA741 so that SID cannot set in. In a similar manner, the SID for other single-amplifier biquads can be carried out. Beyond this threshold value, the active filters will exhibit jump resonance. The reader is referred to Borys [2.72, 2.73, 2.74] for an explanation of the relationship between various distortion measures.

Example 2.14 Determine the level at which SID may set in for the single amplifier band-pass filter tunable using a resistor (see Fig. E.2.5b) using SPICE.

The input voltage maximum at the opamp inverting input can be found from the frequency responses plotted in Fig. 2.43b. If it exceeds a certain level, slew-induced distortion sets in.

```
*SA Bandpass distortion Allen's method

vin 1 0 ac 1 v

R11 1 12 15900
R12 12 0 200
C11 12 13 1000 pf
C12 12 14 1000pf
R16 13 14 31800
E11 0 15 13 0 100000
R14 15 16 1 k
C13 16 0 15.9 uf
E12 14 0 16 0 1

.control
destroy all
let ii = 0
while ii < 5
```

```
alter R12 = 200 + 100 * ii
ac lin 100 20k 60 k
let ii = ii + 1

plot mag(ac1.v(13)) mag(ac2.v(13)) mag(ac3.v(13)) mag(ac4.v(13)) mag(ac5.v
(13))
end
.endc
```

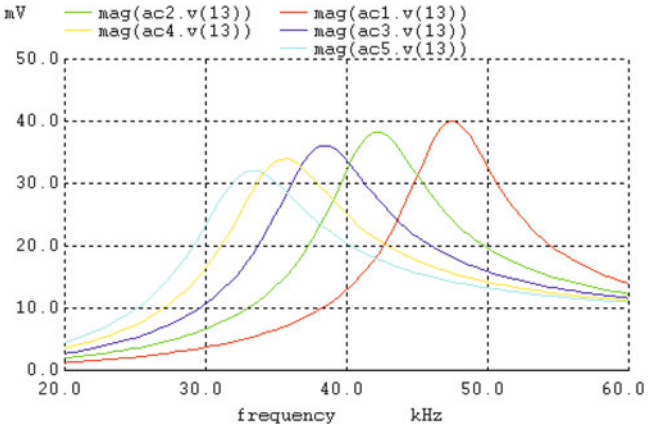

2.13 Problems

P.2.1. A first-order all-pass filter can be obtained by using the circuit of Fig. P.2.1. Analyze the circuit and compare it with the first-order all-pass filters using the opamp of Fig. 2.8a, b. Show that the circuit of Fig. P.2.1b realizes a second-order all-pass transfer function. Discuss the limitations of the circuit.

P.2.2. A bridged-T RC network is shown in Fig. P.2.2a. Derive the transfer function of this circuit and discuss its utility as a notch filter. The circuit

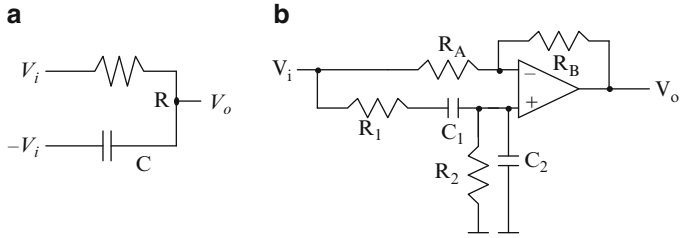

Fig. P.2.1 (**a**) (**b**)

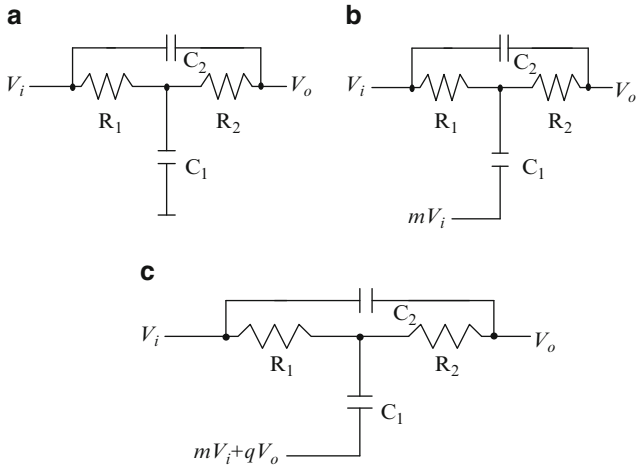

Fig. P.2.2

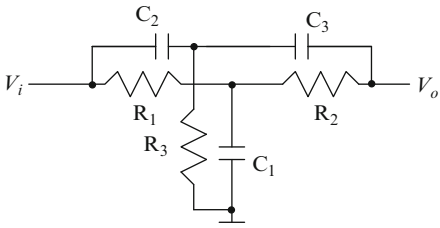

Fig. P.2.3

can be modified to realize a notch or all-pass transfer function using the configuration of Fig. P.2.2b. Analyze the circuit and determine the conditions for realizing notch and all-pass transfer functions. Discuss the limitations of this circuit. Positive feedback can be given to enhance the pole-Q using the modification as shown in Fig. P.2.2c. Derive the transfer function and establish the relationship between the pole-Q and the amount of positive feedback. Suggest a circuit for realizing $mV_i + qV_o$.

P.2.3. A parallel-T RC network is illustrated in Fig. P.2.3. Derive the transfer function of the circuit. This is a third-order network. Find the condition for pole-zero cancellation so that a second-order notch transfer function can be realized.

P.2.4. Hilberman [2.75] has shown that input and ground can be complements in an active RC filter. Using this concept, show that an all-pass filter can be easily obtained from the Tow–Thomas biquad. Compare the circuit with the all-pass filter realized using the feedforward technique in a Tow–Thomas biquad (Fig. P.2.4).

P.2.5. Second-order active RC filters can be built around the GIC. Two such circuits, Fig. P.2.5a due to Mikhael and Bhattacharya [2.76] and Fig. P.2.5b

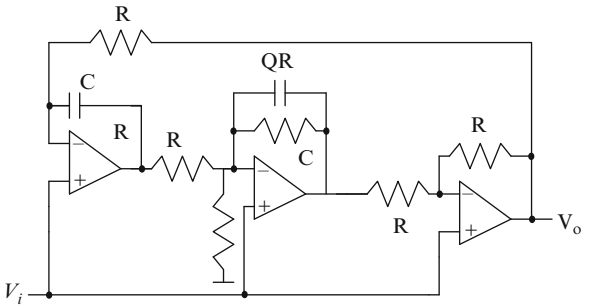

Fig. P.2.4 (Adapted from [2.75] ©IEEE 1973)

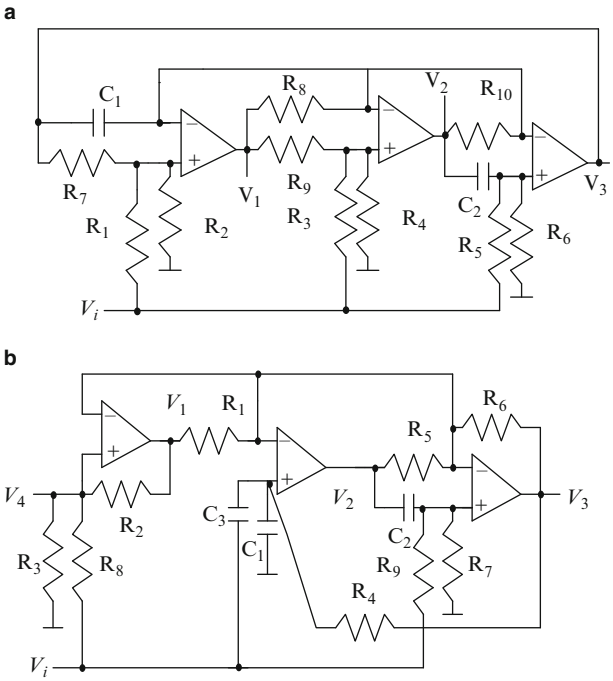

Fig. P.2.5 (Adapted from [2.14] ©IEEE 1984)

Padukone, Mulawka, and Ghausi [2.77] are shown below. Derive the transfer functions of both these circuits together with design equations and analyze the sensitivity of these filters due to opamp finite bandwidth.

P.2.6. A biquad due to Wilson, Bedri, and Bowron [2.78] based on two first-order all-pass filters is presented in Fig. P.2.6. Derive the transfer function of the

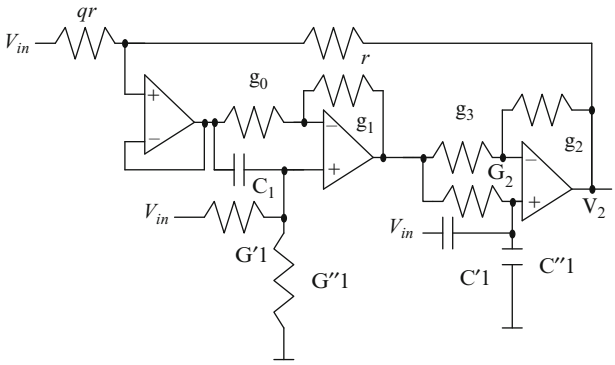

Fig. P.2.6 (Adapted from [2.14] ©IEEE 1984)

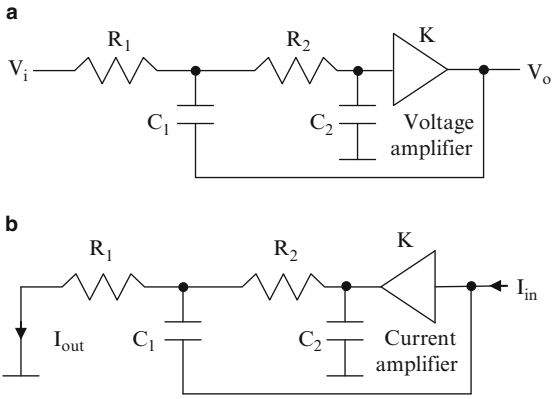

Fig. P.2.10 (**a**) (**b**)

circuit together with the design equations and analyze the effect of opamp finite bandwidth on performance.

P.2.7. Analyze the effect of finite opamp bandwidth on the pole-frequency and pole-Q of the active RC filter of Fig. 2.11b. Discuss the condition for instability.

P.2.8. Analyze the active R filters of Fig. 2.27 considering a two-pole model of the opamp. Discuss the stability of these circuits.

P.2.9. Derive the expressions for peak magnitude of the general second-order transfer function given in Appendix B.

P.2.10. A current-input current-output circuit can be obtained from the voltage-input voltage-output type active RC filter using voltage amplifiers (see, e.g., Fig. P.2.10a) by using the *adjoint technique*. In this technique, the output voltage terminal is fed the input current, the input voltage terminal is grounded, and the output current is tapped at this terminal as shown in Fig. P.2.10b. Discuss in which other cases the technique is applicable.

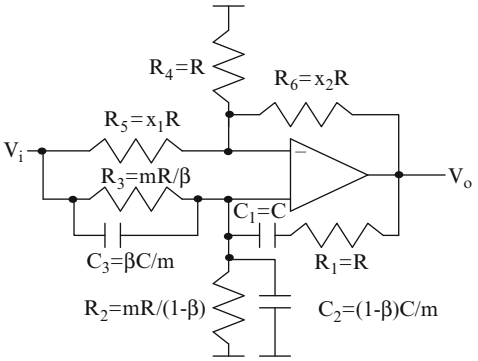

Fig. P.2.12 (Adapted from [2.79] ©IEEE 1973)

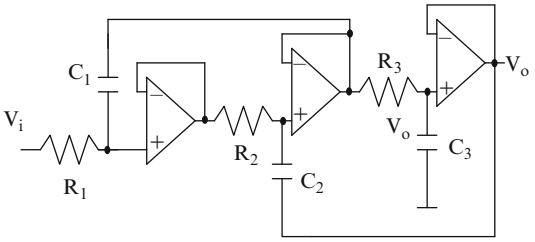

Fig. P.2.13

P.2.11. Derive expressions for the output noise of Tow–Thomas biquad of Fig. 2.18a. Assume that all opamps are identical.

P.2.12. An all-pass network can be realized using the circuit [2.79] of Fig. P.2.12. Derive the design equations and compare with the Steffen all-pass circuit of Fig. 2.13. Choose m for obtaining the minimum GSP. Examine the effect of the opamp finite bandwidth.

P.2.13. A high-order active RC filter due to Bach [2.80] using only unity gain buffers is shown in Fig. P.2.13. Derive the transfer function of this circuit and analyze the effect of finite bandwidth of the opamp. Suggest a design procedure. Derive a high-pass filter from this circuit and the design equations.

P.2.14. Denoting the pole of a second-order filter as p, with a denominator of the transfer function given as $s^2 + s\frac{\omega_p}{Q_p} + \omega_p^2$, show that $\Delta p/p$ in terms of variations in pole-Q and pole-frequency is given by $\frac{dp}{p} = \frac{d\omega_p}{\omega_p} - j\frac{dQ/Q}{\sqrt{4Q_p^2 - 1}}$ [2.81]. This means that it is important to reduce $\frac{d\omega_p}{\omega_p}$ which is $2Q_p$ times more than $\frac{dQ_p}{Q_p}$. Show also that $\frac{d|T(s)|}{|T(s)|} = \frac{dQ_p}{Q_p} + j2Q_p\frac{d\omega_p}{\omega_p}$ and also that $\frac{d|T(s)|}{|T(s)|} = 2Q_p\frac{dp}{p}$ at the frequency$\omega = \omega_p$.

P.2.15. Considering single-pole and two-pole models for the opamps, evaluate the bandwidth of both the amplifiers [2.82] of Fig. P.2.15a, b. Discuss the stability and improvement in bandwidth.

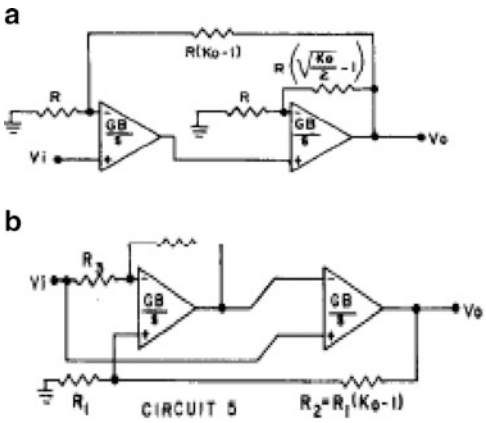

Fig. P.2.15 (**a**) (**b**) (Adapted from [2.82] ©IEEE 1977)

P.2.16. Analyze the performance of integrators using the compensated amplifiers of Fig. P.2.16a–e using two and three opamps [2.83].

P.2.17. Analyze the finite gain amplifiers shown [2.84] in Fig. P.2.17a, b and derive conditions to obtain the flat gain response.

P.2.18. Derive the expression for input impedance of the single-amplifier circuit [2.85, 2.87] of Fig. P.2.18. Analyze the nature of the input impedance. Considering the nonideal frequency response of the opamp, derive the input impedance and compare it with the results using an ideal opamp.

P.2.19. Repeat the problem for the circuit [2.86, 2.87] of Fig. P.2.19. Compare the results with those of Fig. P.2.18.

P.2.20. Derive the input impedance of the circuit [2.88] of Fig. P.2.20. Derive conditions under which a grounded FDNR in series with a capacitor can be realized.

P.2.21. Derive the transfer function of the active distributed network [2.89] of Fig. P.2.21a derived from Sallen–Key and multiple feedback type active RC filters. Using SPICE, simulate the frequency response and discuss the design procedure to realize a given specification. Note that a uniform distributed RC network can be modeled as a π network with irrational impedances as shown in Fig. P.2.21b.

Note that $Y = \frac{\sqrt{sc/r}}{\sinh \sqrt{src\,d^2}}$ and a shunt admittance of $(P-1)Y$ where $P = \cosh \sqrt{src\,d^2}$.

P.2.22. Analyze the positive impedance converter or active transformer [2.90] of Fig. P.2.22 and derive an expression for input impedance when the load impedance is Z_L.

P.2.23. Show that the circuit of Fig. P.2.25 realizes a floating inductance [2.90]. Discuss the behavior with nonideal opamps.

P.2.24. Derive the transfer function of the circuit [2.90] of Fig. P.2.24 and discuss its possible application.

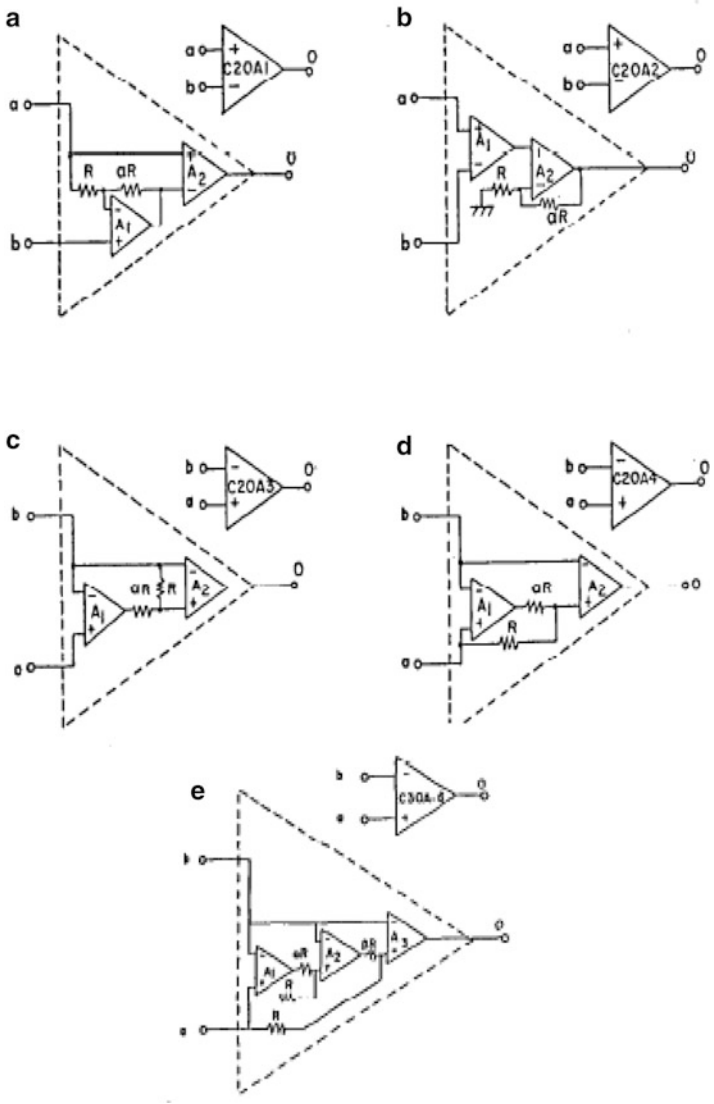

Fig. P.2.16 (Adapted from [2.83] ©IEEE 1987)

P.2.25. Derive the transfer functions of the 2 two-amplifier based filters [2.91] of Fig. P.2.26 and analyze their sensitivity to passive components and gains k1 and k2.

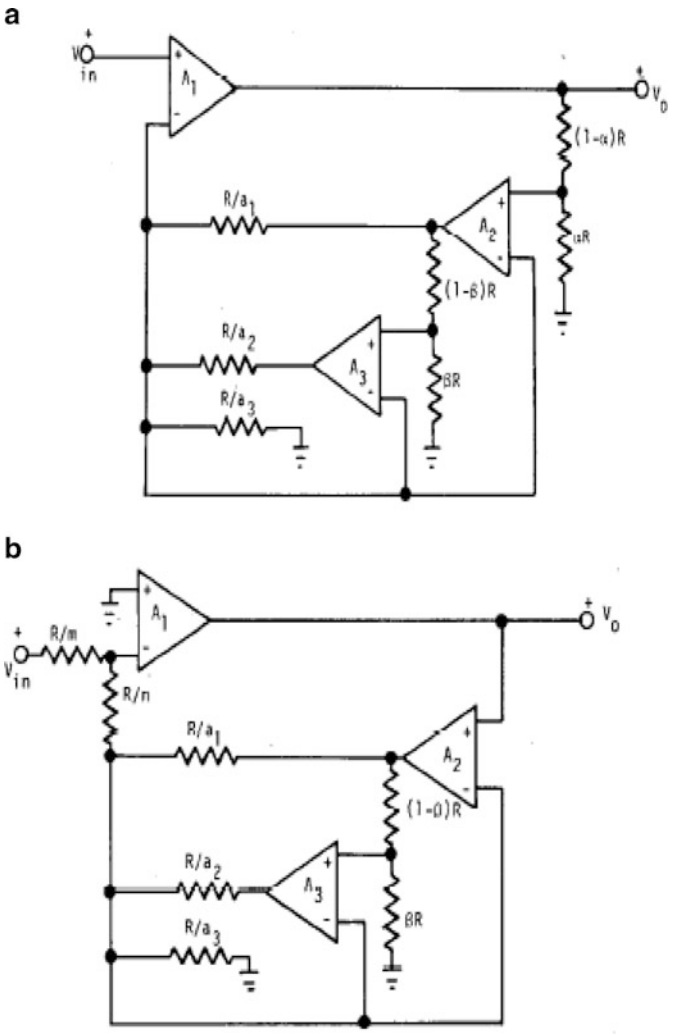

Fig. P.2.17 (**a**) (**b**) (Adapted from [2.84] ©IEEE 1980)

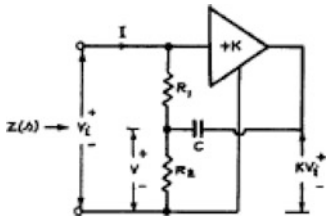

Fig. P.2.18 (Adapted from [2.87] ©IEEE 1970)

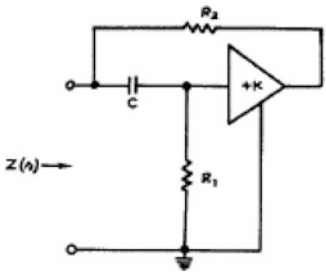

Fig. P.2.19 (Adapted from [2.87] ©IEEE 1970)

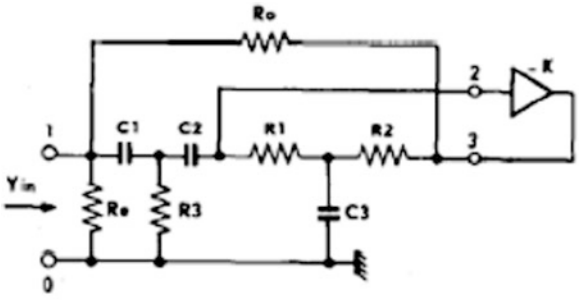

Fig. P.2.20 (Adapted from [2.88] ©IEEE 1974)

P.2.26. Derive the transfer function of the second-order filter [2.92] of Fig. P.2.26 using first-order all-pass networks. Compare with Tarmy–Ghausi modified by the Moschytz realization (Fig. 2.25a).

P.2.27. Analyze the two-amplifier-based active RC filters [2.93] of Fig. P.2.27a, b. Derive expressions for pole-frequency and pole-Q sensitivities.

P.2.28. Derive the transfer functions corresponding to both outputs of the active R filter of Fig. P.2.28 [2.94]. Derive conditions for realizing low-pass, band-pass, high-pass, notch, and all-pass transfer functions.

P.2.29. Derive the transfer functions of the transadmittance filters [2.95] of Fig. P.2.29a, b. Convert them into voltage-mode filters and discuss their utility.

P.2.30. A current conveyor is presented in Fig. P.2.30. This has the property that $V_x = V_y$, $I_z = I_x$, and $I_y = 0$. The input y is buffered and is available at the *x* terminal with a series resistance of Rx. The input current is mirrored and is available at the output terminal. The output terminal has finite output resistance and output capacitance to ground. Derive (a) an integrator, (b) a voltage amplifier, and (c) a current amplifier and obtain their transfer functions. Determine the bandwidth in cases (b) and (c) (Fig. P.2.30).

P.2.31. A second-order filter using a current conveyor CCII is shown in Fig. P.2.31. Derive its transfer function and sensitivity of pole-*Q* and pole-frequency to finite voltage transfer gain between the *y* and *x* terminals, finite current gain between the *x* and *z* terminals, and finite *Rx* and finite *Ro* and *Co* at the *z* terminal.

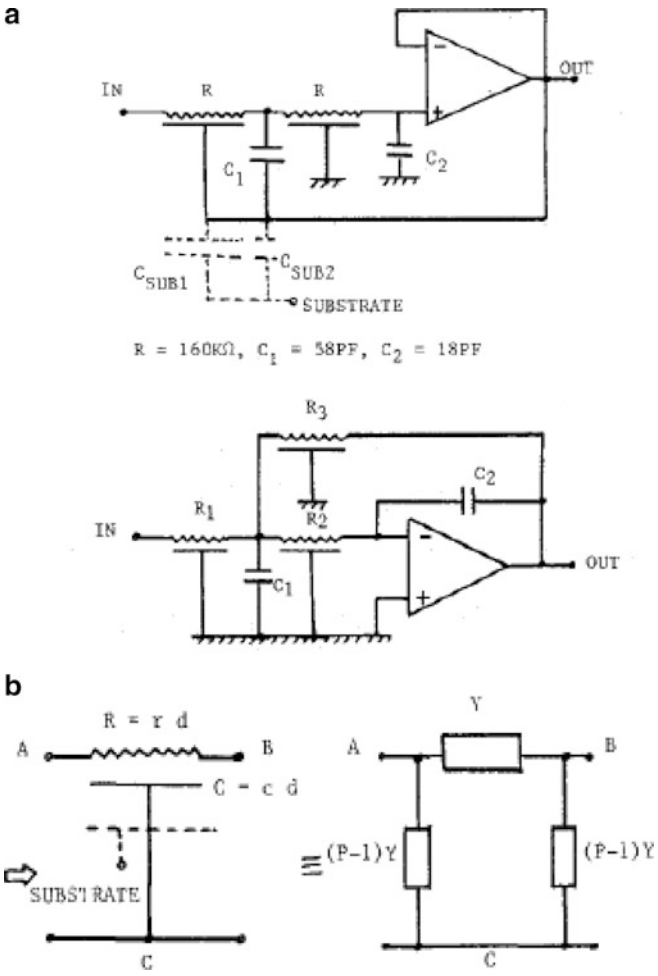

Fig. P.2.21 (**a**) (**b**) (Adapted from [2.89] ©IEEE 1987)

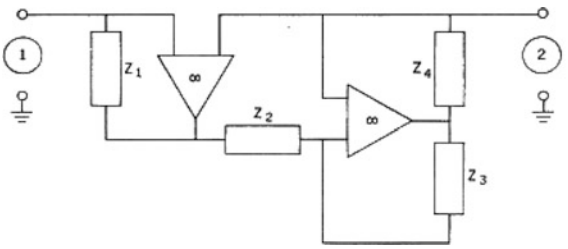

Fig. P.2.22 (Adapted from [2.90] ©IEEE 1971)

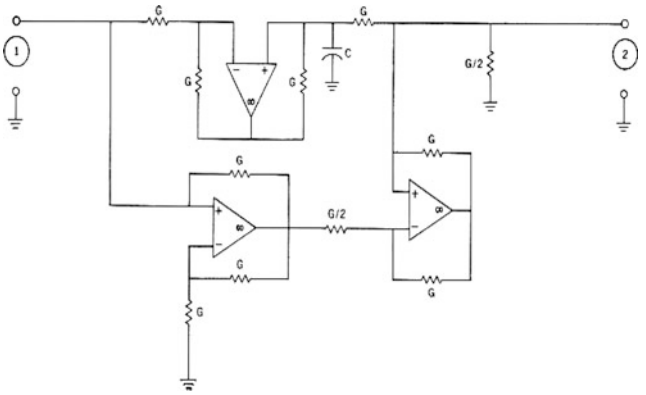

Fig. P.2.23 (Adapted from [2.90] ©IEEE 1971)

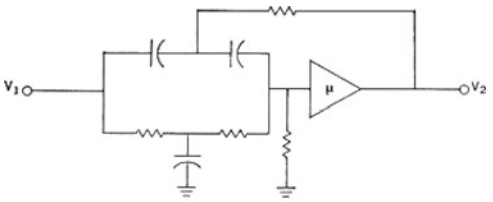

Fig. P.2.24 (Adapted from [2.90] ©IEEE 1971)

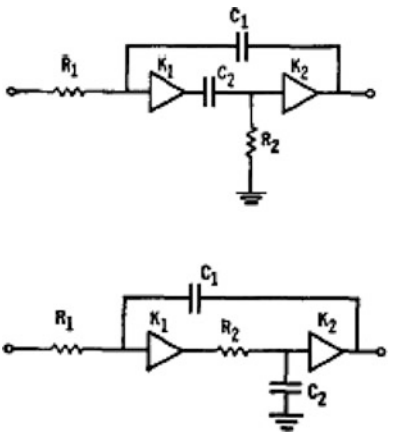

Fig. P.2.25 (Adapted from [2.91] ©IEEE 1971)

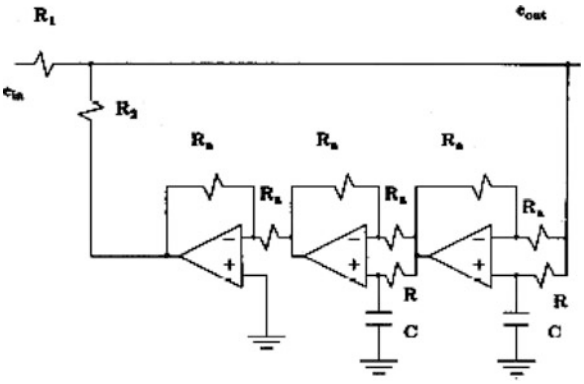

Fig. P.2.26 (Adapted from [2.92] ©IEEE 1968)

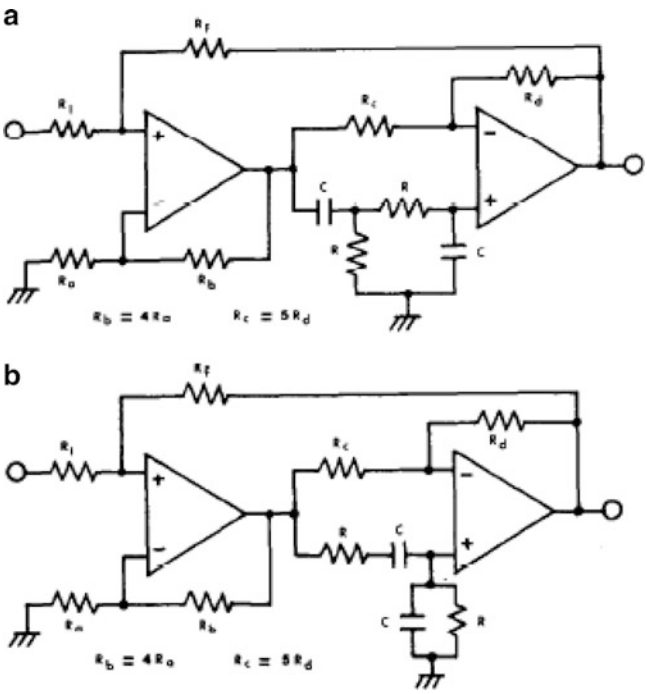

Fig. P.2.27 (**a**) (**b**) (Adapted from [2.93] ©IEEE 1978)

P.2.32. Derive the current-output–current-input transfer function of the circuit [2.96] of Fig. P.2.32. Analyze the effect of nonidealities of CCII.

P.2.33. Construct a state variable voltage mode and current mode biquad based on the Tow–Thomas biquad using a second-generation current conveyor. Derive the transfer functions and analyze the effect of nonidealities.

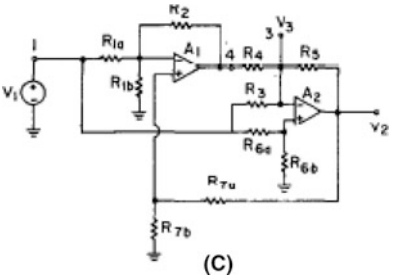

Fig. P.2.28 (Adapted from [2.94] ©IEEE 1977)

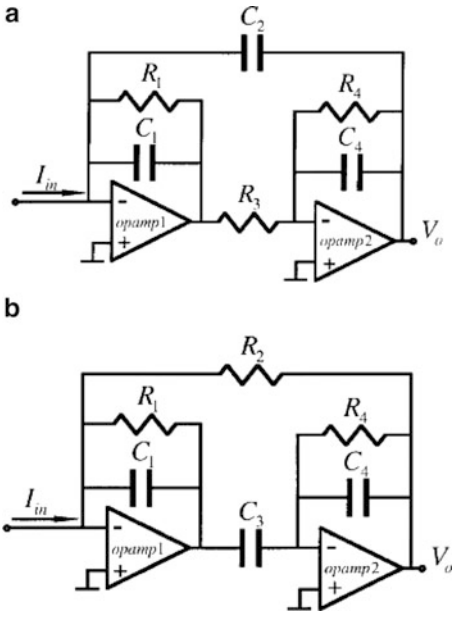

Fig. P.2.29 (Adapted from [2.95] ©IEEE 1997)

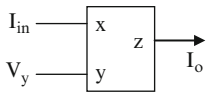

Fig. P.2.30

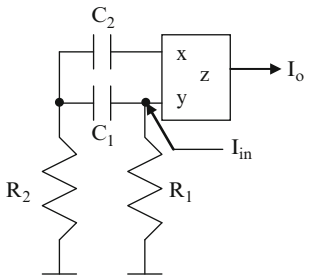

Fig. P.2.31

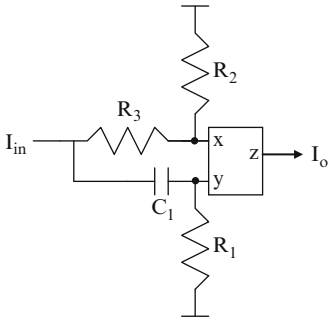

Fig. P.2.32 (Adapted from [2.96] ©IEEE 1990)

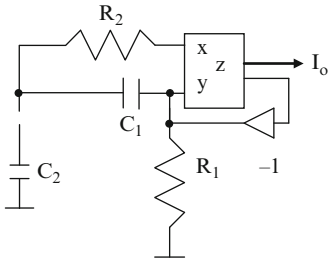

Fig. P.2.35 (Adapted from [2.97] ©IEEE 1987)

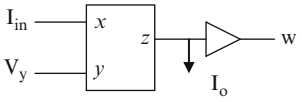

Fig. P.2.36

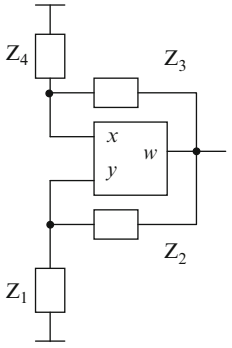

Fig. P.2.38 (Adapted from [2.98] ©IEEE 1996)

P.2.34. Derive a CCII-based biquad exactly identical to a KHN active RC biquad. (It should realize high-pass, low-pass, band-pass, and notch transfer functions.)

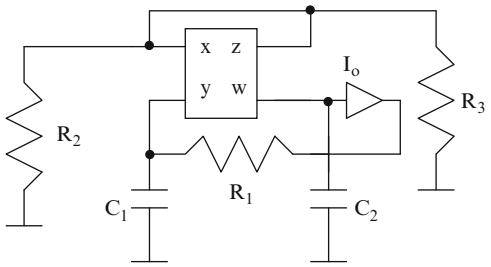

Fig. P.2.39 (Adapted from [2.99] ©IEEE 1999)

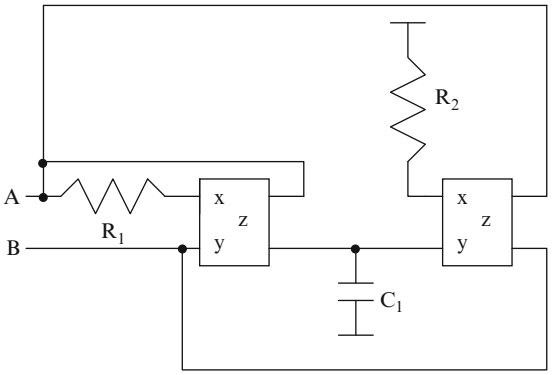

Fig. P.2.40 (Adapted from [2.100] ©IEE 1998)

P.2.35. Analyze the circuit of Fig. P.2.35 [2.97] and derive the condition for oscillations. This uses a first-generation current conveyor denoted as CCI which can be considered as a CCII with another current output that feeds back to the y terminal; that is, $V_x = V_y$, $I_z = I_x$, and $I_y = -I_z$.

P.2.36. A current conveyor CCII can be augmented with a buffer connected to the z terminal y to provide a voltage output at the w terminal. This device is known as CFOA. Derive the transfer function of a finite gain-inverting amplifier using CFOA and evaluate its performance as compared with an opamp-based finite gain-inverting amplifier. Also consider the current mirror pole (between the x and z terminals) in your evaluation (Fig. P.2.36).

P.2.37. Discuss the stability of an integrator using CFOA considering the current mirror pole and other parasitics R_x, R_t, and C_t. Note that x, y, and w correspond to inverting input, noninverting input, and output of the CFOA, respectively.

P.2.38. Derive the expressions for frequency of oscillation and condition for oscillation for the CFOA-based oscillator [2.98] of Fig. P.2.38 by choosing proper impedances for various Z_is.

P.2.39. A FTFN (four-terminal floating nullor) [2.103] is a useful active element. It is described as $V_x = V_y$, $I_x = I_y = 0$, and $I_w = -I_z$. An oscillator using FTFN [2.99] is shown in Fig. P.2.39. Derive expressions for the frequency

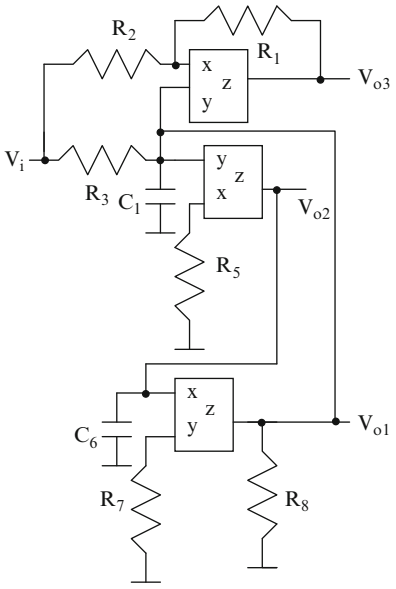

Fig. P.2.41 (Adapted from [2.101] ©IEE 1990)

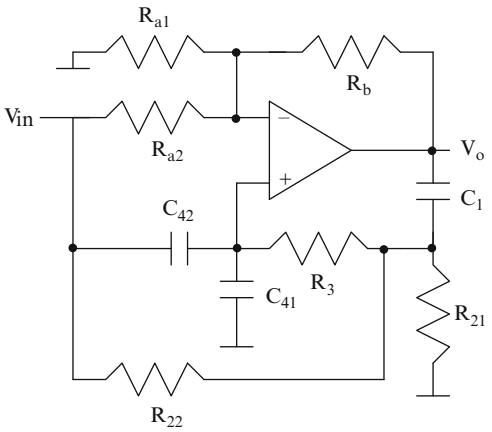

Fig. P.2.42 (Adapted from [2.102] ©IEEE 1980)

of oscillation and condition for oscillation. Analyze the circuit with resistor R_1 connected between the y and z terminals of the FTFN.

P.2.40. Derive the expression for the input impedance of the floating impedance simulator [2.100] of Fig. P.2.40 considering the nonidealities of the current conveyors.

P.2.41. A multifunction biquad using current conveyors due to Singh and Senani [2.101] is presented in Fig. P.2.41. Derive all the transfer functions.

P.2.42. The adjoint concept can be used to derive current mode circuits using current amplifiers. Derive a current-mode biquad from the active RC filter of Fig. P.2.42 due to Sedra, Ghorab, and Martin [2.102] and the Friend–Deliyannis biquad of Fig. 2.11a.

References

[2.1] Sedra, A.S., Brackett, P.O.: Filter Theory and Design: Active and Passive. Matrix, Beaverton, Champaign (1978)
[2.2] Moschytz, G.S.: Linear Integrated Networks: Fundamentals. Van Nostrand-Reinhold, New York (1974)
[2.3] Moschytz, G.S.: Linear Integrated Networks: Design. Van Nostrand-Reinhold, New York (1975)
[2.4] Deliyannis, T., Sun, Y., Fidler, J.K.: Continuous-Time Active Filter Design. CRC Press, Boca Raton (1999)
[2.5] Tsividis, Y.P., Voorman, J.O. (eds.): Integrated Continuous-Time Filters. IEEE Press, Piscataway (1993)
[2.6] Schaumann, R., Ghausi, M.S., Laker, K.R.: Design of Analog Filters: Passive, Active RC, and Switched Capacitor. Prentice Hall, Englewood Cliffs (1990)
[2.7] Ghausi, M.S., Laker, K.R.: Modern Filter Design. Prentice-Hall, Englewood Cliffs (1981)
[2.8] Temes, G.C., Mitra, S.K. (eds.): Modern Filter Theory and Design. Wiley, New York (1973)
[2.9] Daryanani, G.: Principles of Active Network Synthesis and Design. Wiley, New York (1976)
[2.10] Huelsman, L.P., Allen, P.E.: Introduction to the Theory and Design of Active Filters. McGraw-Hill, New York (1980)
[2.11] Bruton, L.T.: Active RC Circuits. Prentice-Hall, Englewood Cliffs (1980)
[2.12] Unbehauen, R., Cichocki, A.: MOS Switched-Capacitor and Continuous-time Integrated Circuits and Systems. Springer, Berlin (1989)
[2.13] Budak, A.: Passive and Active Network Analysis and Synthesis. Waveland Press, Prospect Heights (1991)
[2.14] Ghausi, M.S.: Analog active filters. IEEE Trans. Circuits Syst. **CAS-31**, 13–31 (1984)
[2.15] Soundararajan, K., Ramakrishna, K.: Characteristics of non-ideal operational amplifiers. IEEE Trans. Circuits Syst. **CAS-21**, 69–75 (1974)
[2.16] Wilson, G.: Compensation of some operational-amplifier based RC-active networks. IEEE Trans. Circuits Syst. **23**, 443–446 (1976)
[2.17] Soliman, A.N., Ismail, M.: Active compensation of Opamps. IEEE Trans. Circuits Syst. **26**, 112–117 (1979)
[2.18] Ravichandran, S., Rao, K.R.: A novel active compensation scheme for active-RC filters. Proc. IEEE **68**, 743–744 (1980)
[2.19] Boutin, N.: Active compensation of op-amp inverting amplifier using NIC. Electron. Lett. **17**, 978–979 (1981)
[2.20] Ananda Mohan, P.V.: Active compensation of Opamp Inverting Amplifier using NIC. AEU **42**, 192–194 (1988)
[2.21] Brackett, P.O., Sedra, A.S.: Active compensation for high-frequency Op-Amp circuits with applications in active RC filters. IEEE Trans. Circuits Syst. **23**, 68–72 (1976)
[2.22] DeBoo, G.J.: A novel integrator results by grounding its capacitor. Electron. Des. **15** (1967)
[2.23] Thomas, L.C.: The biquad: part-I- some practical design considerations. IEEE Trans. Circuit Theory **CT-18**, 350–361 (1971)

[2.24] Akerberg, D., Mossberg, K.: A versatile active RC building block with inherent compensation for the finite bandwidth of the amplifier. IEEE Trans. Circuits Syst. **21**, 75–78 (1974)
[2.25] Tsividis, Y.P.: Integrated continuous-time filter design-an overview. IEEE J. Solid-State Circuits **29**, 166–176 (1994)
[2.26] Ponsonby, J.E.B.: Active all-pass filter using a differential operational amplifier. Electron. Lett. **2**, 134–135 (1966)
[2.27] Sallen, R.P., Key, W.L.: A practical method of designing active RC filters. IEEE Trans. Circuit Theory **CT-2**, 74–85 (1955)
[2.28] Gray, P.R., Meyer, R.G.: Analysis and Design of Analog Integrated Circuits, 2nd edn. Wiley, New York (1982)
[2.29] Friend, J., Harris, C.A., Hilberman, D.: STAR: an active biquadratic filter section. IEEE Trans. Circuits Syst. **22**, 115–121 (1975)
[2.30] Fleischer, P.E.: Sensitivity minimization in a single amplifier biquad circuit. IEEE Trans. Circuits Syst. **CAS-23**, 45–55 (1976)
[2.31] Deliyannis, T.: High Q-factor circuit with reduced sensitivity. Electron. Lett. **4**, 577 (1968)
[2.32] Moschytz, G.S.: Gain sensitivity product – a figure of merit for hybrid integrated filters using single operational amplifiers. IEEE J. Solid-State Circuits **SC- 6**, 103–110 (1971)
[2.33] Moschytz, G.S., Horn, P.: Reducing non-ideal opamp effects in active filters by minimizing the gain-sensitivity product. IEEE Trans. Circuits Syst. **CAS-24**, 437–445 (1977)
[2.34] Ford, R.L., Girling, F.E.J.: Active filters and oscillators using simulated inductance. Electron. Lett. **2**, 52 (1966)
[2.35] Chandra, G., Tadeparthy, P., Easwaran, P.: Single amplifier bi-quadratic filter topologies in transimpedance configuration. IEEE Trans. Circuits Syst. **55**, 502–507 (2008)
[2.36] Ananda Mohan, P.V.: On single amplifier bi-quadratic topologies in transimpedance configuration. In: Proceedings of TENCON 2009-IEEE Region 10 Conference. doi:10.1109/TENCON.2009.5395967, pp. 1–6 (2009)
[2.37] Antoniou, A.: Realization of gyrators using operational amplifiers and their use in RC active network synthesis. Proc. IEE **116**, 1838–1850 (1969)
[2.38] Ananda Mohan, P.V., Ramachandran, V., Swamy, M.N.S.: New General Biquadratic Active RC and SC Filters. Proc. IEE, Part G, ECS **131**, 51–55 (1984)
[2.39] Kerwin, W.J., Huelsman, L.P., Newcomb, R.W.: State-variable synthesis for insensitive integrated circuit transfer functions. IEEE J. Solid-State Circuits **2**, 87–92 (1973)
[2.40] Ananda Mohan, P.V., Ramachandran, V., Swamy, M.N.S.: Formulas for dynamic-range evaluation of second-order discrete-time filter. IEEE Trans. Circuits Syst. **30**, 321 (1983)
[2.41] Ananda Mohan, P.V., Ramachandran, V., Swamy, M.N.S.: Nodal voltage simulation of active RC networks. IEEE Trans. Circuits Syst. **32**, 1085–1088 (1985)
[2.42] Soliman, A.M.: History and progress of the Tow–Thomas bi-quadratic filter. Part I: generation and Op amp realizations. J. Circuits Syst. Comput. **17**, 33–54 (2008)
[2.43] Moustakas, E., Chan, S.: Sensitivity considerations in a multiple-feedback universal active filter. IEEE Trans. Circuits Syst. **24**, 695–703 (1977)
[2.44] Tarmy, R., Ghausi, M.S.: Very high-Q insensitive active RC networks. IEEE Trans. Circuit Theory **CT-17**, 358–366 (1970)
[2.45] Moschytz, G.S.: High-Q factor insensitive active RC network similar to the Tarmy-Ghausi circuit, but using single-ended operational amplifiers. Electron. Lett. **8**, 458–459 (1972)
[2.46] Mulawka, J., Bialko, M.: Modifications of Tarmy-Ghausi active filter. Electron. Lett. **10**(18), 380–381 (1974)
[2.47] Toker, A., Ozoguz, S., Cicekoglu, O., Acar, C.: Current-mode all-pass filters using current differencing buffered amplifier and a new high-Q band-pass filter configuration. IEEE Trans. Circuits Syst.-II: Analog Digit. Signal Process. **47**, 949–954 (2000)
[2.48] Soliman, A.M., Fawzy, M.: A bandpass filter using the operational amplifier pole. IEEE J. Solid-Sate Circuits **SC-12**, 429–430 (1977)

[2.49] Ananda Mohan, P.V.: A novel band-pass filter using the amplifier pole. IEEE J. Solid-State Circuits **14**, 649–651 (1979)
[2.50] Tobey, T.E., Greame, J.G., Huelsman, L.P.: Operational Amplifier: Design and Applications. McGraw-Hill, New York (1971)
[2.51] Rao, K.R., Srinivasan, S.: A bandpass filter using the operational amplifier pole. IEEE J. Solid-State Circuits **SC-8**, 245–246 (1973)
[2.52] Ananda Mohan, P.V.: Low-pass and notch filters using the operational amplifier pole. Proc. IEEE **67**, 1160–1162 (1979)
[2.53] Ananda Mohan, P.V.: Novel active filters using the amplifier pole. Electron. Lett. **16**, 378–380 (1980)
[2.54] Mitra, A.K., Aatre, V.K.: Low sensitivity high-frequency active R filters. IEEE Trans. Circuits Syst. **23**, 670–676 (1976)
[2.55] Rao, K.R., Srinivasan, S.: Low-sensitivity active filters using the operational amplifier pole. IEEE Trans. Circuits Syst. **CAS-21**, 260–262 (1974)
[2.56] Schaumann, R.: Low-sensitivity High-frequency tunable active filters without external capacitors. IEEE Trans. Circuits Syst. **CAS-22**, 39–44 (1974)
[2.57] Orchard, H.J.: Inductorless filters. Electron. Lett. **2**, 24–25 (1966)
[2.58] Riordan, R.H.S.: Simulated inductors using differential amplifiers. Electron. Lett. **3**(2) (1967)
[2.59] Bruton, L.: Network transfer functions using the concept of frequency dependent negative resistance. IEEE Trans. Circuit Theory **16**, 406–408 (1969)
[2.60] Allstot, D.J., Brodersen, R.W., Gray, P.R.: Design techniques for MOS switched capacitor ladder filters. IEEE Trans. Circuits Syst. **CAS-25**, 1014–1021 (1978)
[2.61] Yoshihoro, M., Nishihra, A., Yanagisawa, T.: Low-sensitivity active and digital filters based on the node voltage simulation of LC ladder structures. In: Proceedings of IEEE International Symposium on Circuits and Systems, AZ, pp. 446–449 (1977)
[2.62] Ananda Mohan, P.V.: Operational simulation of high-pass RLC filters. Electron. Lett. **24**, 779–780 (1988)
[2.63] Martin, K., Sedra, A.S.: Exact design of Switched capacitor band-pass filters using coupled biquad structures. IEEE Trans. Circuits Syst. **CAS-27**, 469–475 (1980)
[2.64] Laker, K.R., Schaumann, R., Ghausi, M.S.: Multiple-loop feedback topologies for the design of low-sensitivity active filters. IEEE Trans. Circuits Syst. **26**, 1–21 (1979)
[2.65] Bruton, L.T., Trofimenkoff, F.N., Treleaven, D.H.: Noise performance of low-sensitivity active filters. IEEE J. Solid-State Circuits **SC-8**, 85–91 (1973)
[2.66] Trofimenkoff, F.N., Treleaven, D.H., Bruton, L.T.: Noise performance of RC active quadratic filter sections. IEEE Trans. Circuits Syst. **CT-5**, 524–532 (1973)
[2.67] Bachler, H.J., Guggenbuhl, W.: Noise analysis and comparison of second-order networks containing a single amplifier. IEEE Trans. Circuits Syst. **27**, 85–91 (1980)
[2.68] Bachler, H.J., Guggenbuhl, W.: Noise and Sensitivity optimization of a single-amplifier biquad. IEEE Trans. Circuits Syst. **26**, 30–36 (1979)
[2.69] Billam, P.J.: Practical optimization of noise and distortion in Sallen and Key filter sections. IEEE J. Solid-State Circuits **14**, 768–771 (1979)
[2.70] Allen, P.E.: Slew-induced distortion in operational amplifiers. IEEE J. Solid-State Circuits **12**, 39–44 (1977)
[2.71] Allen, P.E.: A model for Slew-induced distortion in single-amplifier active RC filters. IEEE Trans. Circuits Syst. **25**, 565–572 (1978)
[2.72] Borys, A.: A relationship between different measures of non-linear distortion in single-amplifier active filters. IEEE Trans. Circuits Syst. **30**, 842–846 (1983)
[2.73] Borys, A.: A note on general Gain-sensitivity product and complementary transformation. IEEE Trans. Circuits Syst. **37**, 1324–1325 (1990)
[2.74] Borys, A.: Slew-induced distortion of single-amplifier active filters using the gain-sensitivity-product concept. IEEE Trans. Circuits Syst. **CAS-31**, 306–308 (1984)

[2.75] Hilberman, D.: Input and ground as complements in active filters. IEEE Trans. Circuit Theory **CT-20**, 540–547 (1973)
[2.76] Mikhael, W.B., Bhattacharyya, B.B.: A practical design for insensitive RC-filters. IEEE Trans. Circuits Syst. **CAS-22**, 407–425 (1975)
[2.77] Padukone, P.R., Mulawka, J., Ghausi, M.S.: An active biquadratic section with reduced sensitivity to operational amplifier imperfections. J. Franklin Inst. **310**, 27–40 (1980)
[2.78] Wilson, G., Bedri, Y., Bowron, P.: RC-active networks with reduced sensitivity to amplifier gain-bandwidth product. IEEE Trans. Circuits Syst. **CAS-21**, 618–626 (1974)
[2.79] Sedra, A.S., Brown, L.: A simple all-pass network with complex poles and zeros. IEEE Trans. Circuit Theory. **CT-**, 445–446 (1973)
[2.80] Bach, R.E.: Selecting RC values for active filters. Electronics **33**, 82–85 (1960)
[2.81] Moschytz, G.S.: A note on pole, frequency and Q – sensitivity. IEEE J. Solid-State Circuits **SC-6**, 267–269 (1871)
[2.82] Geiger, R.L.: Amplifiers with maximum bandwidth. IEEE Trans. Circuits Syst. **24**, 510–512 (1977)
[2.83] Michael, S., Mikhael, W.B.: Inverting integrator and active filter applications of composite operational amplifiers. IEEE Trans. Circuits Syst. **CAS-34**, 461–470 (1987)
[2.84] Natarajan, S., Bhattacharyya, B.B.: Design of actively compensated finite gain Amplifiers for high-frequency applications. IEEE Trans. Circuits Syst. **CAS-27**, 1133–1139 (1980)
[2.85] Prescott, A.J.: Loss compensated active gyrator using differential-input operational amplifiers. Electron. Lett. **2**, 283–284 (1966)
[2.86] Berndt, D., Dutta Roy, S.C.: Inductor simulation using a single unity gain amplifier. IEEE J. Solid-State Circuits **SC-4**, 161–162 (1969)
[2.87] Dutta Roy, S.C., Nagarajan, V.: On inductor simulation using a unity-gain amplifier. IEEE J. Solid-State Circuits **SC-5**, 95–98 (1970)
[2.88] Molo, F.: Parallel resonator with a resistance and a frequency dependent negative resistance realized with a single operational amplifier. IEEE Trans. Circuits Syst. **CAS-21**, 783–788 (1974)
[2.89] Ahuja, B.K.: Implementation of active distributed RC anti-aliasing/smoothing filters. IEEE J. Solid-State Circuits **SC-17**, 1076–1080 (1982)
[2.90] Mitra, S.K.: Synthesizing active filters. IEEE Spectr. 46–63 (1969)
[2.91] Soderstand, M.A., Mitra, S.K.: Gain and sensitivity limitations of active RC filters. IEEE Trans. Circuit Theory **CT-18**, 600–609 (1971)
[2.92] Comer, D.J., McDermid, J.E.: Inductorless bandpass characteristics using all-pass networks. IEEE Trans. Circuit Theory **15**, 501–503 (1968)
[2.93] Dalpadado, R.N.G.: A class of high-Q high-frequency two amplifier active RC networks. IEEE Trans. Circuits Syst. **CAS-25**, 1099–1101 (1978)
[2.94] Kim, H.K., Ra, J.B.: An active biquadratic building block without external capacitors. IEEE Trans. Circuits Syst. **CAS-24**, 689–694 (1977)
[2.95] Carlosena, A.V., Cabral, E.: Novel transimpedance filter topology for instrumentation. IEEE Trans. Instrum. Meas. **46**, 862–867 (1997)
[2.96] Higashimura, M., Fukui, Y.: Realization of current-mode all-pass networks using a single current conveyor. IEEE Trans. Circuits Syst. **37**, 660–661 (1990)
[2.97] Abuelmaatti, M.T.: Two minimum component CC II based RC oscillators. IEEE Trans. Circuits Syst. **34**, 980–981 (1987)
[2.98] Abuelmaatti, M.T., et al.: Novel RC oscillators using current feedback operational amplifiers. IEEE Trans. Circuits Syst. **43**, 155–157 (1996)
[2.99] Bhaskar, D.R.: Single resistance controlled sinusoidal oscillator using single FTFN. Electron. Lett. **35**, 190 (1999)
[2.100] Ananda Mohan, P.V.: Grounded capacitor based grounded and floating inductance simulation using current conveyors. Electron. Lett. **34**, 1037–1038 (1998)
[2.101] Singh, V.K., Senani, R.: New multifunction active filter configuration employing current conveyors. Electron. Lett. **26**, 1814–1816 (1990)

[2.102] Sedra, A.S., Ghorab, M.A., Martin, K.: Optimum configurations for single amplifier biquadratic filters. IEEE Trans. Circuits Syst. **27**, 1155–1163 (1980)
[2.103] Allen, P.E., Holberg, D.R.: CMOS Analog Circuit Design. Oxford University Press, New York (2002)

http://www.springer.com/978-0-8176-8357-3

VLSI Analog Filters
Active RC, OTA-C, and SC
Mohan, P.V.A.
2013, XV, 618 p. 451 illus., 37 illus. in color., Hardcover
ISBN: 978-0-8176-8357-3
A product of Birkhäuser Basel